ACOUSTOELECTRIC STUDIES IN CADMIUM SULPHIDE THIN FILMS

by

Iain McLaren Mason, B.Sc. (Eng.) (Cape Town).

Thesis presented for the degree of Doctor of Philosophy of the University of Edinburgh in the Faculty of Science.

May, 1968.

ACKNOWLEDGEMENTS.

I wish to express my gratitude to Professor W.E.J. Farvis for his guidance throughout this work.

I would like to thank E.A. Ash, M.B.N. Butler, J. Froom, J.D. Maines, D.P. Morgan, E.G.S. Paige, C.P. Sandbank and many others for their co-operation hospitality and illuminating comments.

The project was, in part, sponsored by Standard Telecommunication Laboratories Ltd., Harlow, Essex.

I am indebted to the English Electric Group, and specifically to The Marconi Company Ltd., Chelmsford, Essex, for the award of a research studentship covering the entire period of study.

Finally, I would like to acknowledge the support of my wife during the latter stages of research.

ABSTRACT.

Mechanical properties of the substrate are shown to exert a primary influence on surface wave propagation in vapour deposited Cadmium Sulphide thin film structures. The implications of substrate anisotropy are numerically explored, and it is shown to be an adequate approximation to regard a suitably oriented CdS-on-Sapphire system as mechanically isotropic with respect to waveguide dispersion.

Acoustoelectric coupling dispersion is discussed within an acoustic ray waveguide framework, and it is concluded that no theoretical objection exists to obtaining thin film acoustic surface wave gain rates comparable to those currently obtained in single crystal bulk wave amplifiers.

Thermodynamic stabilization is shown to be prerequisite to the successful operation of high field CdS thin film devices. Available techniques for the suppression of impurity and secondary phase effects are discussed, and a post-evaporation heat treatment procedure, aimed both at compensation of native atom astoichiometries and at drift mobility enhancement through copper recrystallization catalysis is described.

Observations of thin film high field photocurrent saturation, post-threshold localized field redistribution and acoustoelectric bunching-type noise are diagnosed as characterizing inhomogeneous low gain rate surface wave noise amplification processes.

CONTENTS

CHAPTER 3 (contd.)

CHAPTER 1.

BACKGROUND TO THE RESEARCH.

1.1 INTRODUCTION.

Two proposals due to Krömer [1, 2], the first (1958), that certain energy band structural properties giving rise to a negative effective mass might be used to obtain negative resistance effects in semiconducting crystals, and the second (1959), that these effects might be employed in a practical device, (the NEMAG), for amplification and generation, were important in that they caused attention to be drawn to the then virtually unexplored device area of high field, differential negative resistance, bulk effects in solids.

Somewhat earlier, Voigt (1910) [3] had pointed out the contribution of internal electric fields to the elastic stiffness of a piezoelectric medium. The classical theory of wave propagation in piezoelectric media, which served to emphasize this stiffening concept, was developed by Kyame (1949) [4], (and independently by Koga et.al. (1957) [5]) and extended by Meijer et.al.(1953) [6] and Kyame (1954) [7] to cover the case of piezoelectric semiconductors.

In a closely related field, Weinreich (1956) [8], extending investigations by Parmenter (1953) [9] and others, was led to predict that the electronic contribution to acoustic attenuation in a non-piezoelectric conductor could become negative if the electron drift velocity were to exceed the velocity of sound.

In 1960, Nine [10] reported the observation of photosensitive attenuation of

longitudinal and shear ultrasonic waves travelling respectively parallel to and normal to the hexagonal axis of single crytals of Cadmium Sulphide, but failed to consider, as a possible mechanism, piezoacoustoelectric interactions. Shortly afterwards Hutson (1960) [11], investigating an anomalous phonon drag effect observed during thermoelectric power measurements in Zinc Oxide, measured the electromechanical coupling constants of both CdS and ZnO. Extending Kyame's work on wave propagation, he realized that piezoelectric coupling to electrons could cause directionally dependent, relaxation type acoustic dispersion and attenuation, quantitatively similar to that observed by Nine.

Two fundamentally important discoveries emerged from a study, undertaken by Hutson et.al. (1961) [12] of the photosensitive ultrasonic attenuation of CdS as a function of the externally applied field. The first confirmed White's prediction that for electron drift velocities greater than the velocity of sound, the sign of the acoustic attenuation reversed. The second showed, somewhat surprisingly, that even in the absence of an input signal, if a sufficiently long external d.c. drive pulse was applied to the crystal, a growing acoustic flux could be detected by a transducer mounted at the crystal anode.

Shortly after these experiments, following a proposal by A. Rose after careful elimination of the alternative possibilities, Smith (1962) [13] concluded that the current saturation observed to set in approximately 0.1 μ sec after application of a super-critical (>1600 V/cm) voltage pulse to semiconducting CdS and CdSe crystals, could best be attributed to the amplification of non-injected hypersonic waves. Efforts to detect these waves, however, proved unsuccessful. Hutson (1962) [14] proposed that this current saturation should be regarded as a depletion of forward momentum of the electron stream (or as

an electron flow counter to the direction of electron drift) as energy was transferred to the growing acoustic flux in the crystal. Experimental confirmation of this hypothesis was provided, for photosensitive CdS, by Wang (1962) [15] in a series of measurements of acoustoelectric currents and fields as a function of the applied drift field.

Detecting the buildup of acoustic flux in uniform crystals of CdS using a series of transducers mounted successively at the crystal anodes, McFee (1963) [16] obtained strong correlation between current saturation and the build-up of acoustic flux in the system, and provided additional confirmation of White's (1962) [17] theory that in a current saturated condition, the entire crystal could be regarded as a resonant cavity supporting standing coherent sound waves (the loss suffered by the backward wave component reflected from the anode being exceeded by the gain of the forward wave component). Current oscillations observed during decay of the current from its ohmic to its saturated value were attributed initially, and in many cases perhaps correctly, to the building of such an acoustic standing wave system. However, in a sample oriented for longitudinal wave amplification, current saturation was observed to set in at drift fields only one half as large as those required to give longitudinal wave gain. Furthermore, the period of oscillatory decay of the photocurrent from its ohmic value was found to be both field dependent and longer than the round trip transit time.

In several CdS crystals mounted in the conventional coherent wave gain configuration, Kroger et.al. (1963) [18] reported the observation of an acoustic wave propagating with an anomalously low velocity. The same (principal) authors later observed, in apparently uniform samples of CdS, continuous oscillations of period dependent, in addition to the crystal length, upon such

parameters as the temperature, the electron density, and the voltage applied to the crystal - Kroger et.al. (1964) [19]. Both phenomena were interpreted as involving the collective propagation of momentum by the phonon field in acoustically amplifying crystals.

The observations of Smith, McFee and Kroger et.al. triggered, especially in the Japanese schools, a considerable accumulation of data concerning the non-ohmic and oscillatory high field behaviour of piezoelectric semiconducting and semi-insulating crystals. (Local irradiation of the latter was reported by Okada and Matino (1963) [20] to result in undamped coherent photocurrent oscillations (See Chapter 4, section 7)). It gradually became apparent that the inhomogeneous nature of semi-insulating CdS crystals available for acousto-electric high field studies in many cases contributed significantly to the anomalies observed, and the critical evaluation, by progressively refined techniques, of material homogeneity became a regular and essential feature of significant industrial and academic acoustoelectric research reports.

In 1961, Ridley and Watkins (1961) [21] had proposed that bulk negative resistance could be obtained by heating carriers in a high mobility sub-band with an electric field, thereby inducing transfer to a higher energy, lower mobility sub-band. In a second proposal (- 1961 - [22]) they had pointed out that bulk negative resistance could result from an increase in the capture cross section of repulsive centres as a field heated the mobile electron population. Ridley (1963) [23] later showed it to be thermodynamically favourable for layer-like field redistributions to form across the body of any semiconductor biased to within a bulk, N shaped, negative resistance range.

These researches culminated in the observation of high field regions ("domains")

moving through bulk N-type negative resistance samples with velocities, c, characterised by the mechanisms underlying the differential negative resistance * which included:-

(i) for the slow domains (c <1cm/sec) observed in CdS [24], in Au doped Ge [25], in GaAs [26] and in Se [27]; effective field dependent $\Gamma_{\mathrm{A}}^{\mathrm{re}}$combination.

(ii) for the acoustic domains (c ≐ 2 x 10^5cm/sec) observed in GaSb [28], in CdS [29], in GaAs [30] and in Te [31]; high gain rate acousto-electric interaction.

(iii) for the rapid domains (c ≐ 10^7cm/sec) observed in GaAs [32], in InP [33], in GaAsP [34], in InAs [34], in CdTe [35] amd in ZnSe [36]; field induced redistribution of electrons over bands with different effective masses and mobilities.

1.2 ACOUSTOELECTRIC DEVICE FABRICATION.

The design of devices based upon electron-phonon interactions in piezoelectric semiconductors is influenced, to a significant extent, by the technological considerations of material quality, geometrical control and heat dissipation.

Crystals of ZnO, a material superior in many acoustoelectric aspects to CdS, are virtually unobtainable. Commercially available CdS crystals are comparatively expensive (≐ £70/cm cube) and seldom exhibit the high degree of electronic uniformity essential for the unambiguous interpretation of high field experimental results.

---

* Better "negative differential resistivity", since, as was pointed out by Boër (1965), a negative differential resistance could be obscured by the occurence of static layer-like inhomogenities in the specimen.

Sophisticated techniques, including diamond wheel cutting, masked chemical etching, air abrasion, spark erosion and soft lap polishing, have, while time-consuming and expensive, been successfully extended to achieve the required degree of control over the geometry of CdS crystals, which are at once soft and relatively brittle.

The potential application of piezoacoustoelectric effects to acoustic amplification (Hutson et.al. [12] (1961), Zabolotskaya et.al. [37] (1967)) optical scanning, visual display and the synthesis of complex electronic functions by geometrical or electronic field profile shaping (Clemetson [38] (1967), Butler and Sandbank [39] (1967)) is well established. It has been shown to be possible, for example, to show up to twenty separate levels (created by etching or plating) during a domain transit of $\doteq 4\ \mu$ secs through a length of $\doteq$ 8mm. This corresponds to approximately 10^7 bits per second, a rate entirely compatible with present digital systems practice. Unfortunately, a bulk acoustoelectric domain device is not only incompatible with mass production techniques, but is also inherently restricted by thermal considerations to a typical maximum of ten domain transits per second [39].

Vapour evaporation techniques are readily adaptable to mass production. In contrast to bulk crystal machining, control of film geometry may, by masking, be achieved in the fabrication stage. Since thin film components may both rest upon thermally conducting dielectric heat sinks and, if active, operate at power levels considerably lower than equivalent bulk devices, it becomes immediately apparent that thin film, surface acoustic wave, acoustoelectric devices hold many potential advantages over their bulk wave equivalents.

This study has, as its object, exploration of the feasibility of observing

acoustoelectric interactions in vapour-deposited films of CdS, with a view to the eventual exploitation of a family of thin film acoustoelectric devices directly analogous to the family of bulk acoustoelectric devices currently under development.

The study has been divided into two basic areas, viz:-

(i) a study of surface wave propagation in anistropic thin film structures.

(ii) a study of the preparation and high field behaviour of CdS thin films.

These areas are dicussed in turn in the following chapters, and the final chapter is concerned with a review of the progress achieved, together with a delineation of the principal areas for further investigation.

CHAPTER 2.

ULTRASONIC PROPAGATION IN THIN FILMS.

2.1 INTRODUCTION.

Lord Rayleigh [40], extending an earlier analysis by Lamb [41], showed that waves producing retrograde elliptical particle displacements in the sagittal plane could propagate over the plane surface of an isotropic elastic halfspace with a velocity slightly less than that of the familiar transverse body waves. He deduced the nondispersive nature of propagation and found the approximate shape of the displacement ellipse. Oldham [42] subsequently identified as a wave of Rayleigh type the so-called third phase of seismic disturbance. His acute observation that

> "the rate of propagation is, in some way not worked out, a function of the size of the wave"

preceded by over a decade Love's [43] analysis of dispersion in a layered halfspace system, and by a quarter of a century, Stoneley's [44] short note on the importance of the concept of group velocity in the analysis of pulse propagation in dispersive layers. That

> "energy trapping could take place at the surface of separation of two media with similar surface wave velocities, giving rise to an interface wave of Rayleigh type"

was first pointed out by Stoneley [45].

Further advances in the understanding of surface wave propagation over monolayered elastically isotropic halfspaces are reviewed by Ewing, Jardetsky

and Press [46]. Research directed towards the realization of microwave circuit functions using surface waves is currently in progress in Britain under the supervision of E.A. Ash [47].

That certain anomalies in seismological records could be accounted for by continental anisotropy was proposed by Stoneley [48]. Analyses by Synge [49], Buchwald [50, 51], and Buchwald and Davis [52], of Rayleigh-type wave propagation over unlayered anisotropic halfspaces raise important questions concerning the allowable directions and velocities of surface wave propagation with respect to the crystallographic axes, which will be discussed in the following analysis, since the materials of principle interest are elastically anisotropic.

2.2 THE WAVE EQUATION.

In a three dimensional Cartesian coordinate system define the strain tensor as

$$S_{kl} = \frac{1}{2}(u_{k,l} + u_{l,k}) = S_{lk} \qquad (k,l = 1,2,3) \qquad (2.2.1)$$

where $u_{k,l} = \frac{\partial u_k}{\partial x_l}$, u_k representing the displacement of a material point from its mean position, coordinates x_l.

For small strains, Hookes law

$$\sigma_{ij} = c_{ijkl}S_{kl} = \tfrac{1}{2}c_{ijkl}(u_{k,l} + u_{l,k}) \qquad (2.2.2)$$

relates the stress tensor σ_{ij} to the strain tensor, the elastic coefficients, (stiffness constants) forming a tensor of fourth rank (piezoelectric and other effects being disregarded). Thermodynamic arguments, coupled with the criterion of positive definite strain energy, reduce from eighty-one to twenty-one the maximum number of independent elastic coefficients required

to specify completely the elastic behaviour of an ideal elastic medium through the symmetry conditions

$$c_{ijkl} = c_{jikl} = c_{ijlk} = c_{klij} \tag{2.2.3}$$

Equation 2.2.2 may be differentiated with respect to distance to yield, in the absence of body forces, the three relations

$$\frac{\partial \sigma_{ij}}{\partial x_j} = \tfrac{1}{2} c_{ijkl} \frac{\partial}{\partial x_j}\left(\frac{\partial u_k}{\partial x_\ell} + \frac{\partial u_l}{\partial x_k}\right) \tag{2.2.4}$$

$$= \rho \frac{\partial^2 u_i}{\partial t^2}$$

which couple to constitute the well-known wave equation, in which ρ represents the material density.

2.3 PLANE WAVE SOLUTIONS TO THE WAVE EQUATION.

To simplify subsequent analysis* only those particular integrals of 2.2.4 which describe the family of plane waves will be considered. Consider solutions to 2.2.4 of the form

$$u_k = u_k' + iu_k'' = a_k . \exp[i\omega(s_j x_j - t)] \tag{2.3.1}$$

In general, the angular frequency, ω, the amplitude coefficients, a_k, and the slownesses, s_j, may assume complex values. It is convenient here to restrict ω to real values greater than zero. n_j represents unit wave normals (real). Note that $s_j = n_j/v = \frac{k_j}{\omega}$ (where v represents the phase velocity of wave propagation and $\underset{\sim}{k}$ has its usual meaning).

---

* Lighthill's observation [53] "that plane waves are possible (in anisotropic media) only if there is an energy supply transmitting energy parallel to the wavefronts" limits the generality of the following analysis.

Substitution of 2.3.1 into 2.2.4 above gives a set of three homogeneous linear equations which may be written in the form

$$[\rho \delta_{pr} - c_{pqrs} s_q s_s][a_k] = 0 \qquad (2.3.2)$$

where δ_{pr} is the familiar Kronecker delta.

For the a_k to assume nontrivial values it is necessary and sufficient that the s_j should inter-relate to satisfy the equation

$$\det K_{pr} = 0 \qquad (2.3.3)$$

$$(K_{pr} = \rho \delta_{pr} - c_{pqrs} s_q s_s) \qquad (2.3.4)$$

For each set of values s_j satisfying 2.3.3 there exists a corresponding set of three normalised amplitude coefficients

$$d_k = \frac{a_k}{f} \qquad (2.3.5)$$

given by 2.3.2. The constant of normalization, f, is particular to that set, but may otherwise be arbitrarily selected, and in a physical situation might possibly depend on the initial level of excitation of a disturbance.

2.4 WAVE PROPAGATION IN UNBOUNDED ANISOTROPIC MEDIA.

Only concepts believed to be essential to the understanding of the subsequent sections are included. The detailed topology of the phase surfaces introduced is discussed by Lighthill [53], Duff [54] and more briefly by Musgrave [55].

Note firstly, that equations 2.2.2, 2.2.3 may be questioned on theoretical grounds [56, 57], secondly, that the classical theory of elasticity will not

apply for wavelengths comparable with interatomic spacings, and thirdly, that cases may occur where integrals of the wave equation other than those belonging to the family of plane waves are of importance.

Admitting solely real elastic coefficients, Equation 2.3.3 may be expanded to yield a sixth order polynomial in s_1 with real coefficients b_R

$$\sum_{R=0}^{6} b_R s_1^R = 0 \qquad (2.4.1)$$

if a point $P(s_2 s_3)$ is arbitrarily chosen on the real plane $0s_2 0s_3$ (Figure 2.1).

At an arbitrary angle θ to $0s_2$, draw a halfline on this plane through 0, and consider the behaviour of the roots s_1 to 2.4.1 as P is led from the origin along this halfline.

The roots s_1 for P at the origin are in general real and of the form $s_1 = \pm M' ; \pm M'' ; \pm M'''$. As P moves away from 0 the roots change continuously (not necessarily symmetrically) until at some point L two roots coalesce to become complex conjugate. At two further, in general distinct, points $(T_1\ T_2)$ the remaining roots coalesce successively to form a total of three complex conjugate pairs of roots. Should P travel to infinity, the roots will continue to occur in three complex conjugate pairs. Reversing the direction of the halfline results merely in the reversal of the signs of the roots.

Other arbitrary choices of θ lead to the formation of curves in the plane $0s_2 0s_3$ defined by the loci of L T_1 T_2. The plane $0s_2\ 0s_3$ may be rotated with respect to the crystallographic axes, tracing out a surface S in real space time, of the three sheets generated by the curves L T_1 T_2.

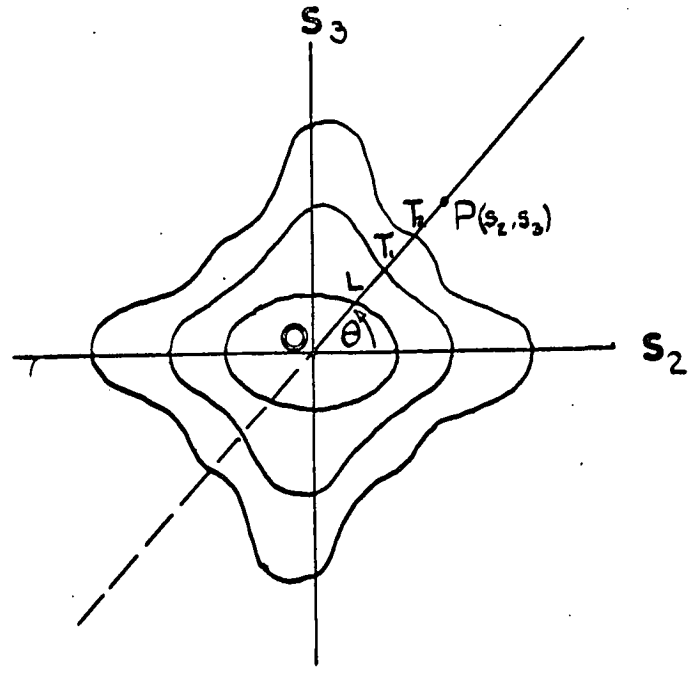

FIGURE 2·1

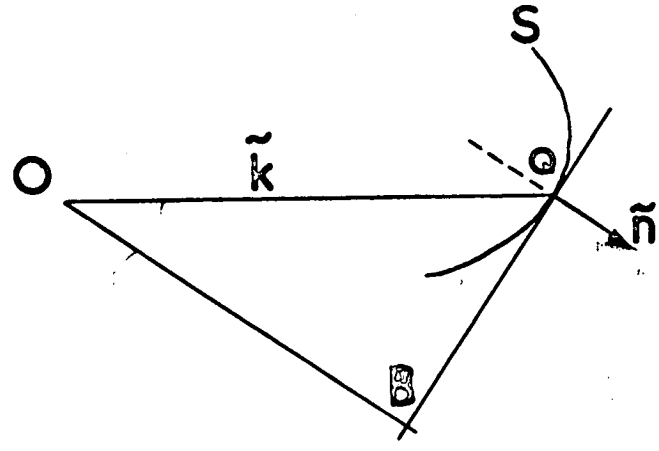

FIGURE 2·2

Setting $\omega = 1$, ($\underset{\sim}{s} = \underset{\sim}{k}$) at each point Q of the curves L T_1 T_2 construct a tangent (Figure 2.2). Then the loci of points B defined by the intersections with these tangents of normals from the origin defines yet another surface W of three sheets in real space time as Os_2 Os_3 is rotated with respect to the crystallographic axes.

If a source of excitation exists at O, the surface W, representing the position at time t = 1 of waves starting from O at t = 0, is known as the wave surface. If Q is a point on the surface **S** , B the corresponding point on the wave surface W, vector $\overline{OQ}$ represents in direction and inverse magnitude the velocity of waves observed at B emanating from O. Consequently, surface S is known as the slowness or reciprocal velocity surface. Vector $\overline{OB}$ represents the group velocity of the wave motion observed at B emanating from O, contributions to which are made by all points Q_i at which the outward normal $\tilde{n}$ is parallel to $\overline{OB}$. Clearly, in Figure 2.2,points O, B and Q are generally collinear only in the degenerate case of isotropy,when all sheets of S, and W reduce to spheres concentric about O.

Real coefficients b_R of the sextic 2.4.1 arise from the restriction of c_{ijkl}, s_2, s_3, to real values. Complex coefficients b_R may represent either an attenuation mechanism, or, in the case of an ideally elastic medium, simultaneous generation of a pair of travelling waves with negative complex conjugate propagation constants. Spatial decrease in amplitude of the standing waves thereby formed need not represent energy dissipation, since standing waves do not represent energy transport [58]. Note that the roots of a sextic with complex coefficients need not occur in complex conjugate pairs, neither need there be an even distribution of positive and negative signs among their imaginary parts.

2.5 WAVE PROPAGATION IN BOUNDED ANISOTROPIC MEDIA.

(page 2-4)

Consider, in Figure 2.3, two parallel sided, homogeneous, infinite anisotropic slabs in a three dimensional Cartesian coordinate system, firmly adherent in the plane $x_1 = -h$, their free faces bound by vacuum in the planes $x_1 = 0$(slab I) $x_1 = -H$(slab II). (Where necessary in the following arguments upper case symbols, equivalent to the lower case symbols defined previously, will be used in the case of slab II, the lower case symbols being retained for slab I).

It is required to examine the restrictions imposed by the boundary conditions of zero normal stress on the faces $x_1 = 0$, $x_1 = -H$; continuity of stress and displacement along the interface $x_1 = -h$; on the coexistence of two wave systems

$$u_p = a_p \exp i\omega(s_j x_j - t) \qquad (a)$$
$$U_p = A_p \exp i\Omega(S_j x_j - t) \qquad (b) \qquad (2.5.1)$$
$$(\Omega = \omega;\ s_1 \neq S_1;\ s_2 = S_2;\ s_3 = S_3)$$

propagating simultaneously in slabs I and II.

Restricting the elastic coefficients to real values, arbitrarily assign s_2 s_3 (real) in equations 2.5.1. Successive substitution of 2.5.1 into the wave equation 2.2.4 gives two sets of three homogeneous linear equations identical in form to 2.3.2. If the amplitude coefficients a_p A_p are to assume nontrivial values, two equations equivalent in form to 2.3.3 must hold, and as s_2 s_3 are assigned, these may be expanded to yield two sixth order polynomials equivalent to 2.4.1 viz:

$$\sum_{R=0}^{6} b_R s_1^R = 0 \qquad (a)$$
$$\sum_{R=0}^{6} B_R S_1^R = 0 \qquad (b) \qquad (2.5.2)$$

which may be solved for s_1 S_1. Given the roots

$$s_1^{(t)} = m^{(t)} \pm in^{(t)} \qquad \text{(a)}$$
$$S_1^{(t)} = M^{(t)} \pm iN^{(t)} \qquad (t,T = 1,2\ldots6) \quad \text{(b)} \qquad (2.5.3)$$

one may, by back substitution obtain the normalised amplitude coefficients corresponding to each root

$$d_k^{(t)} = a_k^{(t)}/f^{(t)} \qquad \text{(a)}$$
$$D_k^{(T)} = A_k^{(T)}/F^{(T)} \qquad \text{(b)} \qquad (2.5.4)$$

Defining $s_2^{(t)} = S_2^{(T)} = s_2$; $s_3^{(t)} = S_3^{(T)} = s_3$; the displacements corresponding to the wave motion are obtained by summation:-

$$u_p = \sum_{t=1}^{6} f^{(t)} d_p^{(t)} \exp[i\omega(s_a^{(t)} x_a - t)]$$
$$U_p = \sum_{T=1}^{6} F^{(T)} D_p^{(T)} \exp[i\omega(S_a^{(T)} x_a - t)] \qquad (2.5.5)$$

The corresponding stresses are

$$\sigma_{ij} = i\omega \sum_{t=1}^{6} c_{ijkl} f^{(t)} d_k^{(t)} s_l^{(t)} \exp[i\omega(s_a^{(t)} x_a - t)]$$
$$\sigma_{ij} = i\omega \sum_{T=1}^{6} C_{ijkl} F^{(T)} D_k^{(T)} S_l^{(T)} \exp[i\omega(S_a^{(T)} x_a - t)] \qquad (2.5.6)$$

Applying boundary conditions, and simplifying,

$$\sigma_{1j}|_{x_1=0} = 0 : c_{1jkl} \sum_{t=1}^{6} d_k^{(t)} s_l^{(t)} f^{(t)} = 0 \qquad \text{(a)}$$

$$u_p|_{x_1=-h} = U_p|_{x_1=-h} : \sum_{t=1}^{6} f^{(t)} d_p^{(t)} \exp[i\omega(-s_1^{(t)} h)]$$
$$- \sum_{T=1}^{6} F^{(T)} D_p^{(T)} \exp[i\omega(-S_1^{(T)} h)] = 0 \qquad \text{(b)}$$

$$\sigma_{ij}|_{x_1=-h} = \sigma_{ij}|_{x_1=-h} : c_{ijkl} \sum_{t=1}^{6} d_k s_l^{(t)} f^{(t)} \exp[i\omega(-s_1^{(t)} h)]$$
$$- C_{ijkl} \sum_{T=1}^{6} D_k^{(T)} S_l^{(T)} F^{(T)} \exp[i\omega(-S_1^{(T)} h)] = 0 \qquad \text{(c)} \qquad (2.5.7)$$

$$\sigma_{1j}|_{x_1=-H} = 0 : C_{1jkl} \sum_{T=1}^{6} D_k^{(T)} S_l^{(T)} F^{(T)} \exp[i\omega(-S_1^{(T)} H)] = 0 \qquad \text{(d)}$$

a set of twelve homogeneous linear equations in the twelve unknowns $f^{(t)}{}_F(T)$ which may be written in matrix form as

$$[A]\,[X] = 0 \qquad (2.5.8)$$

For the coexistence of the two wavesystems 2.5.1 it is necessary and sufficient that nontrivial values $f^{(t)}{}_F(T)$ exist, i.e. that $(s_2, s_3, \omega\ h, H)$ be such that

$$|A| \equiv 0 \qquad (2.5.9)$$

2.6 GENERALIZED RAYLEIGH, STONELEY AND SEZAWA WAVES.

Surface waves may be defined as those waves which, when propagating in a medium with a single or several plane parallel boundaries possess a propagation vector parallel to this or these boundaries. A more convenient definition, due to Rayleigh and adopted for this arguement, defines surface waves to be those waves which, in the case of a semi-infinite medium, cause zero particle displacement at infinite depth.

2.6(a): GENERALIZED RAYLEIGH WAVES.

In the analysis of the bimaterial slab, put $h = +\infty$ (effectively eliminating slab II). In order that u_p may tend to zero as $x \to -\infty$ admit only those roots (2.5.3(a)) of 2.5.2(a) which possess negative imaginary parts.

$$s_1^{(t)} = m^{(t)} - in^{(t)} \qquad (t = 1,2,3) \qquad (2.6.(a).1)$$

Obtain the $d_k^{(t)}$ corresponding to these roots by back substitution. The only relevant boundary condition is that $\sigma_{1j}|_{x_1=0} = 0$.

$$C_{ijkl} \sum_{t=1}^{3} d_k^{(t)} s_\ell^{(t)} f^{(t)} = 0 \qquad (2.6(a).2)$$

For nontrivial $f^{(t)}$ to exist it is necessary and sufficient that

$$\det K_{qt} = 0 \qquad (2.6(a).3)$$

$$K_{qt} = C_{ijrs} d_r^{(t)} s_s^{(t)} \qquad (2.6(a).4)$$

In order that generalized Rayleigh waves should exist in the system, it is necessary and sufficient that 2.6(a).3 be satisfied.

2.6(b): GENERALIZED STONELEY WAVES.

In the analysis of the bimaterial slab, define the interface as $x_1 = 0$, and allow the free boundary planes to extend to $-\infty, +\infty$. In order that u_p may tend to zero as $x \to +\infty$, U_p to zero as $x \to -\infty$, admit only thses three roots (2.5.3(a)) of 2.5.2(a) possessing positive imaginary parts, those three roots (2.5.3(b)) of 2.5.2(b) possessing negative imaginary parts. Evaluate by back substitution the corresponding $d_k^{(t)}$ $D_k^{(T)}$.

The boundary conditions become $u_p|_{x_1 = 0} = U_p|_{x_1 = 0}$; $\sigma_{ij}|_{x_1 = 0} = \sigma_{ij}|_{x_1 = 0}$ giving

$$\sum_{t=1}^{3} f^{(t)} d_p^{(t)} - \sum_{T=1}^{3} F^{(T)} D_p^{(T)} = 0 \qquad \text{(a)} \qquad (2.6(b).1)$$

$$C_{ijkl} \sum_{t=1}^{3} f^{(t)} d_k^{(t)} s_l^{(t)} - C_{ijkl} \sum_{T=1}^{3} F^{(T)} D_k^{(T)} S_l^{(T)} = 0 \qquad \text{(b)}$$

a set of six homogeneous linear equations in six unknowns $f^{(t)}$ $F^{(T)}$.

For generalized Stoneley waves to exist in the system, it is necessary and sufficient that s_2 s_3 be found such that

$$\det L_{ij} = 0 \qquad (ij = 1...6) \qquad (2.6(b).2)$$

where L_{ij} is a 6x6 matrix, the elements of which are given by the coefficients of the unknown $f^{(t)}$ $F^{(T)}$ in 2.6.(b).1.

2.6(c): GENERALIZED SEZAWA WAVES.

In the analysis of the bimaterial slab, put $H = \infty$ and allow U_p to tend to zero as $x_1 \to -\infty$ by admitting only those roots (2.5.3(b)) of 2.5.2(b) which possess negative imaginary parts

$$s_1^{(T)} = M^{(T)} - iN^{(T)} \qquad (T = 1,2,3) \qquad (2.6(c).1)$$

Evaluate by back substitution the D_k d_k corresponding to 2.6(c).1, 2.5.3(a). That $\sigma_{ij\ x = -H} = 0$ is ensured by the initial step in the argument. When the remaining boundary conditions are applied, the following nine homogeneous linear equations in the nine unknowns $f^{(t)}$ $F^{(T)}$ $(t = 1...6 \quad T = 1,2,3)$ are obtained

$$c_{ijkl} \sum_{t=1}^{6} d_k^{(t)} s_\ell^{(t)} f^{(t)} = 0 \qquad (a)$$

$$\sum_{t=1}^{6} f^{(t)} d_p^{(t)} \exp[i\omega(-s_1^{(t)} h)] - \sum_{T=1}^{3} F^{(T)} D_p^{(T)} \exp[i\omega(-s_1^{(T)} h)] = 0 \qquad (b)$$

$$c_{ijkl} \sum_{t=1}^{6} f^{(t)} d_k^{(t)} s_1^{(t)} \exp[i\omega(-s_1^{(t)} h)] - C_{ijkl} \sum_{T=1}^{3} F^{(T)} D_k^{(T)} S_1^{(T)} \exp[i\omega(-S_1 h)] = 0 \qquad (c)$$

(2.6(c).2)

from which the determinantal equation

$$\det M_{ij} = 0 \qquad (2.6(c).3)$$

emerges directly as the characteristic equation governing wave propagation in the system.

2.7 THE PHASE SURFACES FOR BOUNDED MEDIA.

It is required by the adopted definition of a surface wave that displacement tends to zero as distance from the surface of the semi-infinite halfspace tends to infinity. There exists, as a result of this definition, a lower limit to the possible slowness of surface wave propagation, set by the occurrence of real roots to the sextic 2.4.1 within the outer sheet of the slowness surface.

While it may be possible to find directions on the $Os_2\ Os_3$ plane along which real $s_2\ s_3$ values may satisfy the relevant characteristic equation, these directions, at the present state of analysis, must be regarded as discrete. Only in certain cases of elastic symmetry may the characteristic equations be regarded as defining true surface wave slowness curves in real space time, analogous to those defined in Chapter 2, Section 4.

Since roots s_1 to 2.4.1 generally possess, for permissable surface wave velocities, finite real and imaginary parts, surface wave displacement amplitudes will exhibit sinusoidal variation in addition to exponential decay with depth, lie in a plane whose orientation varies with distance from the free surface, and exhibit space dependent eccentricity.

The question of forbidden directions of propagation, discussed most recently by Lim and Farnell [59] is apparently one of surface wave definition. It

would appear that the above analyses cannot be applied to any situation in which the condition, that three and only three of the "halfspace" roots S_1 to 2.4.1 possess negative imaginary parts, fails. If it is necessary, in order to satisfy the boundary conditions, to enter such a situation, the Rayleigh definition of surface wave propagation will be violated, and within this admittedly restrictive definition, one may then consider surface wave propagation to be forbidden.

2.7(a): GENERALIZED RAYLEIGH WAVES.

Generalized Rayleigh waves on ideal elastic media do not, as may be inferred by inspection of 2.6(a).3, exhibit dispersion. As is pointed out by Tseng [60] and by Gazis and Wallis [61], dispersion may however occur for surface wave propagation over unlayered halfspaces for frequency ranges or situations in which the classical analysis (as presented) is inadequate.

The theory of the generalised Rayleigh wave is due largely to Synge [49, 62], Buchwald [50, 51] and Buchwald and Davis [52].

2.7(b): GENERALIZED STONELEY WAVES.

Similarily, classical generalized Stoneley waves show no dispersion. In the degenerate isotropic case the range of existence of these waves is severely limited by the inter-relationship of the elastic properties of the media forming the interface [45, 63, 64]. Consequently, generalized Stoneley waves are to be expected only under highly specialized conditions, which have yet to be extensively studied. Brief mention is made of the generalized Stoneley wave in a study of reflexion and refraction at anisotropic interfaces due to Musgrave [65].

2.7(c): GENERALIZED SEZAWA WAVES.

It follows by inspection from 2.6(c).3 that dispersion in the monolayered halfspace may be normalized with respect to layer thickness h, if ωh is employed as the frequency variable. The equation

$$\det M_{ij} = M(s_2, s_3, \omega h) = 0 \qquad (2.7\,c).1)$$

is then characteristic to such fragments of a surface S in real three dimensional $s_2, s_3, \omega h$ space as may be permitted, by elastic symmetry and the Rayleigh definition of surface wave exponential decay, to exist.

Consider a plane, P, in this space, normal to the plane $\omega h = 0$, passing through the origin O at an arbitrary angle θ to the plane $s_3 = 0$. Assume the elastic symmetry of the system to be such that the surface S is continuous over its range of existence, in $s_2, s_3, \omega h$ space. Then the dispersion of waves with slowness vectors parallel to the intersection of P with $\omega h = 0$ is characterized by the curves of intersection of P with the surface S, general properties of which may be deduced as follows:-

Superimpose, in Figure 2.4, the intersections of the slowness surfaces s_H s_1 for the halfspace and layer with the plane $\omega h = 0$.

(i) A lower limit to surface wave slowness is set, as is described above, by the outer sheet of the slowness curve for the halfspace (T)

(ii) In cases both of zero and infinite layer thickness the analysis of Chapter 2, sections 6(a) and 7(a) is appropriate. In order to retain consistency with this analysis, the slowness of Sezawa wave propagation will be forced in the low and high frequency limits

to the slowness of generalized Rayleigh waves on the substrate and layer respectively.

(iii) The periodicity of the functions $\exp[i(-\omega s_1 h)]\ \exp[i(-\omega S_1 h)]$ implies, at least in certain instances, the existence of an **infinite number of eigenvalues ω h satisfying the characteristic** equation 2.6(c).3 within the range $T_H \rightarrow R_L$ of slowness. In certain cases (e.g. isotropy) the roots s_1 S_1 of Equation 2.5.2 both become purely imaginary outside the outermost slowness curve, T_L, of Figure ~~IV(a)~~ 2.4, the functions $\exp[i(\omega s_1 h)]\ \exp[i(-\omega S_1 h)]$ loose their periodicity, and the existence of an infinite number of eigenvalues of ω h, for a given slowness, can be expected to be curtailed.

Eigenvalues ω h, where they exist, frequently occur in branches over the plane P, coinciding with the curves of intersection of the surface S with the plane P. Each branch characterises a mode of propagation of surface waves in the system.

2.8 WAVE PROPAGATION IN UNBOUNDED PIEZOELECTRIC MEDIA.

The foregoing discussion is based, in the main, upon geometrical arguements in real space time for centrosymmetric anisotropic media. A total of twenty-one of the thirty-two classes to which crystalline media may belong possess no centre of symmetry and, as a result, exhibit piezoelectric effects. The dynamic behaviour of such media is governed by the piezoelectric equations of state [66]

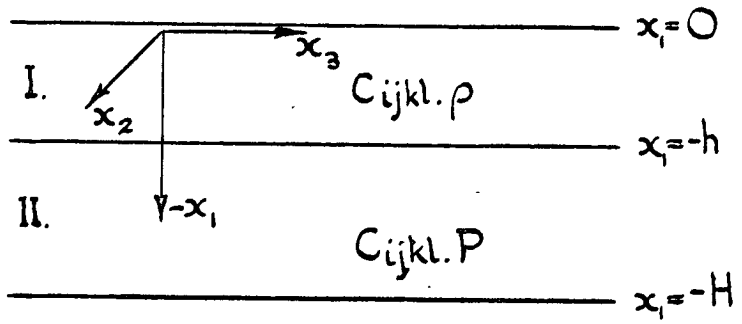

FIGURE 2·3

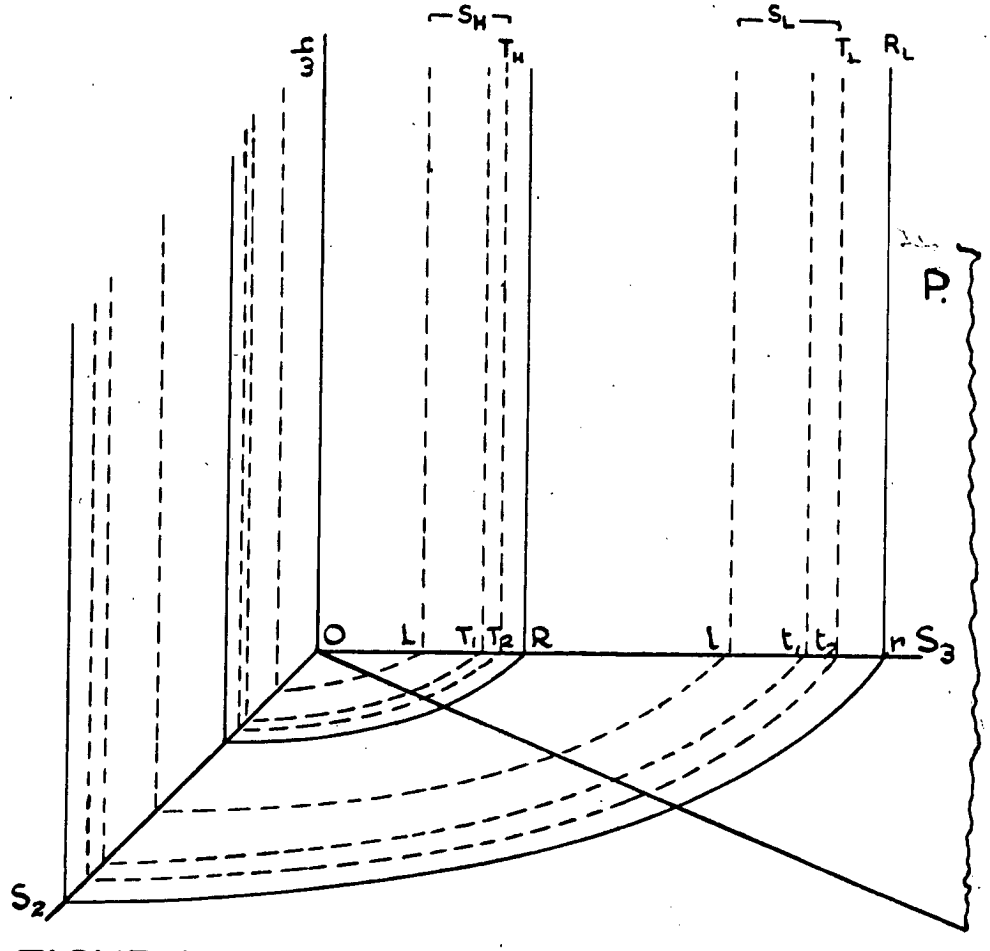

FIGURE 2·4

$$\sigma_{ij} = c^{E}_{ijkl} S_{kl} - e_{ijk} E_K \qquad (a)$$

$$D_i = e_{ijk} S_{jk} + \epsilon^{F}_{ij} E_j \qquad (b) \qquad (2.8.1)$$

coupled with Maxwell's equations.

Substitution of plane wave solutions into the above set of coupled equations yields a set of five linear homogeneous equations. The five-by-five determinant characteristic to these equations is of fifth degree in $(k/\omega)^2$ and may be used to define slowness, velocity and wave surfaces of five sheets in space-time. Two sheets of each surface characterize the well known electromagnetic birefringence, the other three the acoustic trirefringence of the medium under consideration. In general, for a piezoelectric medium, acoustic waves may be visualized as propagating with coupled electric fields, electromagnetic waves as propagating with coupled acoustic vibrations.

The presence of mobile charge in a piezoelectric lattice presents, as was appreciated by Kyame [7], a potential mechanism for acoustic attenuation, and forces dicussion of the phase surfaces into complex space-time.

It will readily be appreciated that any perturbation of the system of equations 2.8.1 is potentially capable of perturbing the dependent phase surfaces. That the effect of carrier drift through a wide bandgap n-type, piezoelectric semiconductor could, under certain conditions, so modify the shape of one or more of the phase surface sheets in complex space-time as to cause the electronic contribution to the attenuation of an ultrasonic wave to become negative was pointed out by D.L. White [17] in a one dimensional analysis * based on Equation 2.8.1.

---

* Mathematical approximations in White's analysis have been shown by Parsons [67] to give rise to certain "anomalies" which do not directly concern this study.

In summary, this well known analysis describes the perturbation of the equilibrium carrier distribution in a piezoelectric semiconductor by a classical, small amplitude plane wave, and, self consistently, shows how the carrier distribution adjusts to the presence of the wave. White's principal assumptions depend for their validity upon true linearity of the basic differential equations of the system, upon mobile carriers being scattered many times per acoustic wavelength, λ, * and upon the bound charge ** equilibrating with the conduction band in a time, t, short compared with the time taken by one wavelength or bunch of acoustoelectrically produced space charge to pass through a given point in the crystal.

Elements of White's theory may perhaps best be explained with reference to the rotating vector diagrams of Figure 2.5. $\underline{J}$ is the alternating current due to perturbation of carriers, $\underline{n}$ is the alternating carrier density, and $\underline{E}$ is the selfconsistent polarization field produced by the strain $\underline{S}$ in the piezoelectric lattice. From conservation of energy arguments it follows that the acoustic power lost to the electrons is given by $\underline{J}.\underline{E} = |J|\,|E| \cos\theta$. Changes in the externally applied field E_{DC} can be shown to cause phase shifts in the system. In particular, the transition $V_d < V_s$ to $V_d > V_s$, (where $V_d = \mu_{elf} E_{DC}$, V_s = velocity of sound) corresponds to a transition of θ from $0 < \theta < \frac{\pi}{2}$ to $\frac{\pi}{2} < \theta < \pi$, causing $\underline{J}.\underline{E}$ to become negative and power to be fed from the drifting electron stream to the acoustic wave.

---

* i.e. that $kl \ll 1$, where $k = \frac{2\pi}{\lambda}$, and l is the electron mean free path (given at room temperature in centimetres by Ioffe's approximation:- $l = 10^{-8}(\frac{m^*}{m_o})^{\frac{1}{2}}\mu$).

** Bound, or trapped, in the sense of not contributing to the d.c. conductivity.

Discussion of acoustoelectric interactions in unbounded systems is resumed in Chapter 4. Further discussion in this, and the following chapter is conducted within White's three principal assumptions (small signal, $kl \ll 1, \omega t \ll 1$).

2.9 ACOUSTOELECTRIC INTERACTIONS IN BOUNDED SYSTEMS.

The considerations of Chapter 2, section 7 may, indirectly, be applied to surface waves propagating over semi-infinite, piezoelectric halfspaces. Displacement is required to tend to zero as distance from the boundary tends to infinity, directions of unattenuated propagation are discrete, and displacements suffer complex exponential decay with depth. However, as in Chapter 2, section 8, the analysis of propagation must be based on the complete set of equations for the system (Equations 2.8.1, coupled with Maxwell's equations plus all the relevant boundary conditions), and must extend into complex space time.

As was axiomatically assumed in the earlier sections of this chapter, particle motions, and accordingly, nontrivial solutions to the equations of motion, are confined to the bounds of the solid. However, the electromagnetic fields associated with particle motions in piezoelectric media are not, and solutions to the coupled set of equations must be sought in the entire space.

The external fields associated with surface waves propagating over piezoelectric halfspaces decay with distance x from the free surface as $\exp[\beta kx]$, where $\beta \doteq (1-(\frac{V_s}{V_L})^2)^{\frac{1}{2}}$, and k is the appropriate propagation constant $(=2\pi/\lambda)$.

---

* V_s is the velocity of surface wave propagation, V_L the velocity of light in free space.

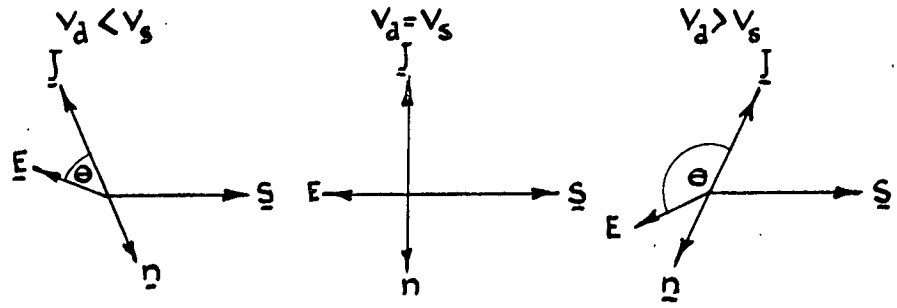

PHASOR DIAGRAMS AE AMPLIFICATION

FIGURE 2·5

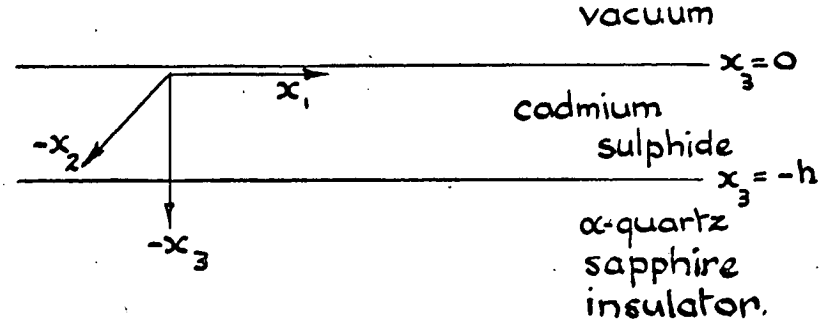

FIGURE 2·6

Thus, while it is in principle feasible to utilize the interaction between surface wave external fields and a free electron beam to obtain amplification of surface waves travelling over a piezoelectric halfspace (the Kaliski amplifier [68]), a severe upper frequency limitation is encountered in attempting to concentrate the beam sufficiently close to the (charging) insulator.

Two variants of the Kaliski surface amplifier were proposed in order to overcome this inherent difficulty. The first, partially realized and analysed, respectively, by Mayo of R.C.A. [69] and Gulyaev et.al. [70], permitted the external field associated with piezoelectric halfspace waves to interact with carriers in a semiconductor located above the halfspace. The second, realized and numerically analysed, respectively, by R.M. White et.al. [71] and Tseng [60], relied upon interaction between surface channeled carriers and the surface wave fields internal to a photosensitive piezoelectric semiconducting halfspace. While a number of "Second-generation" variants of these two bounded acoustoelectric systems have been proposed by Savvinykh et.al. [72], Pustovoit [73], Kaliski [74], Solymar and Ash [75] and others, severe difficulties imposed by the boundary conditions have confined explicit analyses to restricted cases of limited validity.

The acoustoelectric variant of principal interest to this study - a CdS monolayer of finite thickness, h, in firm contact with an effectively semi-infinite insulating halfspace - is shown, schematically, in Figure 2.6.

Suppose, in a manner analogous to the foregoing analysis of generalized Sezawa wave propagation (Chapter 2, sections 6 and 7), the slowness of a postulated surface wave to be arbitrarily assigned in complex space time.

Then its physical existence in the model of Figure 2.6 will depend entirely on its ability to simultaneously satisfy the boundary conditions of stress and displacement continuity at the interface, freedom from normal stress at the surface, and (approximately) continuity of normal electrical displacement and tangential electric field at both surface and interface.

The determinant characteristic to the set of linear equations constructed by combining these boundary conditions with the equations of state and Maxwell's equations (Equations 2.8.1) defines, by anology to Chapter 2, section 7(c), a possibly infinitely degenerate surface in real normalized frequency, complex space time which may, potentially, be perturbed by changes in the parameters defining the system (charge density, carrier drift, mechanical forces). Numerical exploration of this surface is undoubtedly feasible. However, since current channelling, trapping and inhomogeneity effects prevent an experimental approach to any numerically tractable model, and since each surface is particular to the conductivity, mobility, externally applied drift field, and layer thickness of the model, the tedium involved in making such an exploration cannot at present be justified.

The wide conceptual gap between the explicit analyses of acoustoelectric coupling in effectively identical systems due to Kaliski on the one hand and Tseng on the other (low and high frequency limits of the CdS-on-insulator system) may however be bridged by physical arguments.. A numerical framework essential to the formulation of such arguments is presented in the following chapter.

CHAPTER 3.

NUMERICAL STUDIES OF ULTRASONIC PROPAGATION IN THIN FILMS.

3.1 INTRODUCTION.

The first phase and group velocity, shear horizontal (Love), surface wave dispersion characteristics were manually calculated, using four and subsequently seven figure tables, by Jeffreys in 1925. A decade later, having overcome difficulties equivalent to the manual evaluation of shear horizontal characteristics for a triple layered halfspace, the same author published the first known curves for shear vertical (Sezawa) surface wave dispersion over a monolayered halfspace system.[76, 77]

The advent of digital computation facilities led to a relaxation in the difficulties accompanying numerical treatment of elastic boundary value problems. At the present state of the art, it is in principle possible, using sophisticated techniques, to evaluate complete surface wave dispersion characteristics for an infinite number of isotropic layers overlying an isotropic halfspace.

Investigations concerning the influence of the basic structural parameters of an isotropic, monolayered halfspace system on the dispersive characteristics of shear vertical (Sezawa) surface waves, due to Mooney and Bolt [78], are currently being extended at University College, London, by D.P. Morgan and E.A. Ash.

The theoretical work of Synge [49] and Stoneley [48] stimulated a large number of numerical studies of surface wave propagation on crystalline media.

These studies were entirely restricted to the propagation of surface waves over the symmetry planes of media of high elastic symmetry *, and shed little light on the important question of permitted directions of propagation.

The first programme capable of being applied to the study of surface wave propagation in complex space time for an arbitrary choice of symmetry conditions has recently been developed by Lim and Farnell [59, 79]. Their formulation has already yielded information concerning the numerical structure of the anomalously high velocity preudo-surface waves recently discovered on quartz [80] and copper [81], and is currently being extended to the numerical study of anisotropic interface (Stoneley) and monolayered halfspace (Sezawa) waves.

Four significant departures from the classical plane wave treatment of generalized Rayleigh waves should briefly be mentioned. The first, due to Gazis et.al., established a relationship between the permitted directions of surface waves and the bounds of stability of the cubic crystal class.[82] The second, due to Buchwald, avoided the adoption of plane wave solutions altogether by applying Lighthill's Fourier integral method to the problem.[50] The third due to Gazis and Wallis [61], demonstrated high frequency dispersion of generalized Rayleigh-type waves in unlayered cubic crystals by applying relevant boundary conditions to a Born-von Karman lattice model. And finally, the fourth, due (independently) to Kaliski and Tseng, included the joint effects of piezoelectricity and the presence of drifting charge on the attenuation of surface waves travelling in simplified, mechanically non-dispersive systems.[74, 60]

---

* until the pioneering investigations of high symmetry directions of propagation in α-quartz due to Ingebritsen and Tonning (July 1966).[83]

Anderson [84] numerically investigated the dispersion of shear vertical type waves in plates for three solids exhibiting transverse isotropy. Schnitzler of R.C.A. has recently published partial results of the first known numerical analysis of a high symmetry anisotropic monolayered halfspace system (‹001› oriented CdS on the < 001 > and < 011 > faces of Ge). [85]

During the course of this study, partial results of four investigations of surface wave propagation over the principal planes of the only trigonal medium studied to date, α -quartz, were published [59, 83, 86, 87]. Since no numerical information was available concerning surface wave propagation in the anisotropic CdS-on-insulator monolayered halfspace system, the following studies were undertaken.

3.2 SURFACE WAVE DISPERSION IN CdS-ON-"ISOTROPIC" SUBSTRATE SYSTEMS.

In monolayered systems possessing symmetry equal to, or higher than, transverse isotropy (unique axis normal to the free surface), it may be shown that the generalized Sezawa wave decomposes into two uncoupled parts, characterized according to whether particle displacement takes place within (shear vertical, Rayleigh) or normal to (shear horizontal, Love) the sagittal plane. The dispersion of these two uncoupled component parts, may, numerically, be treated separately.

In this section, material anisotropy will be ignored, and fundamental dispersion characterictics determined for a representative selection of CdS monolayered isotropic substrate systems. The elastic parameters for the materials considered are listed in Table 3.1 * (M.K.S. units).

---

* See footnote * on following page.

TABLE 3.1

MATERIAL	LONGIT. WAVE VELOCITY	SHEAR WAVE VELOCITY	RIGIDITY MOD.	RESEMBLES
Layer	4.362×10^3	1.766×10^3	1.504×10^{10}	CdS
Substrate I	11.097×10^3	6.359×10^3	16.118×10^{10}	Sapphire
Substrate II	10.0×10^3	4.85×10^3	6.58×10^{10}	Beryl
Substrate III	7.28×10^3	4.6×10^3	6.63×10^{10}	Apatite
Substrate IV	5.968×10^3	3.764×10^3	3.12×10^{10}	Silica
Substrate V	5.640×10^3	3.280×10^3	2.5×10^{10}	Pyrex
Substrate VI	5.100×10^3	2.840×10^3	1.81×10^{10}	Crown Glass
Substrate VII	3.980×10^3	2.830×10^3	2.18×10^{10}	Flint Glass

3.2(a) SHEAR HORIZONTAL WAVES IN MONOLAYERED ISOTROPIC SYSTEMS.

Simple harmonic, horizontally polarized, plane waves satisfy the monolayered halfspace boundary conditions of zero normal stress at the free surface, stress and displacement continuity at the interface if

$$\tan(\gamma\, kH) = \frac{\mu_2}{\mu_1}\sqrt{\frac{1-\frac{c^2}{\beta_2^2}}{\frac{c^2}{\beta_1^2}-1}} \qquad 3.2(a).1$$

** $\gamma = \frac{c^2}{\beta_1^2} - 1$, k is the propagation constant, H the layer thickness, c the phase velocity of surface wave propagation; μ is

---

* In transversely isotropic systems, the modulus c_{44} resembles the isotropic rigidity modulus for shear vertical surface wave motion, whereas the corresponding modulus for shear horizontal wave motion is $\frac{1}{2}(c_{11} - c_{12})$. A second order inconsistency between the data presented for shear horizontal and shear vertical dispersion in a truely transversely isotropic system may exist

** Reference [46], pages 209-210.

the rigidty modulus and β the velocity of shear wave propagation. The subscripts 1 and 2 refer, respectively, to the monolayer and the halfspace.

No relevant solutions to this equation exist if $\beta_2 < \beta_1$. Real roots kH occur for $\beta_1 < c < \beta_2$. For fixed c, the existance of a multiplicity of roots kH is implied by the repetitive nature of the "tan" function. Varying c over the permitted range $\beta_1 < c < \beta_2$, roots kH occur in an infinity of branches, each branch corresponding to a different mode of propagation in the system. It is easily shown that the different modes correspond to differing numbers of nodal planes within the layer *.

A simple programme for the solution of Equation 3.2(a).1 was written in Atlas Autocode and processed on the Edinburgh Regional Computing Centre KDF9 computer for a CdS layer lying on each of the seven listed substrate materials. Results for the fundamental mode of propagation (no nodal plane) are given, graphically, in Figure 3.1(a).

It should be noted that similar results may be obtained from the nomograms published by Sato [88].

3.2(b) SHEAR VERTICAL WAVES IN MONOLAYERED ISOTROPIC SYSTEMS.

By applying criteria of non-destructive travelling wave interference and total internal reflection to acoustic ray propagation in a monolayered system, Tolstoy and Usdin [89] were able, without formulating the question as a boundary value problem of the wave equation, to derive the following explicit characteristic equation for vertically polarized wave propagation:

---

* Reference [46], pages 209-210.

$$C\Lambda = \cos\left[(r + s)\,H - \epsilon\right] - AT\cos\left[(r-s)\,H - \bar{\epsilon}\right] \qquad (3.2(b).1)$$

A, C are the longitudinal-longitudinal and shear-longitudinal free surface reflection coefficients; $T\,\Lambda$ are moduli of the longitudinal-longitudinal and longitudinal-shear interface reflection coefficients; $-(\bar{\epsilon} + \epsilon)$, $-\epsilon$ are the corresponding changes in phase suffered upon total reflection from the interface, $r = k(\frac{c^2}{\alpha_1^2} - 1)^{\frac{1}{2}}$ and $s = k(\frac{c^2}{\beta_1^2} - 1)^{\frac{1}{2}}$. k, c, H and β_1 are defined as in Equation 3.2(a).1. α_1 is the velocity of bulk longitudinal wave propagation in the layer.

A short programme for the location of roots to this equation in the c - kH plane was evaluated on the Glasgow University KDF9 computer. It emerged that the programme was competent for root seeking only in the range $\beta_2 > c > \alpha_1$. (For $c < \alpha_1$, r becomes imaginary, corresponding to the fact that longitudinal waves in the layer cannot have phase velocities less than α_1).

Access to a complementary programme, written by Hadi [90], based on an isotropic boundary value formulation, and competent for root seeking only in the range $c < \alpha_1$, was kindly provided by Professor E.A. Ash, and a complete picture of dispersion in monolayered halfspace systems emerged.

Hadi's programme was subsequently upgraded by D.P. Morgan and again kindly made available. Complete correspondence between the independent numerical computations of Morgan and Mooney and Bolt [78] made an upgrading of the Tolstoy KDF9 programme unnecessary.

Shear vertical fundamental dispersion curves for an isotropic CdS layer firmly adhering to each of the seven listed substrate materials are given in Figure 3.1(b). Phase and group velocity dispersion curves for two cases of particular

interest (CdS-on-Sapphire, CdS-on-Silica) are given in Figures 3.2 and 3.3. An approximate surface particle amplitude ratio curve for the fundamental mode in CdS-on-Sapphire, interpolated from data published by Mooney and Bolt [78] is given in Figure 3.3. For detailed interpretation of this curve, the reader is referred both to the original reference and to the discussion in section 7 of this chapter.

3.3 DISCUSSION.

Note, in Figure 3.1, firstly that systems are strongly dispersive (fundamental mode) for wavelengths comparable with the layer thickness, and secondly, that dispersion of the fundamental shear vertical (shear horizontal) mode takes place between the Rayleigh (bulk shear wave) velocities of substrate and layer.

In the case of the higher modes, both shear vertical and shear horizontal curves exhibit a low frequency cut-off at a phase velocity equal to the velocity of transverse waves in the substrate. This cut-off effect may be traced through Figure 2.4 to the occurence of real roots to the sextic polynomial 2.4.1 for $c>\beta_2$ forbidding, within the adopted definition of a surface wave, exponential decay of displacement with depth. Attempted higher mode excitation with a sub-cut-off frequency will probably, within a few wavelengths, result in energy conversion into halfspace bulk and lower order mode surface waves. Under normal circumstances no high frequency cut-off is experienced, the higher mode phase velocities tending to the propagation velocity of shear waves in the layer.

These observations are in accordance with the established results of Mooney and Bolt [78] and others. Note however that they pertain only to the degenerate

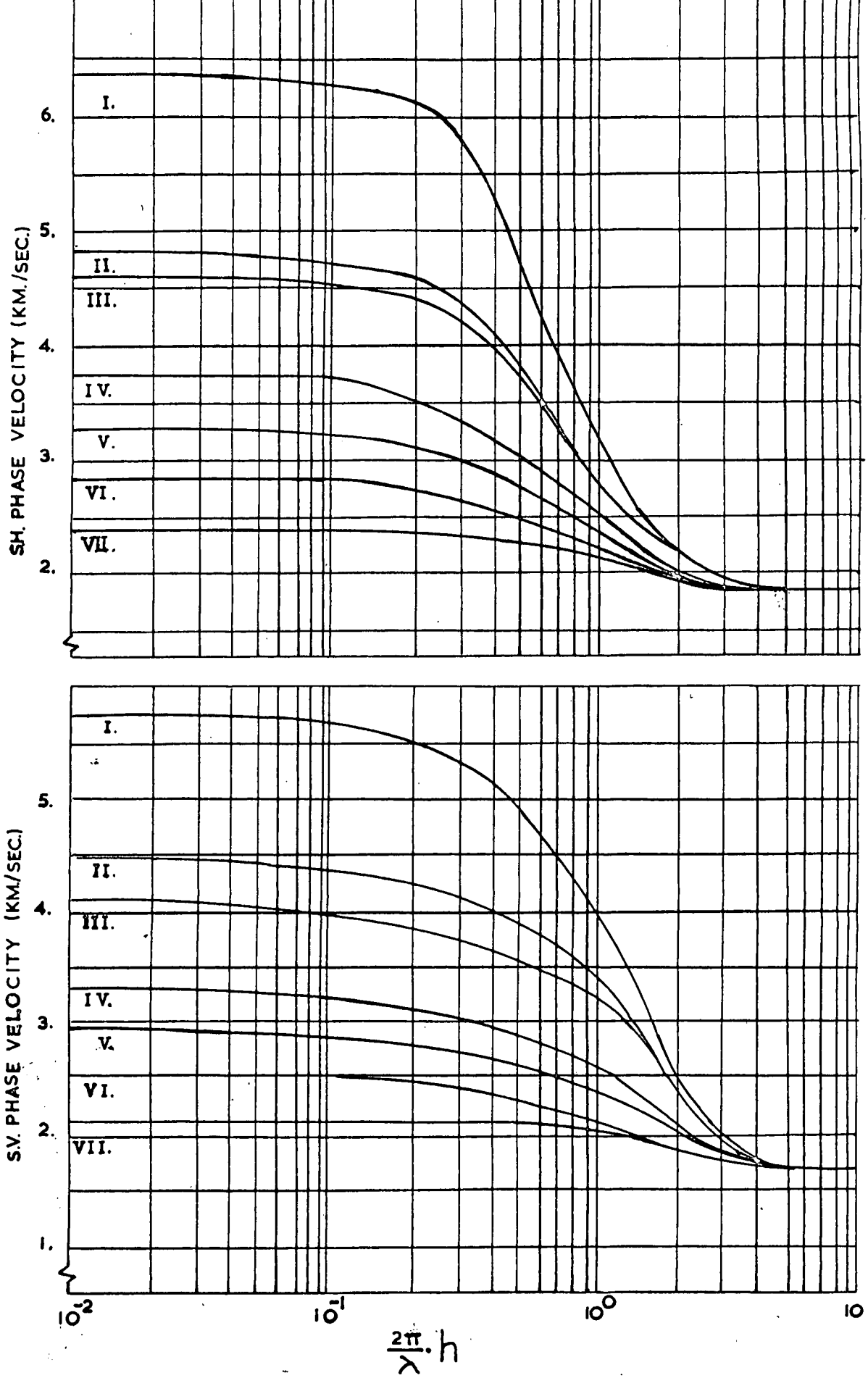
SH. PHASE VELOCITY (KM./SEC.)
6.
5.
4.
3.
2.
I.
II.
III.
IV.
V.
VI.
VII.
SV. PHASE VELOCITY (KM/SEC.)
5.
4.
3.
2.
1.
I.
II.
III.
IV.
V.
VI.
VII.
10^{-2}
10^{-1}
10^{0}
10^{1}
$\frac{2\pi}{\lambda} \cdot h$

FIGURE 3.1

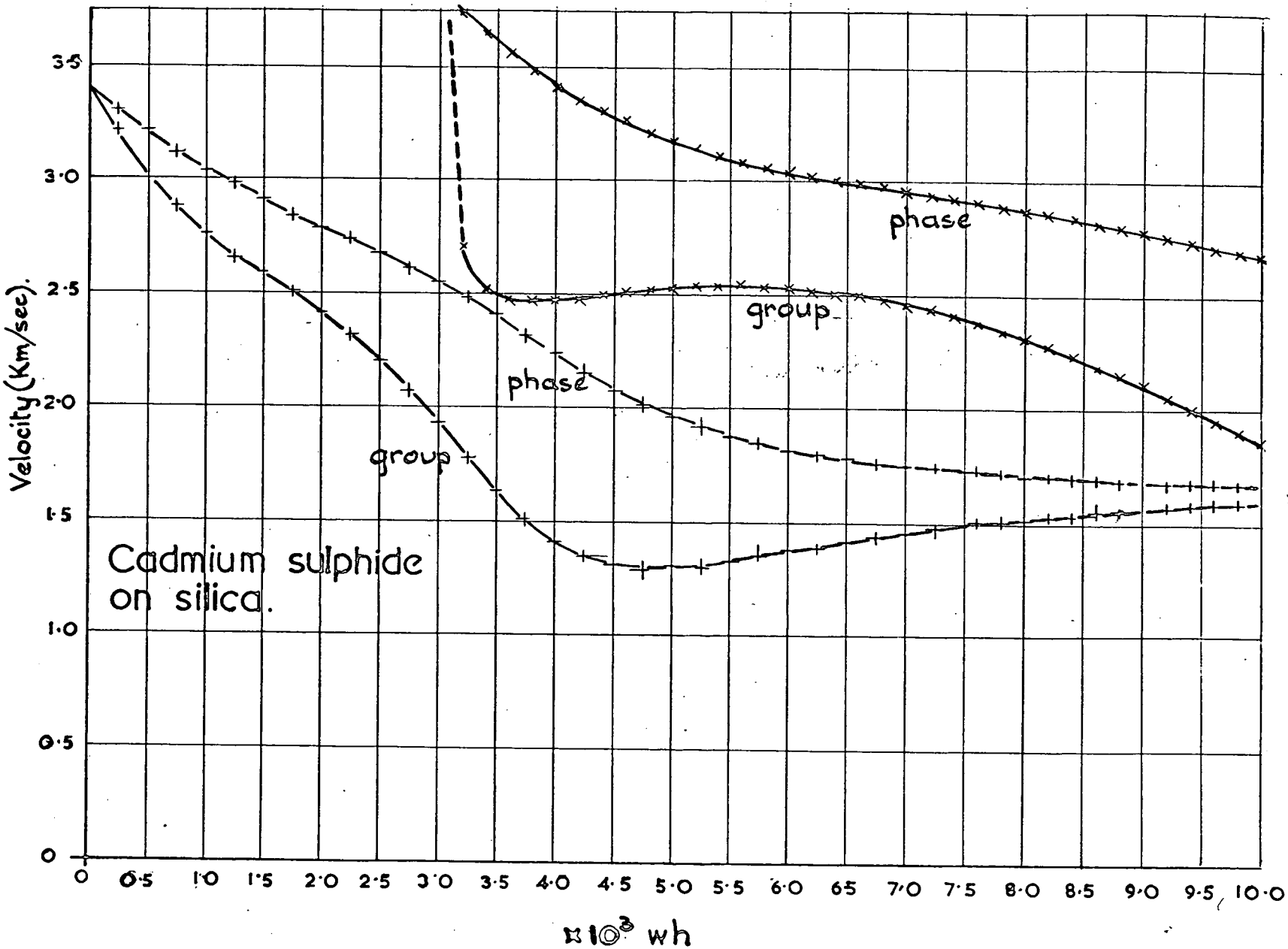
Velocity (Km/sec).
3·5
3·0
2·5
2·0
1·5
1·0
0·5
0
0 0·5 1·0 1·5 2·0 2·5 3·0 3·5 4·0 4·5 5·0 5·5 6·0 6·5 7·0 7·5 8·0 8·5 9·0 9·5 10·0
× 10³ wh
phase
group
phase
group
Cadmium sulphide
on silica.

FIGURE 3·2A

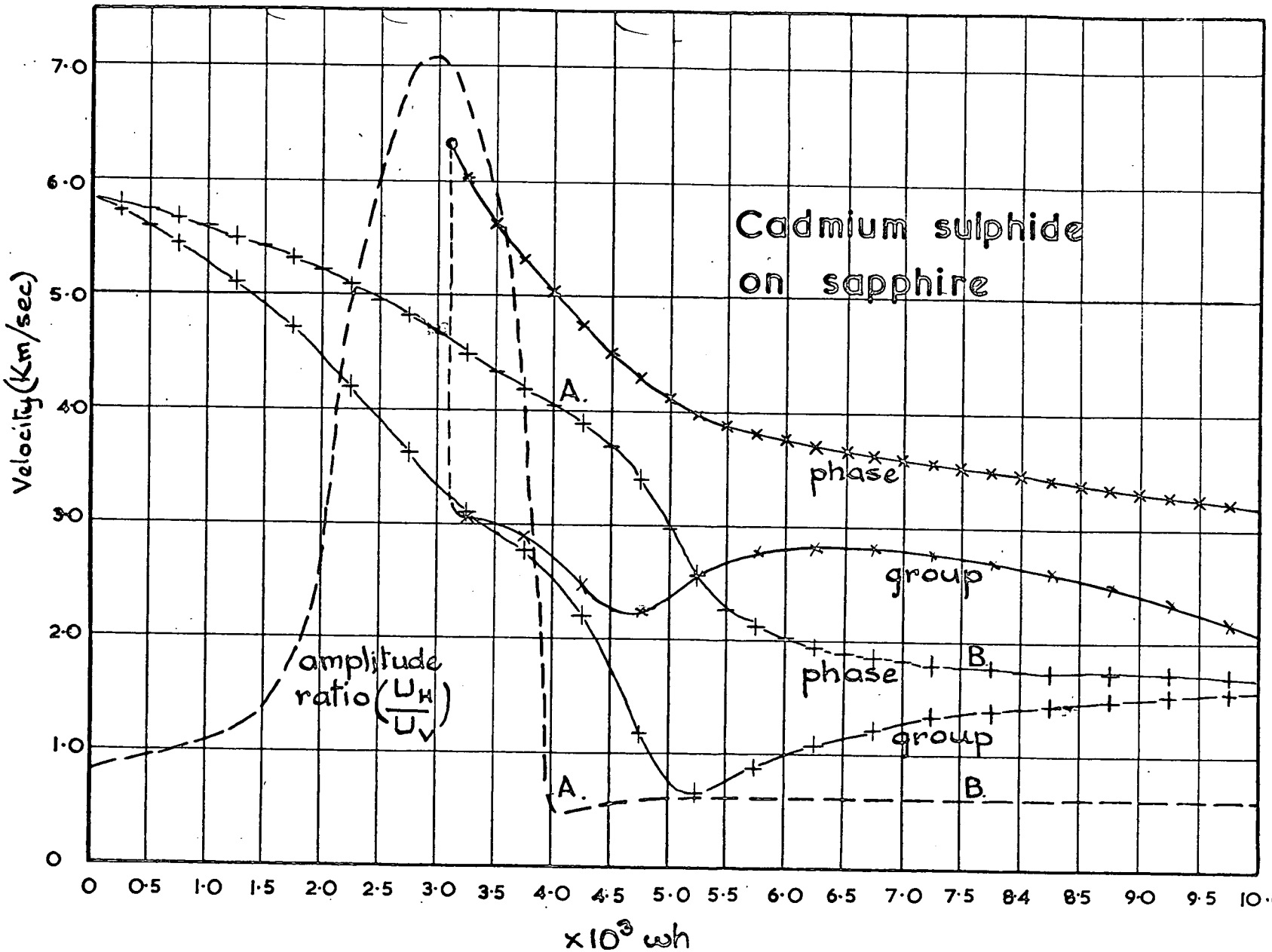
Cadmium sulphide
on sapphire
phase
group
phase
group
A.
A.
B.
B.
amplitude
ratio $\left(\frac{U_H}{U_V}\right)$
Velocity (Km/sec)
7·0
6·0
5·0
4·0
3·0
2·0
1·0
0
0 0·5 1·0 1·5 2·0 2·5 3·0 3·5 4·0 4·5 5·0 5·5 6·0 6·5 7·0 7·5 8·4 8·5 9·0 9·5 10·0
$\times 10^3$ ωh

FIGURE 3.2B

isotropic case. No account has been taken of the anisotropy inherent in crystalline media which may, within the adopted requirement of exponential decay with depth, threaten the very existence of surface waves in the system.

Effects which might be overlooked in directly applying conclusions derived from a study of the "equivalent isotropic" monolayered system to an anisotropic layer overlying an anisotropic halfspace are listed below:-

(i) For propagation parallel to forbidden * directions of either layer or halfspace generalized Rayleigh wave propagation "anomalous" cut-offs may be experienced. Schnitzler's analysis [85] of the <001> CdS layered <001> and <011> faces of Ge provides an interesting example of this predicted phenomenon.

(ii) Dissociation of Love and Rayleigh components of the generalized Sezawa wave may occur with changes in frequency.

(iii) Higher modes may be considerably modified. In particular, notice that roots s_1, to Equation 2.2.4 possess in general finite real and imaginary parts outside the outer ~~substrate~~ film bulk slowness sheet. The periodicity of the function $\exp[i(-\omega s_1 h)]$ in Equations 2.6(c).3 will persist in this region, and the higher modes will no longer necessarily tend at high frequencies to the shear wave velocity of the layer.

(iv) The energy propagation vector is not in general colinear with the surface wave velocity vector. Since dispersion is concerned with a frequency dependent transition of the "centre of gravity" of

---

* The precise physical meaning of a forbidden direction is currently a matter for debate. See Chapter 2, section 6, and the analyses of Lim and Farnell [59].

energy from substrate to layer, or vice versa, a situation is accessable in which the direction of energy propagation may be frequency dependent.

(v) Pseudo-surface wave dispersion may well occur in an anisotropic monolayered halfspace system.

If isotropically derived dispersion ourves are to be applied with any confidence to an experimental system employing an anisotropic material as substrate (e.g. CdS-on-Sapphire), it is mandatory so to orient the crystal cut as to permit quasi-isotropic surface wave propagation over the halfspace.

3.4 NUMERICAL ANALYSIS OF ANISOTROPIC SURFACE WAVE PROPAGATION.

The analytical sequence set out in Chapter 2, section 5 was applied directly to the numerical analysis of surface wave propagation over the unlayered principal planes of sapphire and α-quartz. The programme employed was designed on a modular basis capable of extension to the analysis of any plane wave variant of the general anisotropic plate problem. Since the analytical sequence in Chapter 2, section 5 is selfexplanatory, no flow diagram will be given. The following remarks are confined to the general structure of the routines.

Zeros of a high degree polynomial such as Equation 2.4.1 are notoriously sensitive to slight changes in the coefficients b_R. Analogue methods of coefficient evaluation (e.g. Lagrangian interpolation) are consequently of little use, and brute force Cramer expansion of the wave equation determinant must be resorted to. The resulting ten digit coefficient accuracy did not, in the cases examined, give rise to apparently rounding errors in the remainder of the

programme. It should, in this context, be pointed out that pathological cases might arise in which the phase surfaces are so sensitive to small changes in the input data (i.e. elastic coefficients and material density) as to be poorly defined by the accuracy of currently available experimental techniques. Any attempt at precise numerical analysis of such pathological surfaces should take this factor, in general outside the control of the analyst, into account.

In the cases examined, Bairstow's process was found to rapidly converge onto the zeros of the sextic characteristic polynomial 2.4.1. In cases where 2.4.1 assumed a bicubic form, Tartaglia's method was adopted in order to avoid rounding errors accumulating from the successive use of Bairstow's process and an approximate complex number square root finding routine.

A rough search and plot routine at fixed intervals of slowness was used to locate changes of sign in the real and imaginary parts of the determinant characteristic to unlayered halfspace propagation (Equation 2.6(a).3) A "false root" pivotal condensation technique, which may best be described graphically (Figure 3.3), then rapidly converged onto the required root.

Programming was severely hampered by the absence of complex number facilities in the available compiler. It was found to be valid to regard the 001 plane of sapphire as effectively elastically isotropic with respect to surface wave propagation. The predicted "anomalies" in Sezawa wave dispersion introduced by system anisotropy were accordingly deemed to be of secondary interest to the experimental investigation, and analysis of the anisotropic monolayered halfspace,* was not pursued at any length.

---

* impeded by unreliable evaluation of the required nine-by-nine complex determinant.

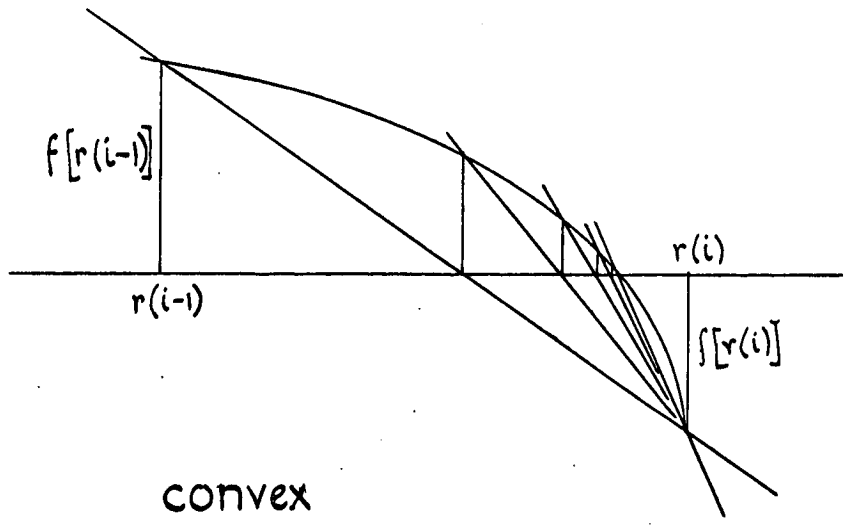

convex

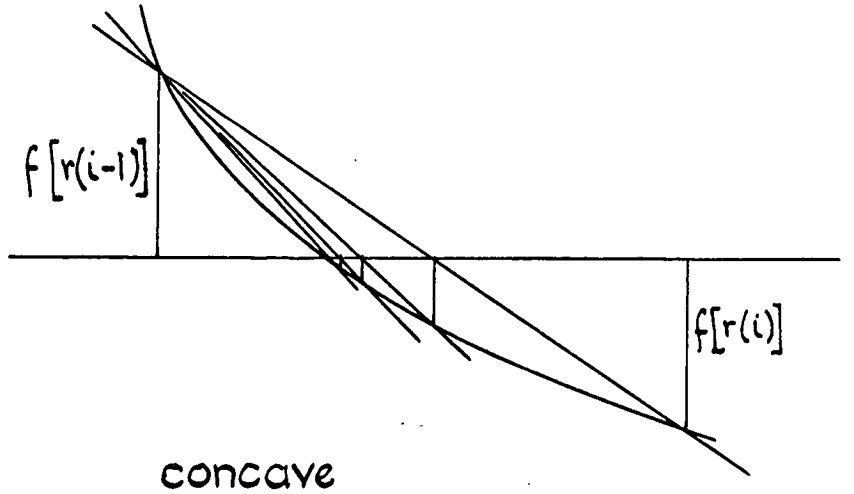

concave

FIGURE 3.3

3.5 SURFACE WAVE PROPAGATION OVER THE PRINCIPAL PLANES OF QUARTZ AND SAPPHIRE.*

For clarity of presentation, only selected sections of the curves of intersection of generalized Rayleigh wave slowness cylinders with the principal planes of quartz and sapphire are plotted. (Figures 3.4, 3.5 and 3.6). Complete curves of intersection may be obtained from these plots by appealing to the elastic symmetry of the trigonal crystal system.

Curves for propagation over the ‹001› plane of both quartz and sapphire are in substantial agreement with the results of Lim and Farnell**. The curve for propagation over the ‹010› plane of quartz is also confirmed by the results of these workers. Experimental verification of the curve for propagation over the ‹100› plane of quartz is provided, in part, by Verevkina et.al. [87] Numerical results for propagation over the ‹100› and ‹010› planes of sapphire, and for propagation over the ‹100› plane of quartz have been communicated, for verification, to Lim and Farnell.

The question of "forbidden" directions of propagation is of direct concern to this study only in so far as it affects surface wave acoustoelectric interactions in vapour deposited CdS thin films. Such directions (numerically characterized by the apparent absence of zeros to the characteristic determinant (2.6(a).3) outside the outer bulk wave slowness sheet) have been shown by Lim and Farnell to be associated with deep, and even infinite penetration of surface wave energy into the halfspace. Since no difficulties were experienced in root seeking on the crystallographic plane of principal experimental interest

---

* Input parameters were obtained from data published in [91] and [167]

** Personal communication.

(<001> plane of sapphire), the numerical structure of surface wave propagation along such forbidden directions as were located,* was not pursued at length.

3.7 SURFACE WAVE ACOUSTOELECTRIC COUPLING.

3.7.1 SYSTEM SPECIFICATION.

In an experimental situation the boundary conditions and the contiuum theory of elasticity, on which the foregoing analyses were based, become open to question, on grounds of surface roughness and crystallite agglomeration, for film thicknesses less the 1000 Å and for frequencies greater than 10^{11} rad./sec. Subsequent discussion must, accordingly, be confined within these limits.

A rigorous general discussion of bounded acoustoelectric interactions, applicable to all possible substrate variants of the CdS-on-Substrate system, is attended by severe analytical, numerical and experimental difficulties. Since the only variant of direct concern is that which optimizes thermal dissipation and the probability of growing high mobility CdS thin films, the physical properties of the seven representative substrates (Chapter 3, section 2) should be considered in some detail.

Silica and α quartz possess coefficients of expansion incompatible with CdS, and are therefore liable, during the thermal treatments involved in the growth of high mobility films, to perturb both the interfacial boundary conditions

---

* E.g. along the Y axis on the <001> plane of α quartz, at 30° to the positive Z axis on the <100> plane of α quartz, and along the X axis on <010> planes of both α quartz and sapphire.

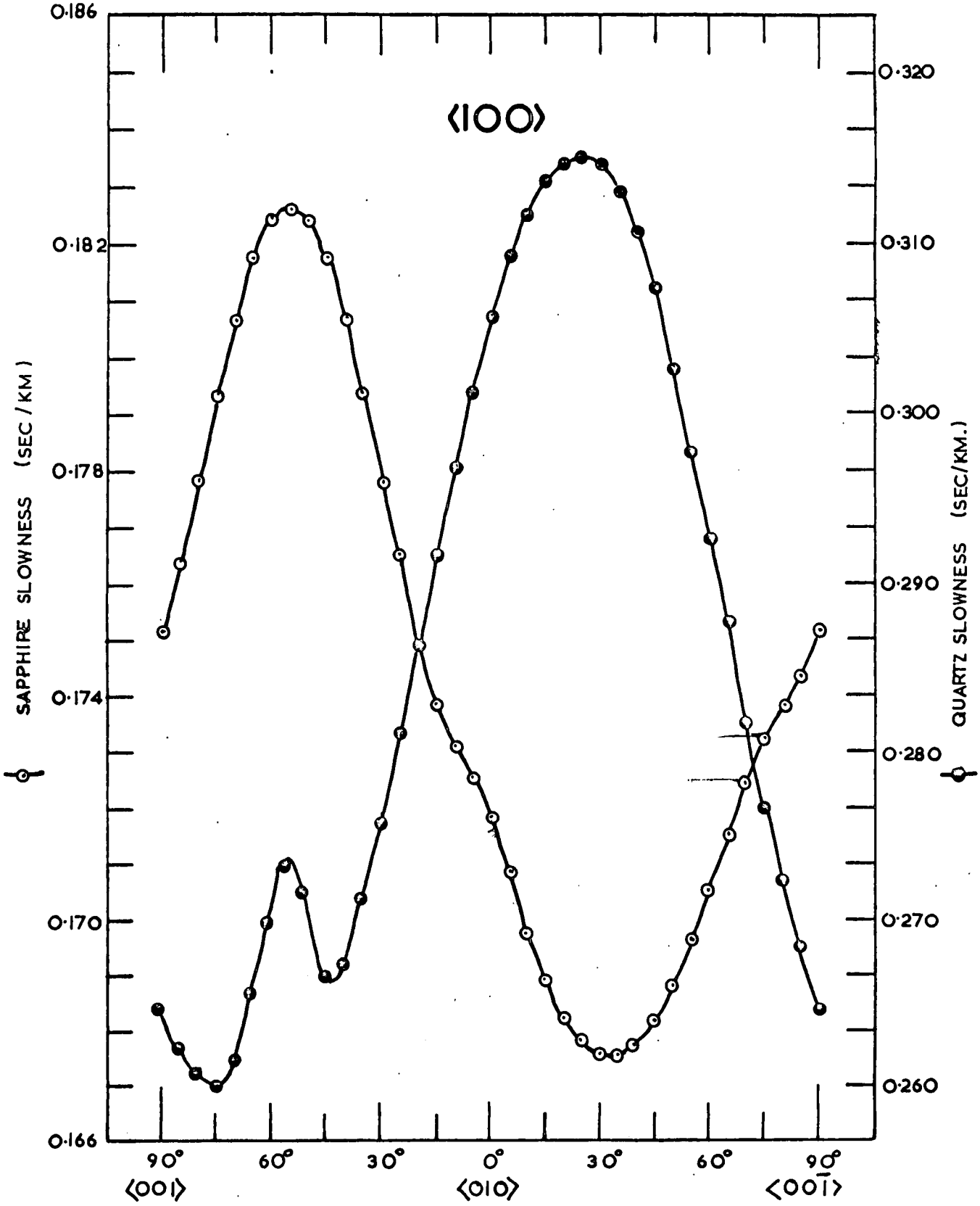
⟨100⟩
0·186
0·182
0·178
0·174
0·170
0·166
SAPPHIRE SLOWNESS (SEC/KM)
0·320
0·310
0·300
0·290
0·280
0·270
0·260
QUARTZ SLOWNESS (SEC/KM.)
90°
60°
30°
0°
30°
60°
90°
⟨001⟩
⟨010⟩
⟨00$\bar{1}$⟩

FIGURE 3·4

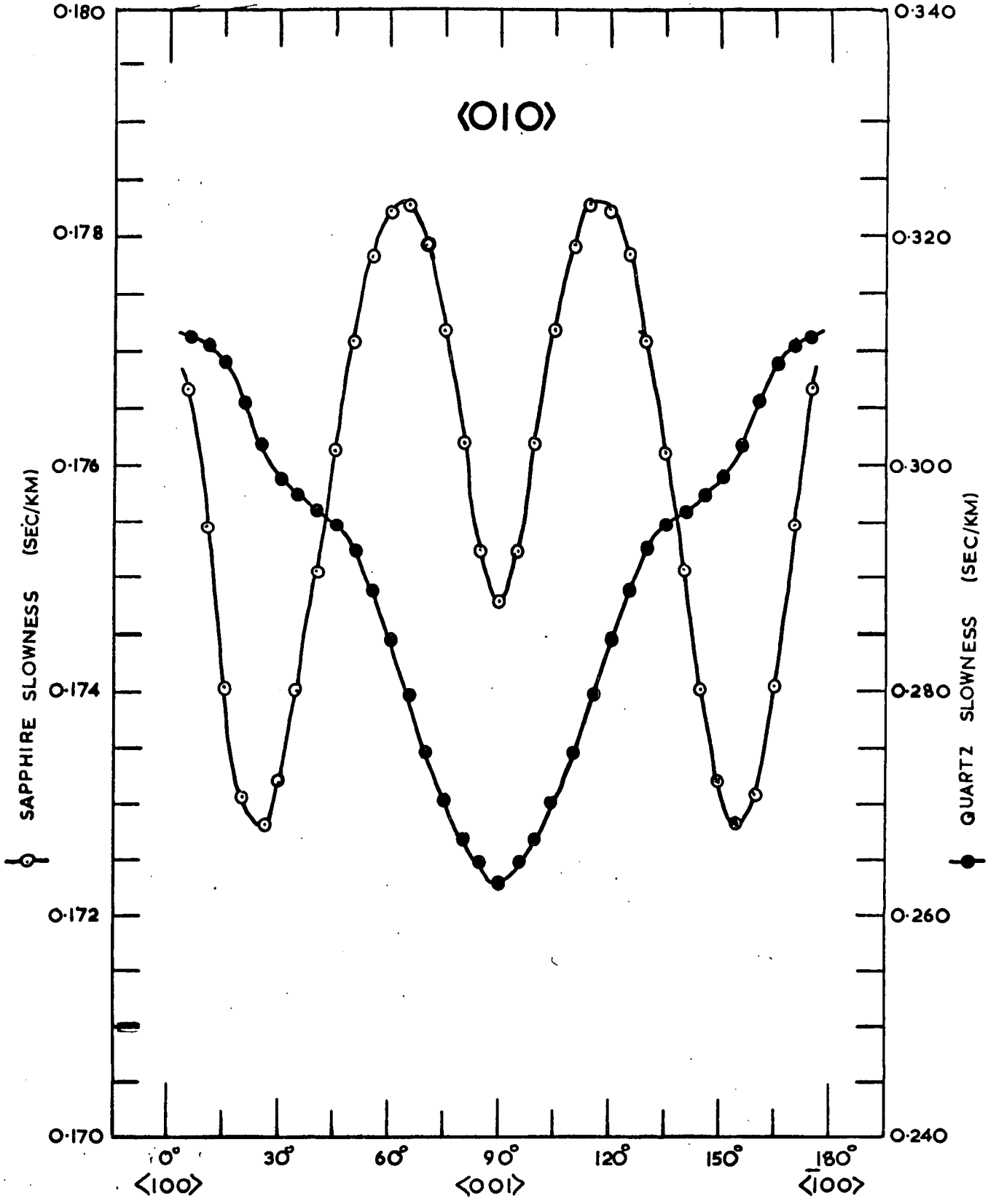
⟨010⟩
0·180
0·178
0·176
0·174
0·172
0·170
SAPPHIRE SLOWNESS (SEC/KM)
0·340
0·320
0·300
0·280
0·260
0·240
QUARTZ SLOWNESS (SEC/KM)
0°
30°
60°
90°
120°
150°
180°
⟨100⟩
⟨001⟩
⟨$\bar{1}$00⟩

FIGURE 3·5

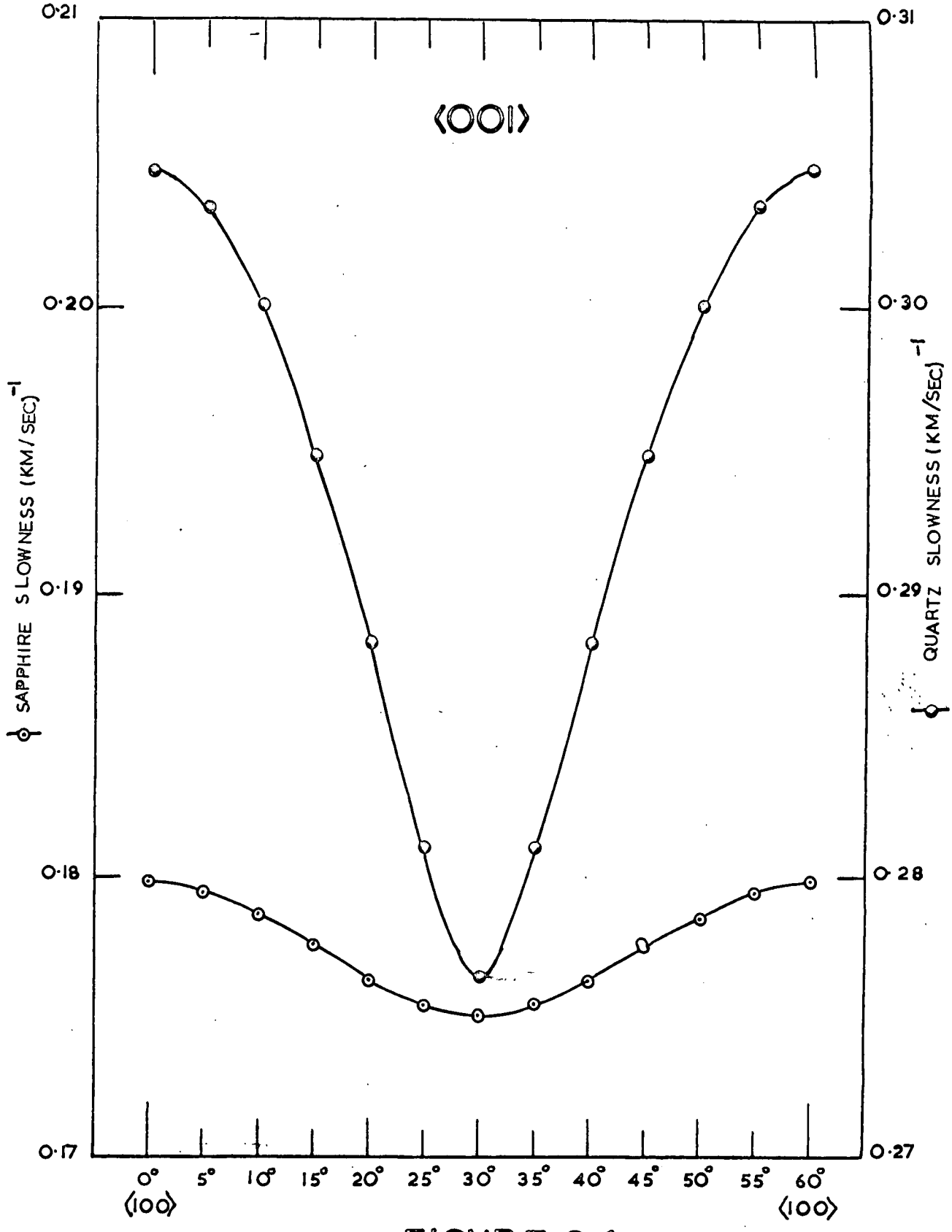
⟨001⟩
0·21
0·20
0·19
0·18
0·17
0·31
0·30
0·29
0·28
0·27
SAPPHIRE SLOWNESS (KM/SEC)⁻¹
QUARTZ SLOWNESS (KM/SEC)⁻¹
0°
5°
10°
15°
20°
25°
30°
35°
40°
45°
50°
55°
60°
⟨100⟩
⟨100⟩

FIGURE 3.6

and the assumption of zero body forces. Films grown on these two materials are, in addition, liable to seek a minimum energy configuration through the creation of electronically important structural defects. The external fields associated with surface waves in α quartz offer potential surface wave electromechanical coupling advantages which must however be weighed against poor thermal conductivity and the hazards associated with surface wave anisotropy.

The chemical and mechanical stability of the three glasses (pyrex, crown and flint) cannot be guaranteed at post-evaporation heat treatment temperatures in excess of 600°C (Chapter 5, section 5). Since glasses are amorphous, the possibility of epitaxial CdS thin film growth does not exist. Finally, the linear expansion coefficient match between CdS and pyrex must be weighed against the relatively poor thermal conductivity of the latter.

Beryl and apatite are not readily available in substrate form and, accordingly, need not be considered further.

The properties of sapphire deserve detailed consideration. A chemically stable, extremely hard, high dielectric strength material, sapphire shows low absorption with respect to GHz ultrasonic bulk waves, is readily available in synthetic form, and may be polished to the tolerances necessary for the boundary conditions (Chapter 2, section 5) to hold over the frequency range of interest. It combines a relatively high thermal conductivity with a coefficient of expansion closely matched to that of CdS. The < 001 > plane is both practically isotropic for surface wave propagation and well suited to the < 001 > epitaxial deposition of CdS monolayers, the system thereby formed combining approximate transverse isotropy with a high degree of surface wave

dispersion. Synthetic sapphire therefore forms an ideal substrate medium for acoustoelectric studies in CdS thin films.

The variant of CdS-on-<001> oriented sapphire is accordingly adopted for discussion in the following subsections.

3.7.2 PIEZOELECTRIC ACTIVITY OF SURFACE WAVES IN CdS-ON-SAPPHIRE.

The wurtzite (hexagonal CdS) structure consists of two interpenetrating close-packed hexagonal lattices, one of Cd (shaded) atoms and the other of S (unshaded) atoms. In the unstrained state each Cd(S) atom lies at the centre of a regular tetrahedron of S(Cd) atoms, charges associated with the two hexagonal lattices are fully compensated, and the structure possesses no dipole moment. The piezoelectric activity of the material may be visualized as originating in mechanical separation of the centres of positive and negative charge (Figure 3.7A) Components of the piezoelectric polarization vector (P_1, P_2, P_3) are related to the strain tensor through the second equation of state 2.8.1.

$$\begin{aligned} P_1 &= e_{15} S_{13} \\ P_2 &= e_{15} S_{23} \\ P_3 &= e_{31} S_{11} + e_{31} S_{22} + e_{33} S_{33} \end{aligned} \qquad (3.7.2.1)$$

Vapour deposited CdS crystallites tend (see Chapter 5, section 6) to possess a unique, one degree, "c" axis orientation normal to the plane of even an amorphous substrate. By direct substitution of the CdS piezoelectric constant matrix into the system of transformation equations given by Cady [91], it may readily be shown that the piezoelectric properties of the film as a whole are unimpaired by random crystallite rotations about the "c" axis.

The principal source of acoustoelectric coupling in CdS lies in the piezoelectric polarization fields associated with lattice strain, which, in effect, modulate the carrier population to produce moving enhancement ("-") and depletion regions ("+"). For bulk wave propagation through CdS it is evident that the carrier drift will be seriously perturbed only by those strain waves which cause polarization in a direction coincident with the direction of propagation (Figure 3.7B after McFee [92]). Once a transverse field system has been set up in the crystal, small depletion regions at the widely separated boundaries will play no significant part in transport through the crystal (Figure 3.7C). For convenience, bulk strain waves producing longitudinal and transverse piezoelectric polarization fields have, respectively, been designated as piezoelectrically active and inactive.

Notice, in contrast to the bulk case, that over the dispersive frequency range, the plane boundaries of a thin film are not widely separated (Figures 3.7D and 3.7E). Depletion and enhancement regions produced by transverse piezoelectric polarization fields may conceivably occupy a substantial proportion of the total film thickness and may therefore play a significant part in transport along the film. The distinction usually drawn between active and inactive bulk waves has, therefore, no direct analogy in a thin film situation.*

3.7.3 "TRANSVERSELY ISOTROPIC" CdS-ON-SAPPHIRE (LOW AND HIGH FREQUENCY LIMITS).

In the normalized high frequency limit, the acoustoelectric coupling problem

---

* The acoustoelectric inactivity of shear horizontal (Love) waves in the system under consideration stems from the total absence of associated piezoelectric polarization fields.

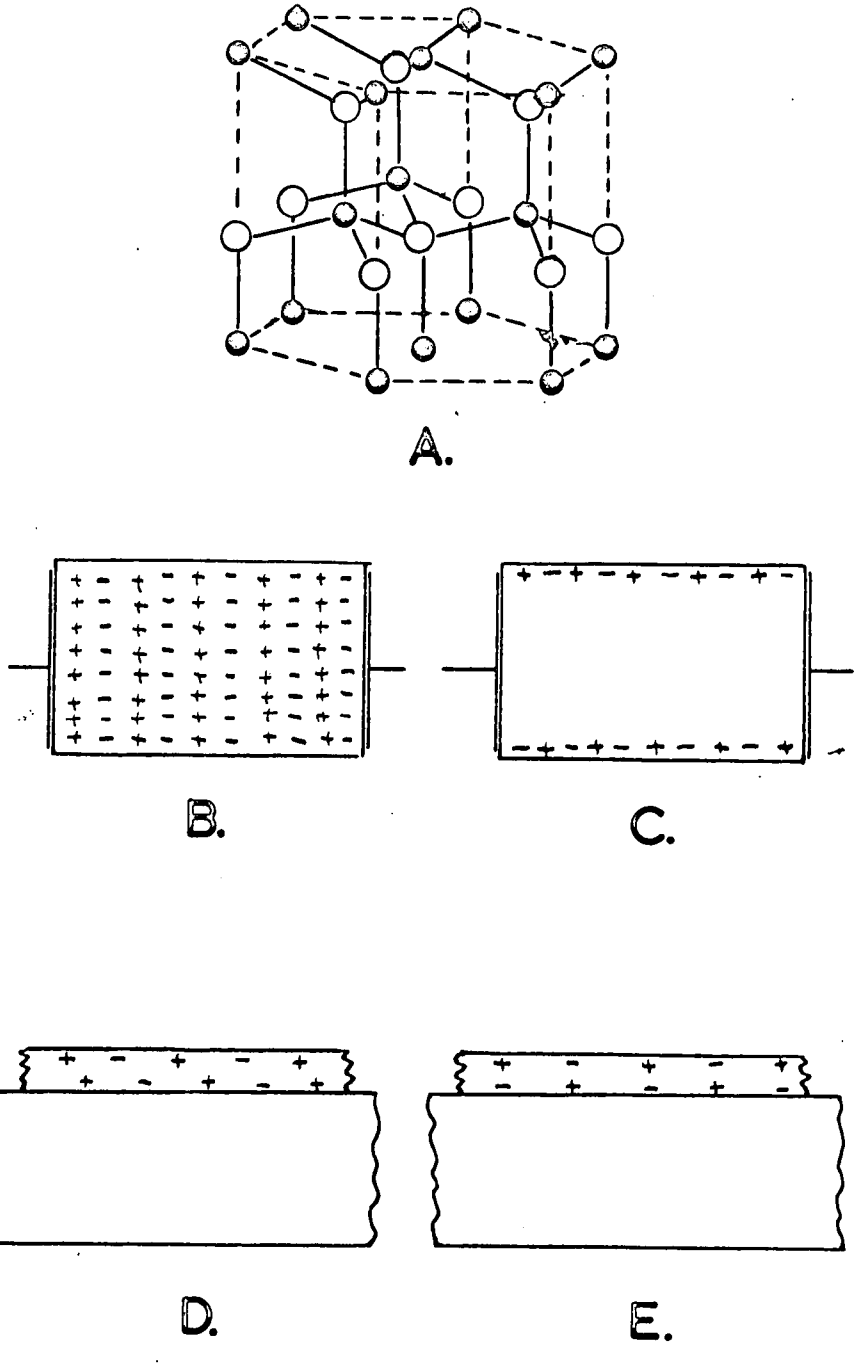

FIGURE 3·7

under consideration may be shown to degenerate to one of Rayleigh wave propagation over the basal plane of single crystal CdS. If current channeling effects are of no consequence, the recent analysis of this variant of the Kaliski amplifier, due to Tseng [60], may be directly adopted.

Under a given set of conditions (conductivity, drift mobility, applied field, frequency), the surface wave propagation constant may be accurately determined only by machine computation. Under certain favourable circumstances, the following explicit approximations may however be derived:-

$$V_R = \left(\frac{c_{eff}}{\rho}\right)^{\frac{1}{2}} \left(1 + \frac{K^2_{eff}}{2} \cdot \frac{\gamma^2 + \frac{\omega}{\omega_D}\left(\frac{\omega_c}{\omega} + \frac{\omega}{\omega_D}\right)}{\gamma^2 + \left(\frac{\omega_c}{\omega} + \frac{\omega}{\omega_D}\right)^2}\right) \qquad (a)$$

$$\alpha = \frac{K^2_{eff}}{2} \cdot \frac{\omega_c}{V_R} \cdot \frac{\gamma}{\gamma^2 + \left(\frac{\omega_c}{\omega} + \frac{\omega}{\omega_D}\right)^2} \qquad (b)$$

$$C_{eff} = V^2_{RO}\,\rho \left(\doteq 1.403 \times 10^{10}\ N/m^2 \text{ for CdS}\right) \qquad (c)$$

$$K^2_{eff} = \frac{V^2_R}{V^2_{RO}} - 1 \quad (\doteq 0.0292 \text{ for CdS}) \qquad (d)$$

$$\omega_c = \frac{\sigma}{\epsilon}, \omega_D = \frac{V^2_e q}{kT\mu}, \gamma = 1 - \frac{\mu dE}{V_R} \qquad (3.7.3.1)^*$$

V_R, V_{RO} are the CdS basal plane Rayleigh wave velocities in the presence, and absence, of piezoelectric stiffening (1.7306 Km/sec, 1.705 Km/sec).

By considering complex roots to Lord Rayleigh's [40] original expression for propagation over an isotropic halfspace, it may be shown [93] that the Rayleigh wave attenuation factor per wavelength (γ') is approximately related to longitudinal (α') and transverse (β') wave attenuation factors by the linear equation

$$\gamma' = A\alpha' + (1 - A)\,\beta' \qquad (3.7.3.2)$$

---

* Equations 113, 114 and 115 of reference 60.

where A is a function only of the Poisson ratio, σ, and is given by

$$A = \frac{16b\ (1 - c^2)}{c^2(3c^4 - 16c^2 - 16b^2 + 24)} \qquad (3.7.3.3)$$

where $b = \frac{V_t}{V_L}$ $(= \frac{1.766}{4.362}$ for CdS) and $c = \frac{V_R}{V_t}$ $(= \frac{1.705}{1.766}$ for CdS).

Substitution of the bulk wave acoustoelectric attenuation factors derived by White into 3.7.3.2 yields

$$\gamma' = \tfrac{1}{2}(K_t^2 + A\ (K_L^2 - K_t^2\ ))\ \frac{\gamma}{\gamma^2 + (\frac{\omega}{\omega}c + \frac{\omega}{\omega_D})^2} \qquad (3.7.3.4)$$

where $K_l^{\ 2}$ and $K_t^{\ 2}$ are, respectively longitudinal and transverse wave coupling constants.

For propagation over the basal plane of CdS, $K_L^{\ 2} = 0$ and $K_t^{\ 2} = 0.035$. For CdS, A = 0.021. Thus an effective Rayleigh wave coupling constant of

$$K_r^{\ 2} = K_t^{\ 2} + A(K_l^{\ 2} - K_t^{\ 2}) = 0.0345 \qquad (3.7.3.5)$$

may be predicted. The origin of the apparent disparity between this figure and that predicted by Tseng (0.0292) may be sought both in the approximate nature of Equation 3.7.3.2 and in the liberties taken with rigor in applying this equation to an acoustoelectrically complex situation. It is however of interest to note that a similar rule-of-thumb calculation for surface wave propagation normal to the basal plane leads to the prediction of a surface wave coupling constant of the order of only 2% of the analogous bulk longitudinal wave coupling constant.

One example of the many "peculiarities" which attend surface wave amplification in the CdS-on-Substrate system should perhaps briefly be mentioned, prior to

discussing amplification in the ultra-low normalized frequency limit. The complex mechanical properties of CdS are sensitive to changes in both drift field and illumination level. Both "external" influences induce changes in the complex coefficients of the CdS wave propagation sextic polynomial 2.4.1 which in turn induce changes in the structure of the roots to this polynomial. Consider the question of amplification along a permitted direction of propagation. A change in drift field could conceivably result in an unfavourable redistribution of positive and negative signs among the imaginary parts of the roots to Equation 2.4.1, causing this previously permitted direction to become forbidden. While the question of energy flow along forbidden directions has yet to be examined in detail, it is conceivable that the drastic change caused by a simple alteration of drift field could cause surface wave energy to be pumped into the substrate through surface wave-bulk wave coupling. The resultant amplification anomaly could either be reversed or compounded simply by altering the level of illumination.

In the low normalized frequency limit, the analysis of coupling in the CdS-on-Sapphire variant degenerates into equivalence with Kaliski's analysis of ultrasonic surface wave amplification in non-piezoelectric dielectrics by means of currents flowing in ultra thin piezoelectric semiconducting boundary layers [94].

The problem was formulated by Kaliski in terms of an isotropic Rayleigh wave-type wave propagation model. To facilitate analysis, channeling effects, fields external to the piezo-semiconductor, and transversal piezocoupling effects were specifically excluded, and only longitudinal strains of the layer were considered. An explicit solution to the resulting set of equations was

obtained using perturbation techniques.*

The derived approximate Rayleigh-type surface wave amplification coefficient differs qualitatively from the analogous expression derived by Tseng (3.7.3.1(b)) only in so far as amplification is found to be an increasing function of the layer thickness. Considering as a numerical example the amplification of 15 MHz surface waves in ultra thin CdS-on-Silica ($h = 0.5$ microns; $\rho = 10^3\ \Omega$ cm), Kaliski predicted an available gain rate of 14.6 dB/cm, which compares favourably with the 21 dB/cm, 8 MHz and 20 dB/cm, 30 MHz Rayleigh wave gain rates observed on the basal plane of $10^4\ \Omega$ cm single crystal CdS by R.M. White et.al. [71] and Vaskova et.al. [95].

A wide conceptual gap exists between, on the one hand, the non-rigorous perturbation analysis of Kaliski and, on the other, the numerical analysis of Tseng. Formidable difficulties are attendant on the rigorous analysis of acoustoelectric interaction in the intervening normalized frequency range of waveguide dispersion. The following subsection is concerned with interaction in this mathematically "forbidden" frequency range.

3.7.4 DISPERSIVE ACOUSTOELECTRIC COUPLING IN CdS-ON-SAPPHIRE.

Physical insight into the dispersive character of acoustoelectric Sezawa wave coupling in CdS-on-Sapphire may be obtained by physically correlating Tolstoy and Usdin's concept of critical angle reflection, non-destructive travelling-wave-interference Sezawa wave dispersion, and the surface particle displacement amplitude ratio dispersion characteristics published by Mooney and Bolt (Figure 3.2B)

---

* For analytical details the reader is referred to the original publication.

Two critical points (A and B in Figure 3.2B), may be located on the dispersion curves. These points correspond to surface wave phase velocities at which the angles of incidence of the longitudinal ($\theta = \sin^{-1} \alpha_1/c$) and transverse ($\gamma = \sin^{-1} \beta_1/c$) components of the travelling wave interference system become critical.

Require the power density of the fundamental mode to remain constant throughout the following discussion. At point A, $c = \alpha_1$, $\theta = \frac{\pi}{2}$, $\gamma = \sin^{-1}(\beta_1/\alpha_1)$, and for the fundamental mode $\omega h \doteq 3500$. At point B, $c = \beta_1$, θ is imaginary, $\gamma = \frac{\pi}{2}$ and $\omega h \doteq 7600$. Thus when:-

$c<\beta_1$; $\omega h > 7600$: both γ and θ are imaginary, the free surface boundary conditions dominate surface wave propagation, and Tseng's [60] acoustoelectric coupling analysis may be applied with confidence to the system.

$c=\beta_1$; $\omega h \doteq 7600$: $\gamma = \frac{\pi}{2}$ and θ is imaginary, the surface wave can be visualized as a vertically polarized, non-destructive interference system propagating normal to the "c" axis of the CdS film. While acoustoelectric coupling might well be expected to show an increase over Tseng's case, it should be emphasized that the analogy to the coupling of transverse body waves propagating over the basal plane of single crystal CdS is incomplete. The discrepancy is illustrated by the corresponding non-zero surface particle amplitude ratio.

$\alpha_1 > c > \beta_1$; $7600 > \omega h > 3500$: $\frac{\pi}{2} > \gamma > \sin^{-1}(\beta_1/c)$ and θ remains imaginary, the travelling wave non-destructive interference pattern becomes more complicated as c increases, γ decreases. Acoustoelectric surface wave coupling, which depends upon the

resultant piezoelectric polarization fields, becomes difficult to predict without specific numerical information. The nett effect of a decrease in ωh is a small increase in the vertical excursion of the surface particles, which implies a possible increase in coupling.

$c=\alpha_1$; $\omega h \doteq 3500$: $\gamma = \sin^{-1}(\beta_1/c)$ and $\theta = \frac{\pi}{2}$, longitudinal waves propagating parallel to the interfacial plane are, for the first time, able to play an active part in the travelling interference pattern. Available energy must now be shared between both longitudinal and shear wave components of the system. This sharing process appears to be mirrored, at the surface, in an abrupt increase in the amplitude of horizontal displacement at the expense of vertical displacement. Since longitudinal bulk waves are piezoelectrically inactive when propagating normal to to the "c" axis of single crystal CdS, it would seem reasonable to expect an abrupt decrease in surface wave coupling over this range.

$\beta_2 > c > \alpha_1$; $3500 > \omega h > 0$: $\gamma = \sin^{-1}\beta_1/c$ and $\frac{\pi}{2} > \theta > \sin^{-1}\alpha_1/c$, the "centre of gravity" of surface wave energy sinks, as ωh decreases, deeper into the substrate, and the system tends to the model of surface wave acoustoelectric interaction investigated by Kaliski. Increase in the vertical excursion of the surface at the expense of the horizontal appears to imply a gradual restoration of acoustoelectric coupling.

In the absence of trapping, the acoustoelectric current caused by depletion of the forward momentum of an electron stream as energy is transferred to a

growing bulk flux wave (frequency ω, phase velocity v_s) may be written*

$$J_{ae} = -\mu_d \frac{\omega_c}{v_s} \frac{e^2}{\epsilon} S_1^2 \left(\frac{\gamma}{\gamma^2 + (\frac{\omega}{\omega_c} + \frac{\omega}{\omega_D})^2} \right) \qquad (3.7.4.1.)$$

Over simplifying an extremely complicated situation, it seems reasonable to assume a linear relationship between the "piezoelectric effectiveness" of a strain amplitude S_1 of given normalized frequency in a CdS-on-Sapphire system and the corresponding ratio of vertical (u_v) to horizontal (u_H) surface particle displacement amplitude. One might, without any ~~rigor~~ rigour, write, for the CdS-on-Sapphire system

$$"J_{ae}" \doteq (\frac{u_v}{u_h})^2 J_{ae} \qquad (3.7.4.2.)$$

The following points,(which hold irrespective of the precise form of the above equation) are illustrated by a study of "J_{ae}" as a function of externally applied field, frequency, and conductivity, in a postulated CdS-on-Sapphire thin film of fixed thickness (0.25μ) and mobility (100 cm^2/V sec) (see Figure 3.8):-

(i) The normalized frequency of maximum gain,$(\omega_c \omega_D)^{\frac{1}{2}} h$,(Chapter 4, section 6) strongly influences the form of the fundamental sheet of the acoustoelectric current surface for a bounded system.

(ii) The zero acoustoelectric gain condition, "J_{ae}" = 0, exhibits a field dependence which reflects the dispersive characteristics of the bounded system.

(iii) The power spectral purity (and hence dynamics) of acoustoelectric domains (Chapter 4) formed in the system will be dictated by the shape of the peaks of acoustoelectric gain.

---

* See Chapter 4, section 2.

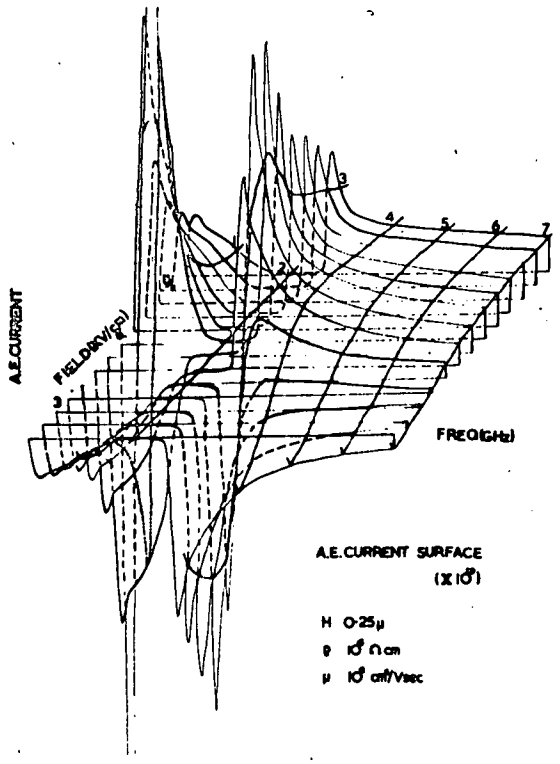

$10^6\ \Omega CM$

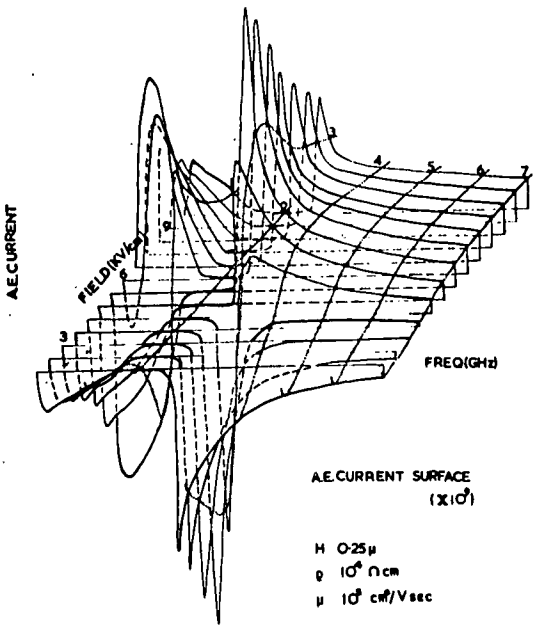

$10^4\ \Omega CM$

— FIGURE 3.8 —

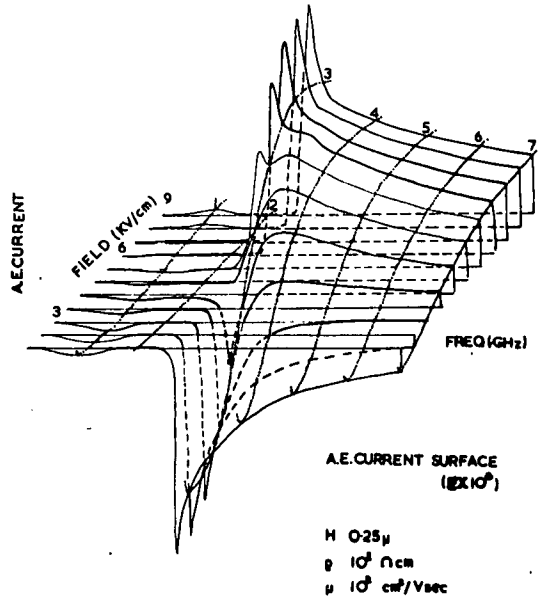

$10^2\ \Omega CM$

(iv) Under certain conditions, high field current saturation effects characteristic of acoustoelectric interaction may exhibit photosensitive multiple "knee" structures reflecting the photosensitive topology of the acoustoelectric current surface.

3.8 CONCLUSIONS.

It has been shown by numerical analysis to be a valid approximation to regard an <001> oriented hexagonal CdS monolayered <001> oriented sapphire half-space system as mechanically isotropic. Dispersion characteristics for surface wave propagation in such a system have been obtained, and the dispersive nature of the acoustoelectric coupling coefficient in the system has been discussed. Since acoustoelectric coupling is not adversely affected by random rotations of the CdS crystallites about the <001> axis, it is concluded that in a vapour deposited CdS thin film-suitably oriented sapphire substrate system, no theoretical objection exists to obtaining acoustic surface wave gain rates of the same order as those currently obtained in acoustic bulk wave amplifiers.

The question naturally arising as to how, for a given flux frequency, acoustic gain is to be shared between the available modes of propagation can only be answered by numerical construction of the surface wave acoustoelectric coupling surface for the particular system under consideration. Such a construction would, in addition, permit location of the sheet degeneracies at which mode coupling might be of importance.

It is to be expected that the available gain of the higher order modes will suffer from diffusion of electrons across nodal planes in the film.

Acoustic scattering at grain boundaries and surface imperfections, thought to play an essential part in mode coupling processes reported in an aluminium wire waveguide, may cause significant distortion of the CdS-on-Sapphire coupling sheets. It has been shown [96, 97] for example, that for definite values of the spatial period of surface roughness of an unlayered body, small in height in comparison to the Rayleigh wavelength, the damping due to scattering, even by fine grain non-uniformities, can be very great for narrow bands of frequency. Similar considerations probably apply for rather broader frequency bands of surface waves in polycrystalline acoustic waveguides [98]. The feasibility of investigating CdS crystallite size by the location of absorption peaks in an obliquely reflected em beam appears worthy of further consideration.

CHAPTER 4.

ACOUSTOELECTRIC INTERACTIONS IN CADMIUM SULPHIDE.

4.1 FIELD INDUCED BULK EFFECTS.

Given the time, mathematical ability and a sufficient number of experimentally inaccessable variables, a large number of plausible theoretical mechanisms might be advanced to explain almost any observed effect in any material in ("steady-state") dynamic equilibrium with its surroundings. Prior to restricting discussion to acoustoelectric interactions in CdS, it is useful to list a few of the known effects of applied field on a single crystal photoconductor.

Neglecting impurity banding, surface, and junction effects, an externally applied field may induce

(i) changes in the forbidden energy gap(s)

(ii) changes in the free carrier wave and distribution functions

(iii) changes in the wave functions of defect levels

(iv) extraction (by tunneling or hopping) of electrons from the valence band to levels in the forbidden gap and thence to the conduction band(s) either directly or by intermediate steps

(v) extraction of holes from forbidden gap levels into the valence band

(vi) carrier heating, which may assist processes (iv) and (v) by impact

(vii) changes in such trapping parameters as capture probabilities

(viii) Joule heating of the lattice

(ix) changes in the spatial distribution of the phonon population by acousto-electric or deformation potential coupling to the carrier stream.

Many of these effects may be inter-related, some, in a given situation, may be thought improbable, and nearly all, in one aspect or another, are poorly understood. In order to preserve both brevity and tractibility it is clearly necessary to impose severe restrictions on the analysis of any high field bulk effect. The absence of such artificial restrictions, and the presence of competing interactions, cannot however be ignored in an imperfect experimental situation.

The following discussion is concerned generally with acoustoelectric interactions in cadmium sulphide, and specifically with the macroscopic consequences of thermal acoustic noise amplification in the frequency range $kl \ll 1$ *. For a more general treatment of acoustoelectric effects and the energy losses by hot electrons, the reader is referred to the multiple part review by Rose of R.C.A. [99].

4.2 ACOUSTOELECTRIC FIELD DEPENDENT CARRIER BUNCHING.

Consider, after Moore [100], Haydl et.al. [101] and others, a homogeneous piezoelectric semiconductor of infinite extent, above absolute zero, through which electrons are drifting faster than the speed of sound. The random acoustic flux coursing through the crystal quasi-parallel to the electron stream may, if amplified sufficiently, be visualized as locking local carriers

---

* The 200 $cm^2/Vsec$ CdS electron mean free path l, and the propagation constant-layer thickness product kh (Figure 3.1) inter-relate with the minimum layer thickness for validity of the boundary conditions (1000 Å), to make dispersion improbable for acoustic frequencies such that $kl \gg 1$.

in potential wells dug by moving strain waves in the piezoelectric lattice.

Define "steady-state" to be a dynamic equilibrium in which favoured waves start from any arbitrary lattice point, grow, forming potential wells, are scattered, and collapse, only to be replaced by other similarily favoured waves. Upon scattering, electrons "acoustoelectrically trapped" in the potential wells return to the mobile electron stream to await recapture by further wells.

Under a constant externally applied drift field, the "trapping" process is, as was pointed out by Moore [100], statistically stationary in time. A mathematical anology to conventional trapping and thermal detrapping from static donor levels accordingly exists, provided the random nature of the acoustic flux is retained under amplifying conditions.

Regard, in the first instance, acoustic flux as a collection of small amplitude plane waves, of frequencies ω_L, giving rise to alternating * piezoelectric polarization fields $\sum_\ell E_L(x)$ and partially neutralizing space charge bunches $\sum_\ell n_{sl}(x)$ superimposed on the equilibrium carrier density $n(x)$. Neglecting carrier diffusion due to $\frac{\partial n(x)}{\partial x}$, the law of internal current may be written as

$$J = q\mu_d(n(x) + \sum_\ell f_\ell \cdot n_{s\ell}(x))(E(x) + \sum_\ell E_\ell(x)) \qquad (4.2.1)$$

where $E(x)$ is the equilibrium field, q is the absolute unit charge, μ_d is the trap controlled drift mobility, and the quantities f_l account for the division of bunched space charge into two

---

* one dimensional propagation $\exp[i(kx - \omega t)]$ space time dependence.

streams in dynamic equilibrium, travelling, respectively, in the conduction band and the forbidden gap.

Provided no phase difference exists between these two streams, and provided a simple trapping model is acceptable [102], the quantities f_1 are real, and are given by

$$\frac{n}{n + n_t} = \frac{t_f}{t_f + t_x}$$

n, n_t and t_f, t_x are, respectively, the densities of free and trapped electrons and the times spent by electrons in the conduction band and in traps. μ_d may, if these two criteria are satisfied, be written as $f_1 \mu_H$, where μ_H is the trap-independent Hall mobility. The question of a phase difference between the two streams, which does not directly concern this study, is considered by Moore and Smith [102], Greebe [103] and others.

The product J in Equation 4.2.1 is composed of four distinct parts, the conventional d.c. drift current, a set of first order currents at frequencies ω_1, a set of non-linear mixing currents at all sum and difference frequency combinations, and finally, a set of direct acoustoelectric currents. The first order currents are responsible for the growth of acoustic waves, and the non-linear mixing currents relate to the mixing of energy among sound waves in the system.[105]

Concentrating attention on the direct current part of J, one may write

$$J_{dc} = q\mu_d n(x) + q\mu_d \cdot \tfrac{1}{2} \cdot \mathrm{Re} \sum_{\ell} (f_\ell \cdot n_{s\ell} \cdot E_\ell^*) \qquad (4.2.2)$$

For small electromechanical coupling, $kv_s \doteq \omega$, where v_s is the phase velocity of sound propagation. It may be shown, for harmonic plane waves, that $J_l \doteq q.n_{sl}.v_s$. The acoustoelectric current term of the above equation may therefore be written as

$$J_{ae} = \tfrac{1}{2} q\mu_d \cdot \sum_{\ell} \mathrm{Re}(f_\ell \cdot n_{s\ell} \cdot E_\ell^*) \qquad (4.2.3)$$

$$= -\tfrac{1}{2} \frac{\mu}{v_s} \cdot \sum_{\ell} \mathrm{Re}(f_\ell \cdot J_\ell \cdot E_\ell^*) \qquad (4.2.4)$$

Applying the principle of conservation of energy to the system, one obtains

$$\frac{dU}{dt} = -\tfrac{1}{2}\mathrm{Re}\sum_{\ell}(J_\ell \cdot E_\ell^*) = -2\sum_{\ell}\alpha_\ell \cdot I_\ell \qquad (4.2.5)$$

where α_L is the attenuation coefficient of the component ω_l, $I_l (= V_s \tfrac{1}{2} c\, S_l^2)$ is the acoustic energy flux; c is the appropriate elastic stiffness constant, and S_l is the corresponding lattice strain.

If the f_l are constant over the frequency range of interest, and are, in addition, real, Weinreich's relation results directly

$$J_{ae} = f \frac{\mu}{v_s} \frac{dU}{dt} \qquad (4.2.6)$$

The attenuation coefficients α_l in Equation 4.2.5 are, (subject to the same restriction of real f_l) given approximately by White's [17] equation

$$\alpha_\ell = \frac{\omega_c}{v_s} \frac{e^2}{2c\epsilon} \left(\frac{\gamma}{\gamma^2 + \left(\frac{\omega_c}{\omega_\ell} + \frac{\omega_\ell}{\omega_D} \right)^2} \right) \qquad (4.2.7)$$

where $\omega_c = \frac{\sigma}{\epsilon}$, $\omega_D = V_s^2/fD_n$, $\gamma = 1 - \frac{f\mu E}{V_s}$, σ is the low field conductivity, ϵ the dielectric constant and D_n is the electron diffusion constant. Substitution of Equation 4.2.7 into Equation 4.2.6 combined with Equation 4.2.5 yields Equation 3.7.4.1.

Consider now the question of build up of a potential well under the influence of the first order currents (Equation 4.2.1), from its initiation to the point in time at which it becomes large enough to induce significant carrier bunching. For an appreciable part of this incubation period (t_i) it may be that the small signal approach is valid. An implicit expression for the distance $l_o = v_s t_i$ which must be travelled under small signal gain conditions prior to the onset of acoustoelectrically induced negative differential conductivity, has been derived by Haydl et.al. [101] *.

$$(2\alpha_m \ell_o)^{\frac{1}{2}} \exp(2\alpha_m \ell_o) = \frac{8\pi^3 \epsilon kT}{K^2 e^2 \alpha_b} \exp(2\alpha_b \ell_o) \qquad (4.2.8)$$

α_m is the acoustic gain rate of the favoured band of random acoustic noise, α_b the corresponding lattice attenuation.

The field dependence of $l_o = v_s t_i$ for one piezoelectric semiconductor is illustrated, after Haydl et.al. [101], in Figure 4.1.

The rate of doing work on a potential well, once a significant number of carriers are locked in its trough, must, since the small signal approach now breaks down, be written out of hand as [99]

$$\frac{dU}{dt} = ne(E - E_a)v_s \qquad (4.2.9)$$

---

* See also the small signal approach of Autin [104].

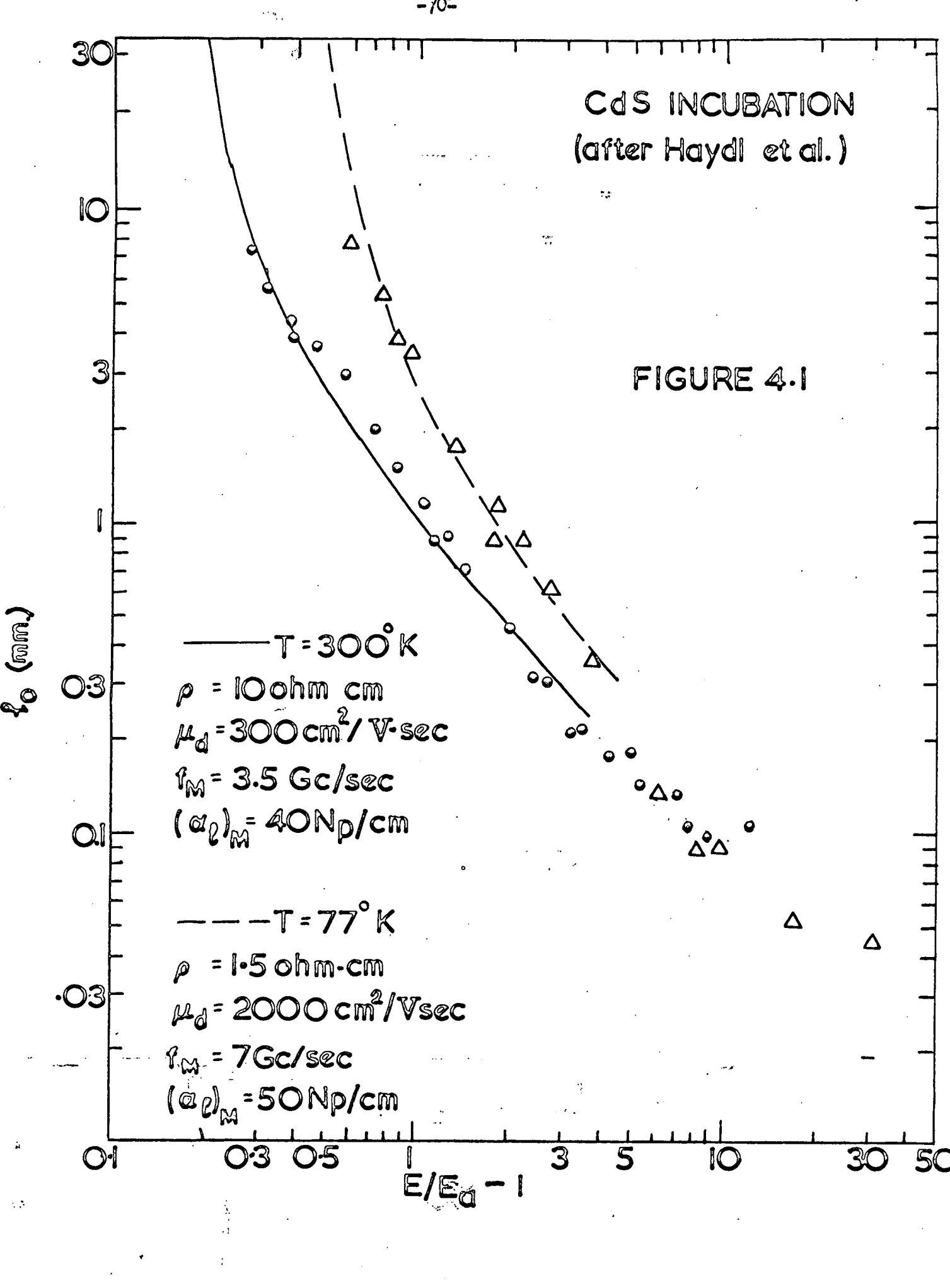
CdS INCUBATION
(after Haydl et al.)
FIGURE 4.1
ℓ_0 (mm)
30
10
3
1
0.3
0.1
.03
0.1
0.3
0.5
1
3
5
10
30
50
E/Ea - 1
——T = 300° K
ρ = 10 ohm cm
μ_d = 300 cm²/V·sec
f_M = 3.5 Gc/sec
$(\alpha_\ell)_M$ = 40 Np/cm
— — —T = 77° K
ρ = 1.5 ohm-cm
μ_d = 2000 cm²/Vsec
f_M = 7 Gc/sec
$(\alpha_\ell)_M$ = 50 Np/cm

The force neE_a causes the bunched carriers to drift at the velocity of sound. The excess force, $ne(E-E_a)$, is transmitted to the potential well by driving the bunched carriers against its flank.

Carrier bunching, of itself, implies a decrease in the local unbunched carrier concentration, an increase in the local resistivity, and an increase in the local field E external to the potential well. The resultant increase in $\frac{dU}{dt}$ causes further carrier bunching, and a convective "feedback" process, terminated either by well collapse or by exhaustion of the local free carrier supply, is set in motion.

In the weak-mixing limit (ultrasonic frequencies) a potential well mean lifetime (initiation to annihilation) t_t may reasonably be regarded as being entirely determined by acoustic lattice processes and hence independent of applied field. In the strong mixing limit (hypersonic frequencies) Prohofsky [105] has shown the piezoelectric-electronic non-linear interaction to be much stronger than the usual crystal anharmonic interactions, and has therefrom deduced that acoustoelectric interactions may be dominant in determining the mean lifetimes of hypersonic waves. For simplicity, the latter case will be excluded from the following discussion.

The (approximately) field independent mean lifetime t_t of a well may, perhaps crudely, be expressed as the sum of the mean incubation time t_i, the mean collapse time t_c, and the mean lifetime in a saturated condition t_l.

$$t_t \doteq t_i + t_l + t_c \qquad (4.2.10)$$

Exhaustion of the free carrier supply will, according to this oversimplified life cycle, occur in a crystal if the acoustoelectric gain is such that $t_i << t_t$.

In Moore's two state model *, the mean lifetimes t_s, t_o in the states S, 0 refer, respectively, to electrons being acoustoelectrically trapped in potential wells or free to move in the conduction band under the influence of the externally applied field. One may, perhaps even more crudely, write

$$\begin{aligned} t_s &\doteq t_t + |\epsilon|\ t_i \\ t_o &\doteq t_c + (1 - |\epsilon|)t_i \end{aligned} \qquad (4.2.11)$$

The detailed form of the convective feedback function **, $|\epsilon| << 1$ is undoubtedly interesting, but will not be discussed here.

Note that t_t and t_c are, to a first order approximation, independent of the applied field. The field dependence of the mean lifetime in a saturated condition, t_1, follows directly from Equations 4.2.8 and 4.2.10.

Inspection of these relations 4.2.8 - 4.2.11 shows it to be reasonable to expect that for $t_i < t_t$, the probability per unit time of electronic transitions $S \rightarrow 0$ (bunched to unbunched states), given by $1/t_s$, decreases with increase in the field applied to the crystal. The probability per unit time of transitions $0 \rightarrow S$ (unbunched to bunched states), given by $1/t_o$, similarly increases with increase in externally applied field. The onset of negative differential conductivity in a piezoelectric semiconductor may, accordingly, be regarded as a necessary consequence of convective acoustoelectric carrier trapping.

---

* successfully applied to the spectral analysis of current noise in amplifying CdS.[100]

** relating to the physical situation in which the effective captive cross-section of a well changes (not necessarily monotonically) as the local field becomes stronger, the gain rate higher and the well deeper (unless limited by non-linearity of the semiconductor).

Summarizing the above analysis, two distinct non-linear consequences of electron drift through homogeneous, infinite, piezoelectric semiconductors exist: current saturation, caused, if $t_i > t_t$, by the internal generation of acoustoelectric current as a direct result of acoustic flux growth; and negative differential conductivity, caused, if $t_i < t_t$, by large signal carrier trapping.

This study is concerned with acoustoelectric interactions in CdS thin films, with particular reference to surface wave domain propagation. The dynamical behaviour of bulk wave domains is, unfortunately, not yet fully established. Currently, available proparation techniques do not, as yet, yield homogeneous thin films. The following sections are, accordingly, devoted to the development of a temporary framework for domain visualization, and to a study of low gain rate acoustoelectric interactions in inhomogeneous specimens.

4.3 THE DYNAMICS OF HIGH FIELD INSTABILITIES.

An attempt is made in the following non-rigorous analysis to extend Boër and Dussel's [106] graphical treatment of the dynamics of slow ($c < 1$ cm/sec) and fast ($c \doteq 10^7$ cm/sec) domains to the case of acoustoelectric domains. Analytical details, since they do not directly concern this study, will, as far as possible, be omitted from the text. Boër and Dussel's notation will however be retained, permitting direct comparison with the original treatment.

The quantities in the following equations should be referred to a co-ordinate system moving through the crystal at the speed of sound when acoustoelectric interactions are under consideration. For simplicity, boundary effects will be ignored, and analysis conducted in one dimension.

With respect to the relevant frame of reference (static in the cases of field dependent free electron density, field dependent mobility, and synchronous in the case of acoustoelectric carrier bunching) Poisson's equation and the law of internal current may be written

$$\frac{\partial E}{\partial x} = \frac{e}{\epsilon\epsilon_o}(n + n_t - p_t) \qquad \text{(a)}$$

$$j = en\mu E - \mu kT \frac{\partial n}{\partial x} + \epsilon\epsilon_o \frac{\partial E}{\partial t} \qquad \text{(b)} \qquad (4.3.1)$$

where e represents the unit charge, $\epsilon\epsilon_o$ the dielectric permittivity, n_t and p_t are the densities of, respectively trapped electrons and holes, and the other symbols have their usual meaning.

Combining these two equations yields a partial differential equation of order, and linearity, determined by the behaviour of the functions $\theta(x, t, E)$. (θ representing μ, n, n_t, p_t or ϵ). In order to contain the problem it is clearly imperative to refer the functions θ to a reasonably well behaved model.

Choosing a simple model, and restricting discussion to the case of small departures from equilibrium, the differential equation may be linearized about certain values of applied field without, possibly, serious loss of information. The standard approach of investigating the ability of particular integrals of the form

$$\phi(x, t) = \phi e^{kx} e^{\lambda t} + \text{const. terms} \qquad (4.3.2)$$

(k:"propagation" constant; λ : time constant; ϕ = n, E, N_t, p_t, j in turn) to satisfy the linearized equation, may then be adopted.

If the model permits λ to be put equal to -ck, solutions represent small,

exponential travelling waves. Unless k is purely imaginary, as x tends to $\pm\infty$ the linearization may become invalid. If the crystal is of finite length L, a finite real part of k may be admitted, provided the further relationship

$$\int_{x}^{x+L} E(x)\,dx = V \qquad (4.3.3)$$

is satisfied (V: externally impressed voltage). If, in 4.3.3, x is the only variable, solutions 4.3.2 must be space periodic, with L an integral multiple of the period length.

Putting $\lambda = -kc$, where c is a constant, 4.3.2 may be rewritten

$$\phi(x, t) = \phi e^{kx} e^{-kct} = \phi(x - cf) = \phi(x') \qquad (4.3.4)$$

If 4.3.4 satisfies the differential equation, time may be eliminated as an independent variable using the Galilean transformation

$$\frac{\partial}{\partial t} = -c\frac{\partial}{\partial x} = -c\frac{d}{dx'} \qquad (4.3.5)$$

Referring Equations 4.3.1 to a co-ordinate frame travelling at a velocity c relative to the original (synchronous or static) frame of reference, one has

$$j = en\mu E - \mu kT\frac{dn}{dx'} - \epsilon\epsilon_o c\frac{dE}{dx'} \qquad (4.3.6)$$

$$\frac{dE}{dx'} = \frac{e}{\epsilon\epsilon_o}(n + n_t - p_t)$$

Provided attention is concentrated solely on the "steady state" situation, (excluding domain growth and annihilation processes), $\frac{dj}{dx'}$ may be set identically to zero.*

Turning now to the models representing acoustoelectric carrier bunching and field dependent recombination/mobility saturation (Figures 4.2.A and 4.2.B

---

* This is equivalent to stating that device current does not change with time once a domain has formed, and involves no conflict with experiment

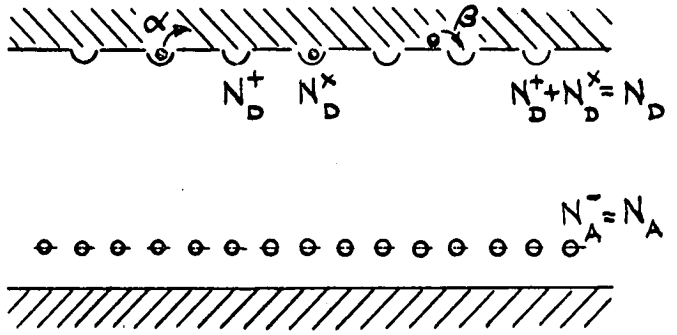

A.

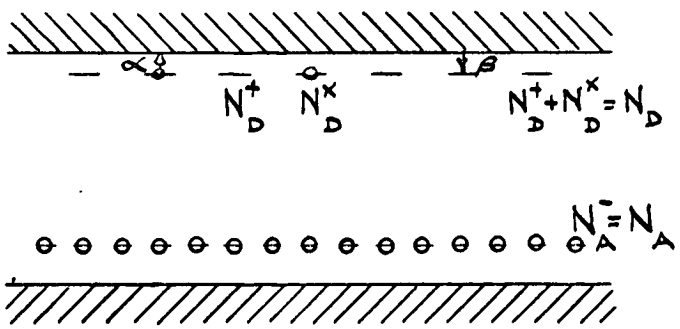

B.

FIGURE 4·2

respectively) notice that in so far as the acoustoelectric mathematical analogy to conventional trapping and thermal detrapping may be pursued, the two models are effectively equivalent, and may be described by the same sets of equations

$$\frac{dN_D^+}{dt} = \alpha N_D^x - \beta n N_D^+ \qquad (4.3.7)$$

$$\rho = e(n + N_A^- - N_D^+) = e(n + N^x - (N_D - N_A))$$

N_D^x and N_D^+ are here defined as the densities of bunched/filled and unbunched (empty) states in potential wells/conventional traps. Provided α, the relaxation time for electrons in bunches/traps, is sufficiently rapid, second derivatives in 4.3.6 may be eliminated by assuming quasi-thermal between bunched/trapped electrons and those in the conduction band

$$N^x = \beta N_D \frac{n}{\alpha} + \beta n \qquad (4.3.8)$$

Equations 4.3.6 may now be written

$$\frac{dn}{dx} = \frac{e}{\mu kT}\left(n\mu E - j_e - c\left\{n + \frac{\beta N_D n}{\alpha+\beta n} - (N_D - N_A)\right\}\right)$$
$$\frac{dE}{dx} = \frac{e}{\epsilon\epsilon_o}\left(n + \frac{\beta N_D n}{\alpha+\beta n} - (N_D - N_A)\right) \qquad (4.3.9)$$

The transferred electron effect may be described by making μ the only field dependent variable in the above set of equations. Both field dependent recombination and acoustoelectric interaction processes may be discussed in terms of a field independent electron relaxation time α (related to detrapping or well collapse) and an effective electron recombination coefficient, β (related to trapping or convective well growth) that is a strongly increasing function of externally applied field.

4.4 SOLUTIONS OF EQUATIONS 4.3.9.

A discussion of the techniques to be employed in the solution of the above equations is beyond the scope of this thesis. Graphical analysis of the behaviour of solution curves on the n-E plane, however, led Boër and Dussel to the conclusion that

> "for field dependent recombination the domain velocity is bounded by velocities of the order of the drift velocity of electrons, times a retarding factor due to trapping, at a field strength corresponding to the second singular point
>
> $$c \doteq \left(\frac{n}{n_t}\,\mu E\right)_{II} \qquad (4.4.1)$$
>
> With increasing influence of traps the trapping factor can be orders of magnitude smaller than unity, and thereby reduce the domain velocity from the value of the drift velocity by this amount.

When referred to the synchronous co-ordinate framework, this statement is in agreement with available observations of acoustoelectric domain velocity. In terms of the analysis provided in Chapter 4, section 2, c must necessarily be small, since $\frac{n}{n_t} \ll 1$ is prerequisite to the onset of acoustoelectrically induced negative differential conductivity. A fall in immediately-post-creation domain velocity has recently been observed by Pohlendt and Wettling in CdS. This fall could possibly correspond to the final stages of convective growth, mirrored in the approach of $\frac{n}{n_t}$ to a "steady state".

The question of solution behaviour for $c < 0$ has yet to be discussed. No mathematical account has yet been given of the complex processes leading to domain formation and annihilation. It is believed however that the picture emerging from the above analysis - of an acoustoelectric domain as being a

high field instability, created for thermodynamic reasons [23] by the effective acoustoelectric removal of mobile carriers from the conduction band, and propagating with a velocity governed basically by the mobile carrier drift velocity but strongly boot-strapped by carrier bunching to the collective velocities of individual, continuously created and annihilated potential wells which build a region of intense acoustic energy tied to the instability - may go some way towards portraying the physical situation, at least in the weak non-linear mixing limit.

It will readily be appreciated that in defective crystals, other processes (either distributed or junction) may induce negative differential conductivity effect at fields far lower than those required to give acoustoelectric gain. These processes may well dominate the formation of inhomogeneous field distributions in imperfect crystals.

4.5 SURFACE WAVE DOMAINS IN CdS-ON-SAPPHIRE WAVEGUIDES.

Acoustoelectric instability ("domain") formation is favoured by the simultaneous presence of a distributed acoustic source, a distributed small signal gain mechanism, and a distributed large signal, convective bunching feedback loop (Chapter 4, section 2)

Low energy electron diffraction experiments on nickel have indicated that the mean square vibrational amplitude of surface atoms is greater than that of atoms in the bulk [108]. An analogous surface wave source is spontaneously presented to a CdS-on-Sapphire waveguide above absolute zero. If the results of the previous analysis (chapter 3, section 7) are accepted, small signal

surface wave gain will occur under the influence of an applied drift field. If, further, a large signal convective bunching feedback loop can be sustained while the system enters an effective negative differential conductivity state, moving domains will form in the waveguide.

The power spectrum of the phonon packet associated with an acoustically dispersed waveguided domain may be influenced by changes in the preincubation externally applied voltage, the postincubation dynamic field distribution and the intensity of illumination (in the case of photosensitive samples). Systemmatic "anomalies" in domain behaviour are to be expected as a necessary consequence of dispersion.

Detailed discussion of the properties of as yet unobserved waveguided domains is premature, and should be deferred until rigorous mathematical treatments of domain formation and small signal surface wave acoustoelectric coupling become available.

4.6 STATIC DOMAINS IN INHOMOGENEOUS LOW GAIN RATE MATERIAL.

The small signal, bulk wave, amplification coefficient reaches a peak when

$$\gamma = -\left(\frac{\omega_c}{\omega} + \frac{\omega}{\omega_D}\right); \quad \omega = \omega_m = (\omega_c \omega_D)^{\frac{1}{2}}, \text{ viz:-}$$

$$-\alpha_{max} = \frac{\omega}{v_s} \frac{e^2}{8c\epsilon} \tag{4.6.1}$$

Since

$$\omega_m = (\omega_c \omega_D)^{\frac{1}{2}} = \left(\frac{\sigma}{\epsilon} \frac{v_s^2 C_i}{kT\mu}\right)^{\frac{1}{2}} \tag{4.6.2}$$

it is evident that $-\alpha_{max}$ is directly proportional to the square root of the dividend σ/μ If the crystal conductivity is low, $-\alpha_{max}$ will be small, and t_i will be correspondingly large. In high resistivity CdS, t_i may well exceed t_t, in which case convective bunching cannot occur.

Current saturation, accompanied by observable acoustic flux output at the crystal anode, may still take place [109], provided the crystal is homogeneous. Consider, however, applying a voltage V to an inhomogeneous low gain rate specimen composed of two homogeneous sections (parts 1 and 2) which differ only in so far as the carrier concentration in part 2 exceeds the carrier concentration in part 1 (Figure 4.3).

Since $E_1 > E_2$, part 1 will achieve a state of acoustic gain while part 2 is still in a state of acoustic attenuation. In this situation, let the flux amplified from the acoustic thermal background in part 1 be totally attenuated in part 2. No acoustic output will then be observed at the crystal anode. Acoustoelectric currents J_{ae1} and J_{ae2} will, respectively, oppose and assist the current J flowing through the specimen. In order to maintain current continuity, fields local to regions of acoustic amplification will substantially exceed their prethreshold values, while fields local to regions of acoustic attenuation will fall well below their ohmic values and may even become negative. The process may, to some extent, be convective since the acoustic gain rate in the high field regions may increase*. Since the conductivity of the adjoining regions differs, it may easily be shown [109] that the static acoustoelectrically induced field redistribution will be accompanied by crystal saturation.

The occurence of current saturation, accompanied by the formation of static, post-threshold, gross field inhomogenities in an inhomogeneous piezoelectric photoconductor, may be regarded as positive indications of localized, low

---

* That this increased gain rate might, in borderline cases, lead to $t_i < t_t$ thereby triggering convective growth, is an interesting possibility, which need not be considered here.

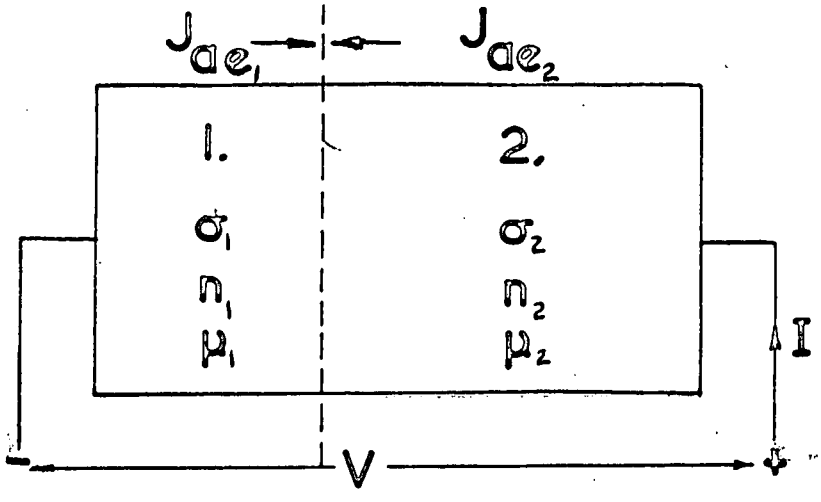

$n_2 > n_1$

FIGURE 4-3

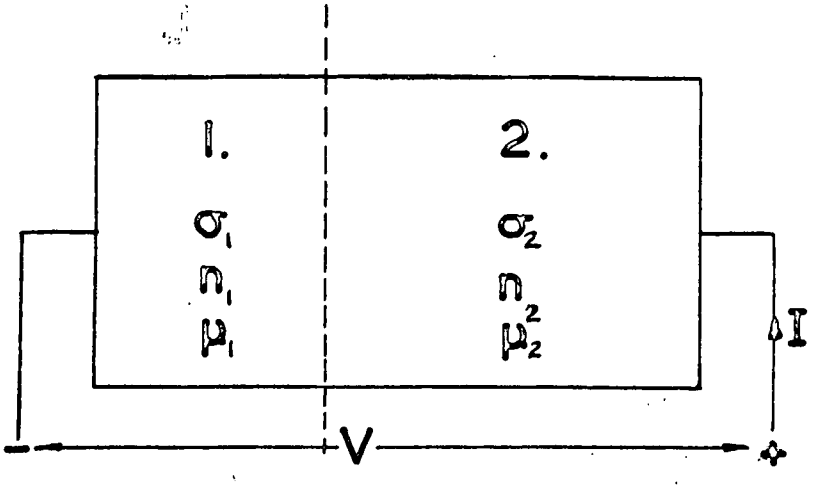

$n_2 < n_1$

FIGURE 4-4

gain rate acoustoelectric amplification.

4.7 CURRENT OSCILLATIONS IN SEMI-INSULATING PIEZOELECTRIC CRYSTALS.

Consider, after Paige [110], a photoconducting, uniform CdS crystal through which electrons are drifting faster than the speed of sound, and in which the phonon distribution has reached a steady state. If the conductivity in the cathode region is suddenly increased, the phonon flux in that region will decay to zero, and flux throughout the crystal will fall, causing a fall in acousto-electric current and a consequent rise in current through the device. Under certain conditions the cathode region may at this juncture revert to an amplifying condition, increasing, after a suitable lag, phonon flux throughout the crystal, and decreasing the current. This fall in current may again switch the cathode to an attenuating state, thereby establishing an oscillating cycle of acoustoelectric origin.

The situation may be represented by a one dimensional model of the form of Figure 4.4 ($n_1 > n_2$). Fluctuating boundary conditions at the inhomogenity interface present significant mathematical difficulties, which may, as has been shown by Froom [111], be resolved in part by numerical analysis. These difficulties are rivalled by the difficulties involved in over-riding inherent material inhomogeneities in order to obtain a situation amenable to experiment.

Acoustically induced current oscillations in semi-insulating piezoelectric crystals remain, as a result, only qualitatively understood.

CHAPTER 5.

PREPARATION AND PROPERTIES OF CdS THIN FILMS.

5.1 INTRODUCTION.

Major research into the preparation and properties of high purity, single crystal CdS may be traced to Frerich's [112] extension of the vapour synthesis techniques established by Lorenz [113]. Crystals of sufficient perfection to permit the interpretation of warm electron experiments have for some time been commercially available.

While thin film vapour deposition methods for CdS were developed by Veith [114] shortly after Frerich's experiments, and in spite of industrial interest in such CdS based thin film devices as the insulated gate TFT, synthesis techniques for high purity, high mobility CdS thin films remain practically in their infancy. Currently, impurity and secondary phase effects compete with the host lattice conduction processes. Hence electrical observations, even at low fields, are frequently irreproducible.

An effort will be made here to relate relevant known aspects of the physics and chemistry of CdS to established film preparation procedures in order to provide a background of information against which the preparation procedures used in this study may be critically examined.

5.2 THE SYNTHESIS OF CdS THIN FILM STRUCTURES.

Procedures for the preparation of thin ($\simeq 1.5\mu$) plates of CdS by polishing

from the bulk single crystal, recently developed by Wilson [115], may have important applications in the future study of acoustoelectric interactions in bounded systems. However, such techniques will not be considered further here.

The high temperatures ($\doteq 1475^{o}C$) and pressures ($\doteq 3.9$ atm) involved in achieving a stoichiometric melt of CdS virtually preclude, on state of the art and economic grounds, the preparation of high purity crystals by liquid-solid transformations.

Growth by gas transport from the vapour phase is subject to fewer limitations, since lower temperatures are involved, and forms the basis of the above mentioned Lorenz-Frerichs process, first applied to the growth of microcrystalline CdS thin films for photocell applications by Jacobs and Hart [116] using the reaction

$$H_2S + Cd(vapour) = CdS + H_2$$

at a pressure of 10mm Hg. More recently, Capella [117] has grown epitaxial CdS films using the reaction

$$H_2S + CdCl_2 = CdS + 2HCl$$

Information concerning the electrical properties of films prepared by these and similar methods appears to be limited.

The literature concerning the vapour evaporation of CdS thin films combines, in the main, evidence of duplication of effort into the partially achieved optimization of variants of the basic techniques employed by Veith [114], together with an apparent poverty of comprehensive information on both the structural and electrical properties of the films prepared and a frequent lack of appreciation of the full complexity of the interactions involved in preparing these films.

It is proposed to review briefly some aspects of the defect chemistry of CdS, prior to examining vapour deposition and post evaporation heat treatments in somewhat greater detail.

5.3 DEFECT INCORPORATION IN CdS.

Brief consideration is given here to the incorporation of native and foreign point defects in CdS. Extensive reviews of the chemistry of imperfect crystals, which forms a study in its own right, are given by Albers [118], Kroger [119], and Woodbury [120].

It is known that nearly all the elements are, to an electronically important extent, soluble in CdS, that even at moderate temperatures the material will react rapidly with its firing environment, and that the existence region of compound CdS in the three dimensional (P-T-Cd_xS_{1-x}) Gibbs phase diagram is small, probably asymmetrical, and easily distorted by certain impurities. As a result of the complexity of defect incorporation, and of certain thermodynamic difficulties, little quantitative data concerning the defect chemistry of CdS exists, and only in a very small number of cases has the microstructure of point defects been established.

Even in the absence of foreign atoms, the electronic properties of CdS are sensitive to thermal history and the partial pressures (P_{Cd} P_S) of the firing environment [119, 121]. During poorly controlled thermal cycling, concentrations of native disorders may well vary, and the appearance and subsequent disappearance of native microprecipitates in successive thermal cycles appears to be possible [122

A total of six basic native point disorders, which may exist singly, in complexes

with gross lattice defects, or in complexes with foreign impurities, may be classified according to Alber's notation as Cd_i, S_i (interstitial); V_s, V_{cd} (vacancies); Cd_s, S_{cd} (substitutional). In simple situations, the first of each pair may act as a donor, the second as an acceptor. Should the density of defects due to foreign atom incorporation be exceeded by the native defect density, the latter may well dominate the conduction processes.

Concerning the incorporation of foreign atoms (e.g. $^{*}O$) at high concentration levels, it is known to be essential to consider the stability of the CdS with respect to the precipitation of second phases (e.g. $CdSO_4$) [123]. In order to preserve overall crystal neutrality, the incorporation of certain elements (e.g. halogens) may be accompanied by the formation of native defects [124].

The impurities $^{*}O$, $^{*}Ag$, $^{*}Cu$, $^{*}Cl$, $^{*}In$, H_2O, are of particular importance to this study, and should be considered in some detail.

$^{*}Cu$ and $^{*}Ag$ diffuse rapidly as interstitials, but may substitute for Cd Halogen coactivators (e.g. $^{*}Cl$) appear to enhance their solubility, though little is known about the chemistry of this impurity system. Electronically, $^{*}Cu$ and $^{*}Ag$ generally form acceptor levels when in true solution; but may readily precipitate during cooling, tending (of particular importance to thin films) to decorate imperfections and lattice disorders [122, 125]. Cu_2S, the possible second phase with $^{*}Cu$, is a narrow band gap (0.6eV), p-type defect semiconductor, is readily precipitated from solution, and may well be responsible [126] for the observed hole conductivity in "p-type" CdS [127].

$^{*}In$ and $^{*}Ga$ appear to be incorporated substitutionally at Cd sites, diffuse rapidly, and are highly soluble. Both behave electronically as donors. These factors are of some importance in the preparation of ohmic contacts to CdS,

and have, of particular note, been used to advantage in the preparation of high Hall mobility ($240 cm^2/Vsec$), low resistivity CdS thin films [128, 129].

*Cl forms a useful coactivator with *Cu in the preparation of photosensitive CdS. It may substitute for S and is thought to associate with V_{cd} during sulphur firing, V_s during cadmium firing [120]. At high concentration levels, the native defects formed in order to preserve crystal neutrality may effectively compensate the electrical activity of *Cl.

The incorporation of *O is complex and poorly understood. It may substitute for S, and it seems reasonable to suppose that the resulting lattice strain may give rise to a vacancy complex or a dislocation at the *O site. During firing it may modify partial pressures in such a way as to control native defect formation [130], and may also reduce CdS [118], thereby increasing the crystal conductivity. Its behaviour in stabilizing ZnS in the wurtzite modification while not necessarily applicable to CdS, should be noted.

The formation of solid solutions CdS-CdO may modify the band structure of the original CdS crystal. *O incorporation may, conceivably, give rise to impurity banding.

Below $\doteq 200^{\circ}C$ an oxidation appears to take place that has been interpreted as an annihilation of sulphur vacancies by occupation with oxygen atoms. The resulting surface acceptor states increase markedly the surface resistivity. Photoadsorption (desorption) with less than (greater than) bandgap light has been noted [132]. Typical time constants involved in achieving a steady state of chemisorption with changes in illumination intensity may be conservatively estimated at 15 minutes [131].

Water vapour is notorious for causing experimental difficulties in less elegant high vacuum systems. Faeth [133] has suggested that the ion $(H_2O)^-$ could be responsible for the coulomb repulsive traps located at between 0.73eV and 0.83eV below the conduction band in CdS and CdS-CdSe single crystals by Bube et.al. and others (see the references cited by Faeth). It should be noted that such centres are not only capable of retarding drift mobilities, but may also, of themselves, give rise to non-acoustoelectric high field current saturation and negative resistance effects.

5.4 VACUUM EVAPORATION OF CdS THIN FILMS.

Early work*, on the correlation between residual gas pressure, substrate temperature, evaporation rate and purity of source material, and the apparent resistivity, photosensitivity and spectral response of one step monosource, high vacuum evaporated CdS thin films, yielded sufficient information for the production of simple thin film photo resistors, raised many as yet unanswered questions concerning the evaporation and condensation kinetics of CdS, and provoked efforts to control the properties of the films produced.

Solid-vapour phase equilibria of II-VI systems are reviewed by Lorenz [140]. Mass spectrometric investigation by Goldfinger et.al. [141] failed to detect molecules of CdS in the vapour phase, suggesting practically complete dissociation upon sublimation according to the reaction

$$2CdS = 2Cd + S_2$$

---

* Veith [114], Aitchison [134], Bromley [135], Nelson [136]. See also the reviews of Bube [137], De Klerk [138] and Shallcross [139] and the references therein.

Further investigations by Somorjai [142] have shown that CdS sublimation is controlled by a complicated charge transfer surface reaction which may be relied upon to preserve approximate stoichiometry of the vapour stream.

Consider an idealized enclosed system, in which sublimation takes place from a finite stoichiometric CdS charge at one site (source) and in which condensation is permitted only at a second site (substrate). Obviously, after a sufficient elapse of time, a stoichiometric (but not necessarily homogeneous) film of Cd, S and CdS will result at the substrate, in spite of the fact that at any given temperature the vapour pressure of sulphur exceeds by orders of magnitude the vapour pressure of cadmium.

Native and foreign defects, and astoichiometries arise firstly, in practical systems, from the selective deposition of components of the native vapour on parts of the apparatus other than the substrate, and secondly, from the presence of chemically active residual gas atoms, which serve to distort both the vapour composition and the above mentioned Gibbs phase diagram.

It is useful to bear in mind that at the economically achievable residual gas pressure levels of 10^{-5} - 10^{-6} Torr, the number of foreign atoms is comparable with the number of native vapour atoms impinging on a given substrate per unit time. From the point of view of reproducible CdS deposition, it is less essential that the absolute level of the residual gas pressure in a practical system should be ultra low ($<<10^{-6}$ Torr) than it is that the vacuum should be clean (i.e. chemically inert) and reproducible.

Addiss [143], apparently for the first time, partially enclosed the source-vapour stream-substrate in a hot wall belljar in an attempt to restrict selective condensation of native components on cold sites in the vacuum chamber.

By empirically adjusting and accurately monitoring the governing variables of their system, Zuleeg and Senkovitz [144] subsequently achieved successful optimization of a one step, monosource high vacuum thin film evaporation process for thin film transistor fabrication.

The first high vacuum coevaporation of CdS crystals from separate Cd and S molecular streams appears to be due to Miller et.al.[145]. A subsequent attempt to balance the sulphur concentration in Cd rich monosource evaporated CdS films by coevaporation from separate CdS and S sources, due to Pizzarello [146] was followed by De Klerk and Kelly's [147] carefully optimized Cd and S separate source coevaporation system designed for the production of high resistivity CdS thin film microwave transducers. Considerable support is lent to the selection of an optimum substrate temperature, T_s, in the temperature range 180°C-200°C, by their observations that at $\doteq 10^{-5}$ Torr the deposition rates of elemental Cd and S are significantly retarded for substrate temperatures, respectively less than 200°C and greater than 50°C, and that for substrate temperatures greater than 180°C formation of the metastable (high pressure, β, impurity) cubic modification of CdS is discouraged.

De Klerk [138] has argued that for substrate temperatures in the range 50°C-200°C condensation is probable only at sites at which Cd and S atoms arrive simultaneously. His conclusion, that the films deposited in his apparatus are stoichiometric, while supported by extensive piezoelectric and crystallographic studies, has apparently not, as yet, been verified by comprehensive physical studies, and it remains open to question as to whether the high values of resistivity reported result from perfect stoichiometry or from a high level of sulphur incorporation in the CdS host lattice (S_i, V_{cd} and S_{cd} act as acceptors).

The preparation of CdS on sapphire films in a small heated chamber at 10^{-9} Torr, using ultrahigh purity source material was recently performed by Hudock [148]. Hall mobility and resistivity values of the order of 150cm^2/V sec, 0.1 - 1.0 Ω cm were reported to result from a 400°C liquid Cd postevaporation heat treatment aimed at impurity reduction by solvent extraction. Such films might be eminently suited to the study of high gain rate acoustoelectric surface wave interactions. Unfortunately, facilities do not at present exist for the duplication of his preparation procedures.

The apparatus assembled in the chamber of an Edwards 19E4 plant and used in this study for the monosource evaporation of CdS thin films, is illustrated in Figure 5.1. The following evaporation procedure was adhered to whenever possible:-

(i) After backing the three substrates *, mounted as shown on a ledge in the centre of the chimney, with a mica seal and a glass slide, the controlling chromel alumel thermocouple was wedged into position and the chamber evacuated.

(ii) The substrates were baked at 300°C for a short time under a pressure of $\doteq 10^{-5}$ Torr. Argon was then bled into the chamber, both in an effort to flush chemically active residual gases, and to facilitate ion bombardment of the substrates.

---

* The (20 x 6.5 x 2) mm^3 sapphire substrates, polished on one face to a flatness of $\lambda/2$, were cleaned by washing in concentrated HCl, an agitated detergent solution, and hot chromic acid in a 30 minute sequence with a deionized water rinse between each stage. After manual scrubbing with cotton wool soaked in isopropyl alcohol, the chemical cleaning procedure was repeated. The substrates were then stored in a recirculating isopropyl alcohol vapour bath.

(iii) Upon termination of the cleaning discharge, the bombardment electrode was withdrawn, the chimney cooled to 193°C, the vacuum chamber re-evacuated to 10^{-5} Torr, the SM10 source carefully outgassed, and the liquid nitrogen cold trap then brought into operation.

(iv) After an interval of two minutes, the mica cover was withdrawn, exposing the substrates to the automatically baffled vapour stream.

(v) During the empirically determined evaporation period, the source current and the substrate temperature were, respectively, manually and automatically held constant, and the vacuum chamber was continuously pumped.

(vi) Evaporation was terminated by cutting the source current. After allowing the chimney to cool to 50°C, air was admitted to the vacuum chamber.

The films produced in this manner were, in general, pinhole free, adherent to the substrate, and varied in colour from brown, through orange, to a light yellow.

Due originally to Brunschweiler [149], and developed at Edinburgh University by Reid [150], this system compares favourably with Addiss', De Klerk and Kelly's, and the idealized system mentioned above in three aspects vital to the preparation of stoichiometric CdS films. Firstly, the sticking probabilities of Cd, S, and CdS molecules on the hot Ta walls of the vapour stream-substrate enclosing chamber were found experimentally to be low. Secondly, the relatively small volume enclosed probably gave a favourable ratio of Cd and S to residual gas vapour pressures in the vicinity of the substrates. Thirdly, the relatively high thermal conductivity substrates were in reasonable thermal contact with, and nearly totally enclosed by the chimney walls, and could therefore, with a

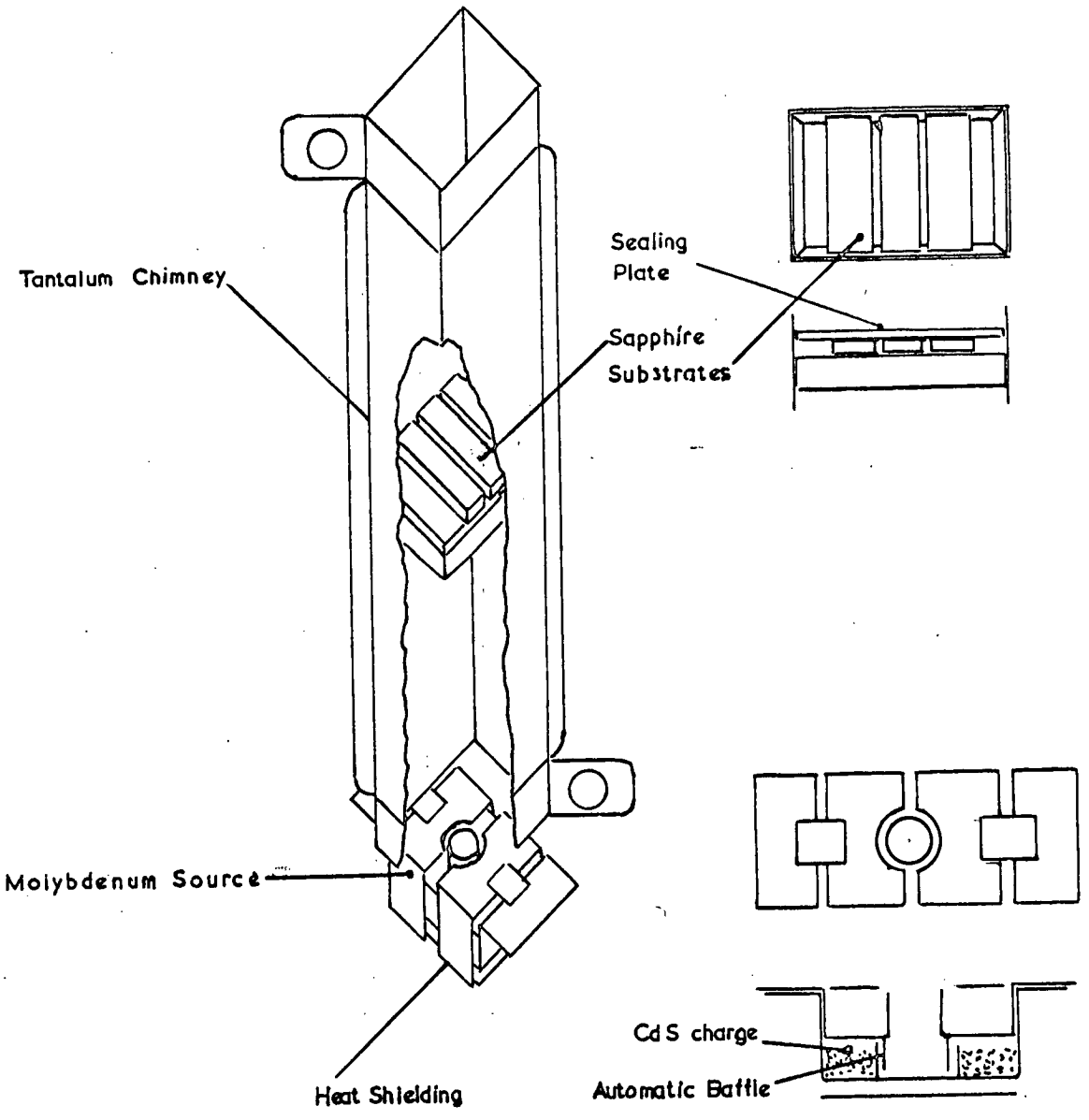
Tantalum Chimney
Sealing Plate
Sapphire Substrates
Molybdenum Source
Heat Shielding
Cd S charge
Automatic Baffle

FIGURE 5·1

high degree of confidence be assumed to be close to the controlled temperature of 193°C during evaporation. (Using a more conventional substrate heating system, Foster [151] discovered, in pathological cases, temperature differentials of up to 100°C between heater block and substrate face).

In spite of efforts to constrict the chimney mouth, some degree of leakage from the source-vapour stream-substrate system was inevitable. As a result of the (unnecessarily) large volume pumped, the difficulties involved in eliminating backstreaming from the Edwards diffusion pump, the undesirably high leakage rate of the vacuum chamber seals, and the unavoidably wide variety of materials evaporated in the plant, it proved, in addition, practically impossible to guarantee the "cleaness" of residual gases in the evacuated chamber. As an inevitable consequence, the interbatch reproducibility of the physical characteristics of films deposited in the apparatus suffered.

The coevaporation method so strongly advocated for the production of high quality CdS films by De Klerk [138] may best be regarded as an optimizable technique for native acceptor doping of the films during deposition. An equivalent technique, involving the coevaporation of CdS and S or Ag has been successfully optimized by Foster [151]. It is believed that coevaporation systems hold no inherent advantages over suitably designed monosource systems in the deposition stages of the preparation of high mobility CdS films.

5.5 POST EVAPORATION HEAT TREATMENT OF VAPOUR DEPOSITED CdS LAYERS

A variety of attempts to control the photoelectronic properties of vapour deposited CdS thin films are reported in the literature. These range from the evaporation of dopant films onto the film surface, through firing of the films

in surrounds of CdS powder doped with the desired level of impurity, to the pre-evaporation addition of dopant to the source material. Meaningful tabulation of the results of investigations in order to establish the state of the art fails, firstly because of the frequent absence of evidence of effective standardization of either the vapour deposition or post evaporation heat treatment procedures employed, and secondly, because of the omission in many cases of secondary experiments essential for effective characterization of the photoelectronic properties of the films produced.

The apparently accidental discovery of CdS thin film recrystallization catalysis above a certain temperature ($\doteq 500^{\circ}C$) by thin (100 Å) Ag, Cu, Pb, Al, Bi, Zn and ZnS layers evaporated onto the film surface is due to Gilles and Van Cakenberghe [152]. Their observations were, in respect of Ag and Cu, confirmed and extended by Addiss [143], who noted the favourable effect of oxygen traces in the inert gas firing atmosphere on recrystallization. Increases in crystallite size of between three and four orders of magnitude are reported, Addiss's claims of post-recrystallization photosensitive Hall mobilities, (suggestive of impurity scattering) of the order of 70 cm^2/V sec are supported by the work of Dresner and Shallcross [153]. No convincing theory explaining the mechanism underlying recrystallization catalysis has yet been advanced.

In a further series of experiments, Dresner and Shallcross [128] successfully attacked the problems involved in preparing high Hall mobility CdS films. Deposited in a partially optimized, monosource, high vacuum (10^{-5} Torr) apparatus, the films were then fired at empirically determined temperatures for varying durations in pure, oxygen diluted and chlorine diluted static inert atmospheres. Dopants (Cu, Ag, In, Ga) evaporated onto the film surface or

added to the firing environment, were used either singly or in combination. They found (i) that oxygen traces accelerated recrystallization

(ii) that above 450°C Cu and Cl dopants diffused readily into the films

(iii) that precipitates of foreign additives formed sources of error in Hall mobility and other electrical studies

(iv) that with careful doping and firing, postevaporation heat treatments were potentially capable of yielding both photosensitive and semiconducting CdS thin films possessing Hall mobilities which approached those obtainable in bulk single crystals.

Access to a representative literature on thermal treatments in air, oxygen, nitrogen, argon, cadmium vapour and high vacuum may be obtained through the references cited by Boër, Esbitt and Kaufman [154]. Sulphur vapour annealing has been performed by Dresner and Shallcross [128].

Since 10^{-5} Torr vacuum annealing at temperatures up to 550°C for periods up to one hour in the apparatus shown in Figure 5.1 failed (See Chapter 6) to yield films of sufficient quality for the unambiguous observation of acoustoelectric interactions, alternative postevaporation heat treatment methods were evaluated.

The method, introduced by Boër, Esbitt and Kaufman [154], of the heat treatment of evaporated CdS layers in a flowing nitrogen atmosphere containing HCl and traces of oxygen and providing a transport of CdS and copper, was found to be attractive for at least three reasons. Firstly, systematic attempts to optimize the annealing procedure are clearly described. Secondly, the flow method employed incorporates potential mechanisms for the simultaneous

reduction of native astoichiometries introduced during deposition, for the controlled incorporation of compensating Cu and Cl atoms in the lattice, for the catalysis (due to the presence of Cu) of recrystallization after the method of Gilles and Van Cakenberghe [152], and for the thermal annealing of mechanical strains present in the as deposited film. And thirdly, confidence may be attached to the accuracy of their secondary experiments characterizing the photoelectronic properties of the recrystallized films produced *, which revealed an unusually low (for thin films) trap density.

The apparatus used in this study for the postevaporation heat treatment of CdS layers is illustrated in Figure 5.2. After due consideration of the optimization data given by Boër et.al., the following experimental procedure was adopted.

Up to 15 pinhole free, evenly CdS coated substrates were placed, axially, evenly spaced, face upwards upon a CdS:Cu powder layer, formed by spreading 100gm CdS powder, doped with an empirically determined weight of fine Cu powder, along the central 50cm of a 100cm long, 36mm i.d. quartz tube.

---

* It is perhaps indicative of the experimental state of the art, and the pressure upon available resources, that Hall mobility measurements are reported for only three layers (138, 220, 225 $cm^2/Vsec$ respectively at room temperature, 150ft-c white unfiltered light). Detailed photoelectronic measurements were performed on only one of these layers (225 $cm^2/Vsec$). The results of further experiments performed on layers recrystallized in the B-E-K apparatus were reported by Boër, Feitknecht and Kannenberg [155].

After sealing the tube ends with gas inlet and outlet fixtures, the tube was symmetrically positioned in a ≐ 50cm long, preheated * tubular furnace. A 3.6 litre/min argon supply was immediately connected to the gas inlet.

During the warm-up period, in order to compensate for the heat lost to the cold quartz combustion tube, the furnace was run under full power (1.25 kW) until a centrally placed, axial, sheathed thermocouple indicated an internal gas temperature of 570°C ** Thermal lag alone carried the indicated gas temperature to a peak of 620°C over a further (7 minute) period, at which stage temperature control was passed to an automatic controller.

Thermal "equilibrium" having been established in the vicinity of 620°C, O_2 was bled at a constant rate (≐ 10cc/min) into the 3.6 litre/min argon stream. A constant proportion (between 4 and 10 per cent) of the mixture was directed through a wash bottle containing a measured amount of 37% aqueous HCl, and returned to the original gas stream immediately prior to its entering the annealing oven.

Heat treatment was continued for an average period of 35 minutes, after which the O_2 and HCl sources were removed and the oven allowed to cool to room temperature under a slightly reduced argon flow. The heat treated films were then removed from the tube, examined, and if unrejected, stored either in a dessicator, or whenever possible, under high vacuum prior to the evaporation and low temperature annealing in of indium contacts.

---

* 600°C wall temperature.

** 7 minutes after introducing the combustion tube.

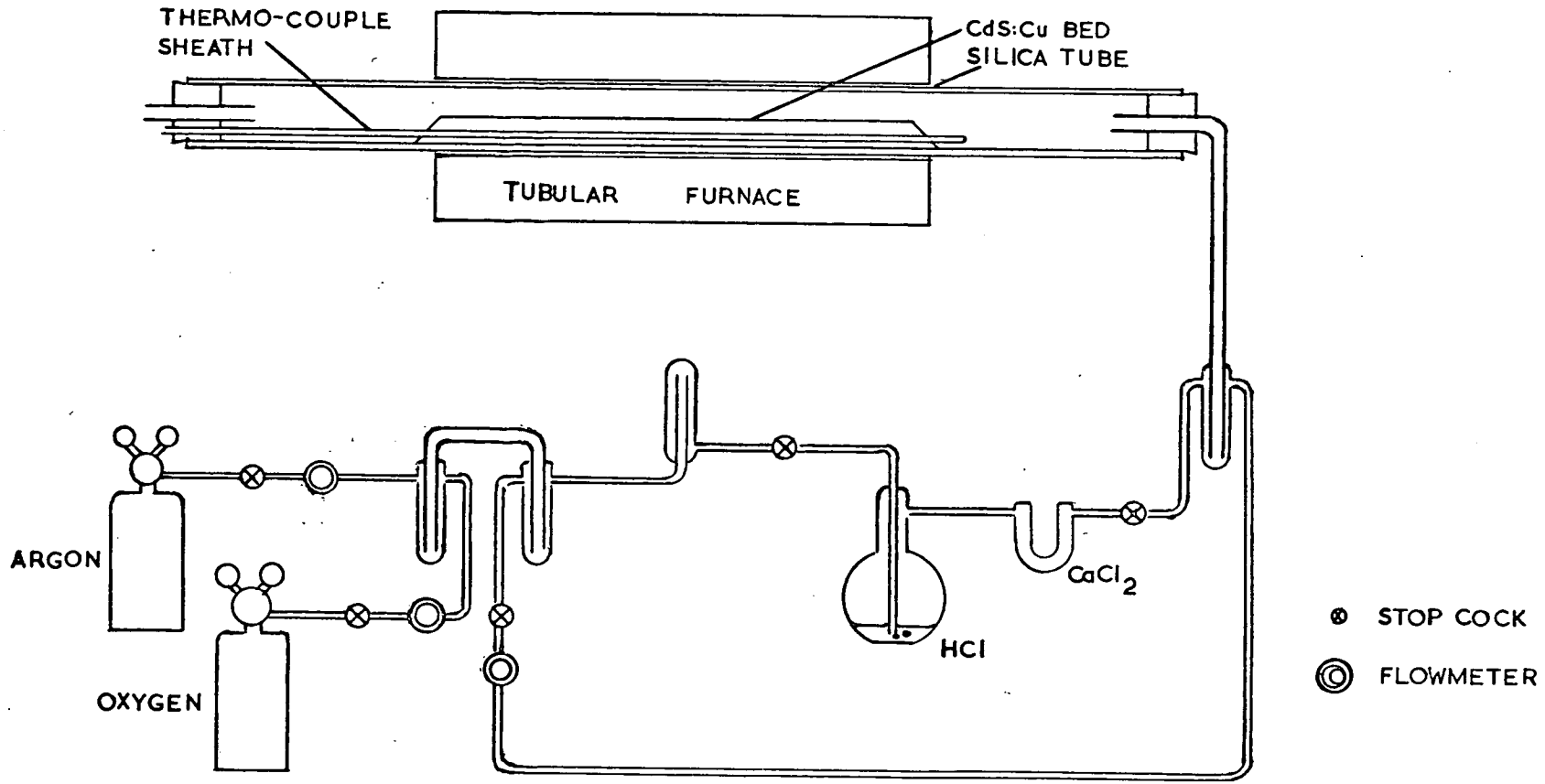
THERMO-COUPLE
SHEATH
CdS:Cu BED
SILICA TUBE
TUBULAR FURNACE
ARGON
OXYGEN
HCl
CaCl2
STOP COCK
FLOWMETER

FIGURE 5·2

A high proportion of the films treated in this manner were rejected as unsuitable for further study on the grounds of localized peeling, crazing, pinholing, discolouration (suggesting gross precipitation of a second phase), powder grain incorporation, and substantial loss of the vapour deposited film. The remaining films (20% yield) ranged in colour from orange yellow to yellow, and showed some evidence of localized, structurally faulty, crystal growth when viewed through crossed polaroids in a standard laboratory microscope.

The chemistry of the interactions promoting improvements in the photoelectronic properties reported by Boër, Esbitt and Kaufman [154] and confirmed, to some extent, in Chapter 6, is undoubtedly complex. Since no evidence exists to support any extension of the broad theoretical outlines proposed by Boër et.al. [154, 155], no such extension will be attempted.

5.6 STRUCTURAL STUDIES OF CdS THIN FILMS.

Basic structural faults in CdS layers may in some cases differ markedly in their origins and behaviours from the behaviour of their bulk CdS structural equivalents. Interfacial dislocations, for example, may arise either as a result of atom disregistry during epitaxial deposition (in which case they may be regularly spaced) or during thermal cycling, as a result of mismatch between the expansion coefficients of film and substrate. Further sources of structural imperfection may be sought, as in faulted bulk crystals, in accidents of nucleation and the (poorly understood) kinetics of crystallite growth. Gross departures from the minimum energy configuration are apparently inevitable in thermally cycled films and the high structual defect density may, at least in part, be regarded as a necessary consequence.

Access to the literature on the crystallography of CdS evaporated films may be obtained through the references cited by Foster [151]. As might well be expected, the fine structures of films are reported to be complex functions of the substrates used, the many deposition and postevaporation heat treatment parameters involved, and the thermal histories of the films. Circumstantial evidence exists in support of the hypothesis that a growth completion between, in most cases randomly oriented nucleates, is in some way responsible for the apparently natural tendency of the "c" axes of vapour deposited CdS crystallites to be oriented within a few degrees of the normal to the substrate plane. It is possible, on the basis of observations of Foster et.al. [156], to postulate that under certain circumstances, growth on one face (the "Cd" face) is particularly favoured.

Such a postulate would lead to an explanation of the fortunate fact, established by the successful operation of CdS vapour deposited transducers, and a prerequisite of any conceivable acoustoelectric thin film device, that CdS crystallites are predominantly "one way up" as opposed to being randomly inverted with respect to one another.

Postevaporation heat treatments have been found [129] to provoke two important crystallographic changes, the first involving a gross increase in crystallite dimension, and the second involving tilts of up to 25° of the c-axis away from the substrate surface normal. Both phenomena may be symptomatic of a search of the system for a minimum energy configuration, and neither directly affects the criteria defining the acoustoelectric activity of surface waves in the system. (Since only one degree of orientation is involved, the CdS-on-Sapphire system would retain effective transverse isotropy for tilts of this order).

The tendency of *Cu, *Ag and *O to congregate at, initiate, or decorate structural faults was noted in Chapter 5, section 3.* Fault initiation as a result of native atom, second phase, and foreign atom microprecipitation is to be expected. It is further conceivable that impurities incorporated during firing or at room temperature may diffuse more rapidly down the intercrystallite grain boundaries. Finally, it is conceivable that structural faults may be stabilized by the presence of impurities. It is concluded that, in unstabilized CdS films, it is reasonable to expect a high degree of astoichiometry in the immediate vicinity of structural faults and thin film grain boundaries. In terms of an equivalent electrical circuit, a thermodynamically unstabilized CdS film may be regarded as a two dimensional aggregate intimately connected by a randomly distributed resistor-junction mesh structure, which may either support, short circuit or oppose conduction through the CdS crystallites. For the successful operation of high field non channel conduction thin film devices of the class proposed in this study, it is imperative that the microscopic short-and open-circuit conditions are suppresed.

5.7 FIELD INDUCED INTERCRYSTALLITE INSTABILITIES IN CdS THIN FILMS.

Since the high field behaviour of such complex structures as randomly repetitive NIPIN junctions are neither per se under study nor fully understood, the following remarks will be confined to a description of how they might

---

* Direct evidence of the selective precipitation of Cu in a CdS film heat treated in a manner identical to that described above, was obtained by Boër et.al. [155].

originate during treatment of the CdS thin film, and to an elementary discussion of the global effects upon conduction introduced by their presence.

5.7.1 REPETITIVE M-S-M AND P-N-P STRUCTURES.

Copper generally forms a blocking contact to CdS, and Cu_2S is ptype. Both materials may precipitate from solid solution upon cooling at structural faults, superimposing on the film an either complete or particulate matrix of Cu.(Cu_2S). The former case is too degenerate to warrant discussion. In the latter case, exhaustion barriers partially ring each crystallite. An externally applied voltage drops mainly across the barriers, widening those reverse biased, and narrowing those forward biased. Double tunnel injection may occur at the former, diffusion at the latter, and radiative recombination may be observed at both [157]. Increase in the external voltage may lead to internal field emission, carrier accelaration, impact ionization from traps and eventually, to catastrophic breakdown should the internal series resistance provided by the crystallites fail to arrest the process.

5.7.2 REPETITIVE N-I-N STRUCTURES.

Such structures may result from incomplete formation of the film, alternatively from the diffusion of (say) $O^{=}$ down the crystallite boundaries. The breakdown sequence is similar to the above. These structures may readily be simulated by drawing a fine scratch across an otherwise well-behaved film.

The above, and other junction structures, may occur in combination or permutation (N-I-P-I-N; N-I-M-I-P-I-N *etc*) randomly throughout a film, and

may give rise to a bewildering variety of global film current voltage characteristics.

The electroluminescent literature, as reviewed by Morehead [157], provides an excellent introduction to the behaviour of similar, if somewhat simpler structures produced by design rather than by accident. The scanning electron microscope may eventually prove a useful tool for the examination of accidental junction structures in thin film CdS.

The phenomenon of second breakdown, (as reviewed for transistors by Schafft et.al. [158]) may also be expected to occur in thin imperfect films. Imagine a voltage dropping across the boundary between two crystallites. If the current density in a small area increases statistically, a hot spot may result. If this spot give rise to an increase in local current larger than the original fluctuation, localized thermal runaway will occur unless arrested by the internal series resistance of the crystallites.

CHAPTER 6.

HIGH FIELD CHARACTERISTICS OF CdS THIN FILMS.

6.1 INTRODUCTION.

Unambiguous confirmation of the theoretical prediction - that in transversely isotropic CdS-on Sapphire systems, acoustoelectric interactions contribute significantly to the attenuation of shear vertical surface waves - is clearly a matter of priority.

Broadband coherent surface wave experiments are undermined by the high insertion losses and inherently narrow bandwidths of conventional surface wave generating devices [159] (Chapter 6, section 2). The hazards frustrating demonstration of thin film surface wave photodependent, field dependent attenuation effects (after Hutson et.al. - see Chapter 1, section 1) are further accentuated by the absence of control over the electronic properties of thin film CdS.

Haynes-Shockley-type time-of-flight experiments are capable of yielding evidence of bulk wave acoustoelectric interactions in CdS platelets (see Le Comber et.al. [160]). Similar charge injection techniques may in future be employed in the study of high field transpost in thin film coplanar devices. Apparatus for the study of drift mobility in semiconducting glass sandwich structures, currently under development at Edinburgh University, might eventually prove adaptable to such a study. However, no technique for the investigation of surface drift mobility is at present available.

Multiple-band pattern illumination of photoconducting (low gain rate) CdS single crystals has recently been reported to give rise to high field current oscillations of period strongly related to the period length of the band pattern and to the velocity of shear waves in the crystals [161]. Such techniques may eventually prove valuable in investigations of dispersion and acoustoelectric coupling in photosensitive, piezoelectric thin film waveguides.

Effective thermodynamic stabilization is prerequisite to any sophisticated, high field, solid state transport investigation (see, for example, Chapter 5, section 7). Since current deposition techniques are unstabilized, experimental efforts were necessarily confined to relatively unsophisticated investigations of the global high field characteristics of available polycrystalline CdS thin films. Thermal acoustic lattice noise was relied upon to present a broadband surface wave input to the films and emphasis was placed on observation of the macroscopic effects of acoustoelectric noise amplification.

6.2 EXCITATION OF SURFACE WAVES ON THE ‹001› PLANE OF SAPPHIRE.

The comb excitation of surface waves on the basal plane of sapphire was performed in order both to verify the existence of such waves and to lay foundations for a study of surface wave photodependent, field dependent attenuation in a CdS-on-Sapphire system.

Two Sokolinskii-type combs were fabricated from 10 x 10 x 1.5 mm^3 duralumin plates, lapped to parallelism and cut (using a 6.7 thou. saw) on one face with a series of forty, 169 μ deep, parallel grooves, set at a mean period of 170 μ. A 0°X cut quartz transducer was "Salol" * bonded to the unruled face

* See footnote * on following page.

of each comb. The resulting structures were mounted in a parallel configuration in pressure contact with a ruby substrate. (Figure 6.1.A).

Longitudinal waves transmitted into the generating comb** launched surface waves of wavelength equal to the comb period by creating periodic stresses on the ruby substrate. After travelling approximately 1 cm across the basal plane surface waves launched longitudinal waves into the receiving comb which, in turn excited the receiving transducer. The output signal*** was amplified (Arenberg P.A. 620; Arenberg W.A. 600 E), video detected, and displayed on the screen of a standard HP 140 A oscilloscope (Figure 6.1.A).

Representative oscillograms are given in Figures 6.1B and 6.1C. The former shows the damping effect of an alcohol drop placed between transmitter and receiver on the substrate surface. Evaporation of the alcohol gradually restored the delayed signal, thereby illustrating its surface wave origin. Notice, in the latter figure (6.1C) trapezoidal distortion of the square R.F. input pulse. This feature is common to all periodic methods of surface wave generation and detection, and originates in oscillatory settling processes beneath the gratings. The oscillatory settling time is given approximately by $2L/c_R$. (where 2L is the total grating length in the direction of propagation and c_R is the surface wave velocity.)

---

* Phenyl Salicylate. Melting point 40°C. The tendency towards supercooling was suppressed by thermally controlling the bonding environment, and agitating the bond edges with a fine brush.

** The generating transducer was excited in inertia drive in the thirh harmonic by an Arenberg. P.G. 650 C (600 V_{max} peak-to-peak R.F. pulses).

*** Typically 95db down on the input signal.

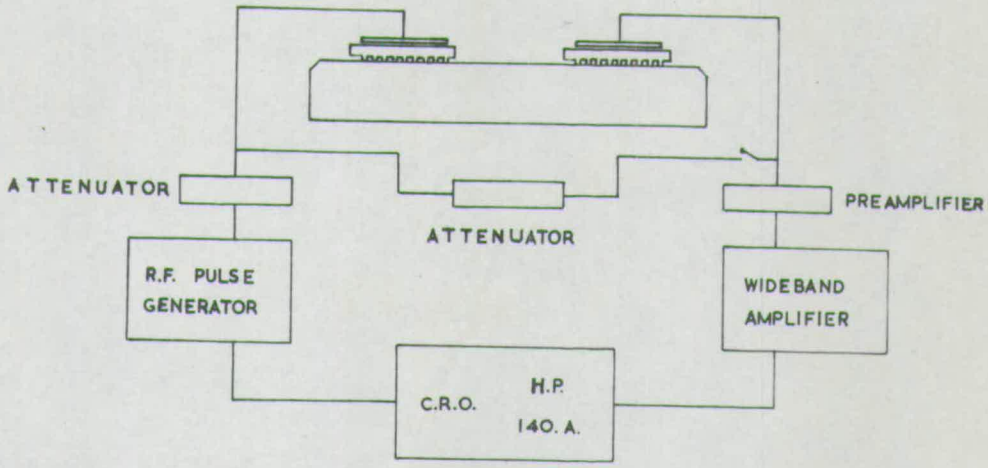

A.

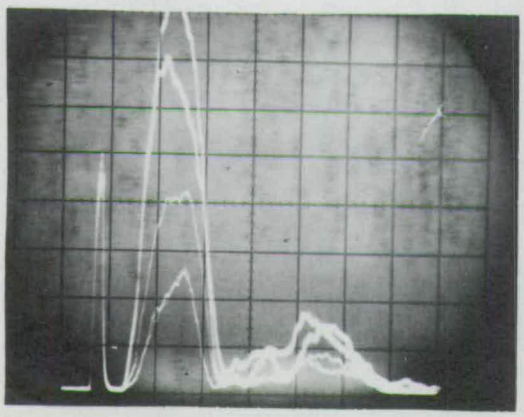

H 5·0 μsec/div.

B.

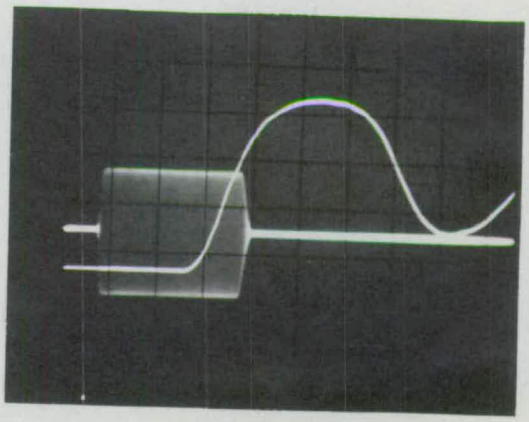

H 1·0 μsec /div.

C.

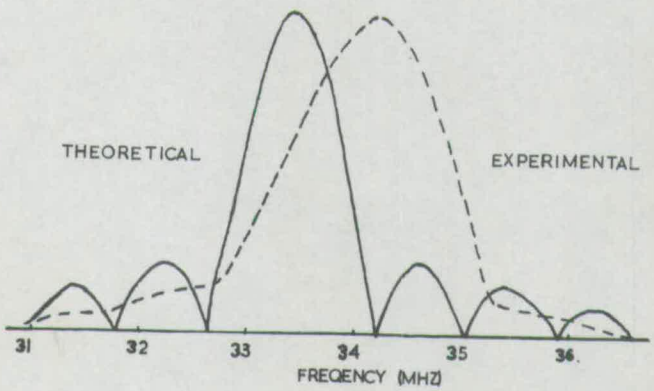

D.

FIGURE 6·1

Inherent bandwidth restrictions of comb generation-detection techniques are discussed by Viktorov [159]. Theoretical and experimental frequency response curves of the ruby surface wave system employed in these experiments are plotted in Figure 6.1D. A numerical search for response of the system at even harmonics of the fundamental comb frequency failed. It is postulated that the surface waves detected by Artz et.al. [162] in the second harmonic mode were generated by periodic asymmetries in the teeth of their combs.

Transmitter-receiver tooth parallelism was achieved by "tuning" both receiver orientation and carrier frequency onto the maximum surface wave signal amplitude. By imposing an artificial upper limit to the sensitivity of the receiver, multiply-reflected bulk waves frustrated attempts to accurately tune the receiving comb to detect 34 MHz surface waves transmitted through 0.5 to 5 μ thick, 2 mm wide vacuum annealed CdS thin film strips. As a result, no meaningful estimate of the attenuation introduced by the vapour deposited films could be made. In common with the earlier 15 MHz CdS-on-Silica experiments performed by R.M. White, no photodependence of the video-detected waveform was observed.

Three explanations for the excessive surface wave damping introduced by the layers may be advanced. Firstly polycrystallinity and surface roughness may have resulted in the distributed generation of bulk waves. Secondly, attenuation present may, effectively, have given rise to a "forbidden" direction of propagation by asymmetrically distributing positive and negative signs among the imaginary parts of the roots to the sextic governing wave propagation in the halfspace (Equation 2.4.1). Thirdly (after R.M. White [163]) acousto-electric interactions may have been responsible for the attenuation observed.

The third explanation is considered unsatisfactory in view of the apparent absence of detected video waveform photodependence.

6.3 HIGH FIELD CHARACTERISTICS OF CdS THIN FILMS.

6.3.1 EXPERIMENTAL DESIGN CONSIDERATIONS.

In the absence of coherent acoustic surface wave transmission, the observation of thin film acoustoelectric interactions must depend on the amplification of thermal surface wave noise which, in turn, requires the attainment of carrier drift velocities greater than the velocity of the surface waves.

Substantial mobility enhancements at low temperatures are, apparently, restricted to CdS single crystals of the highest purity. Since the CdS films under investigation inevitably contained high impurity concentrations, and since temperature reductions correspond to reductions in the level of acoustic noise input to the system, no advantages were to be gained by conducting experiments at low temperatures. Accordingly, no cryogenic apparatus was constructed.

Considerations of specimen inhomogeneity, photosensitivity, surface roughness, and surface wave incoherence weigh heavily against the direct observation of acoustoelectrically amplified flux by optical scattering or coherent surface wave detection techniques. Efforts were, accordingly, devoted solely to the observation and interpretation of the non-ohmic consequences of thermal acoustic surface wave noise amplification (Chapter 4).

6.3.2 EXPERIMENTAL TECHNIQUES.

Parallel sided, eight mm wide, masks screened the central portion of each film during the evaporation (conducted at the lowest achievable residual vapour pressures $\doteq 5 \times 10^{-6}$ Torr) of two coplanar indium strip contacts onto the (occasionally ion bombarded) surface of each film. The contacts were designed to be of sufficient area to ensure a low localised current density, and spaced sufficiently far apart to permit both low gain rate incubation of potential acoustoelectric instabilities and probing of localized field distributions. The contacts were annealed, either in air or in argon, to assist the diffusion of indium donors into the films.

For the purposes of high field investigation, the specimens were mounted in turn on the spring loaded platform of a high voltage testing jig (Figure 6.2). Uniform illumination was delivered through a variety (bandgap OG1, water cell, neutral density) of filters from a 100 watt, tungsten filamented, variac-primatran driven commercial projector lamp.

Monitoring the voltage developed across a 1 kΩ series resistor, noting carefully any irregularities, and immediately, if so indicated, terminating the experiment, the specimens were generally subjected to voltage controlled pulses of gradually increasing amplitude (< 10 kV), slow rise time (1m sec) comparatively rapid fall time (1 μ sec), and two milliseconds plateau, at repetition rates of the order of one pulse per second. (Figures 6.3, 6.4)

Threshold fields (typically 7-10 kV/cm) for interelectrode surface breakdown were found to decrease with increase in illumination intensity, ambient relative humidity, and film age. While rarely of itself completely catastrophic, each

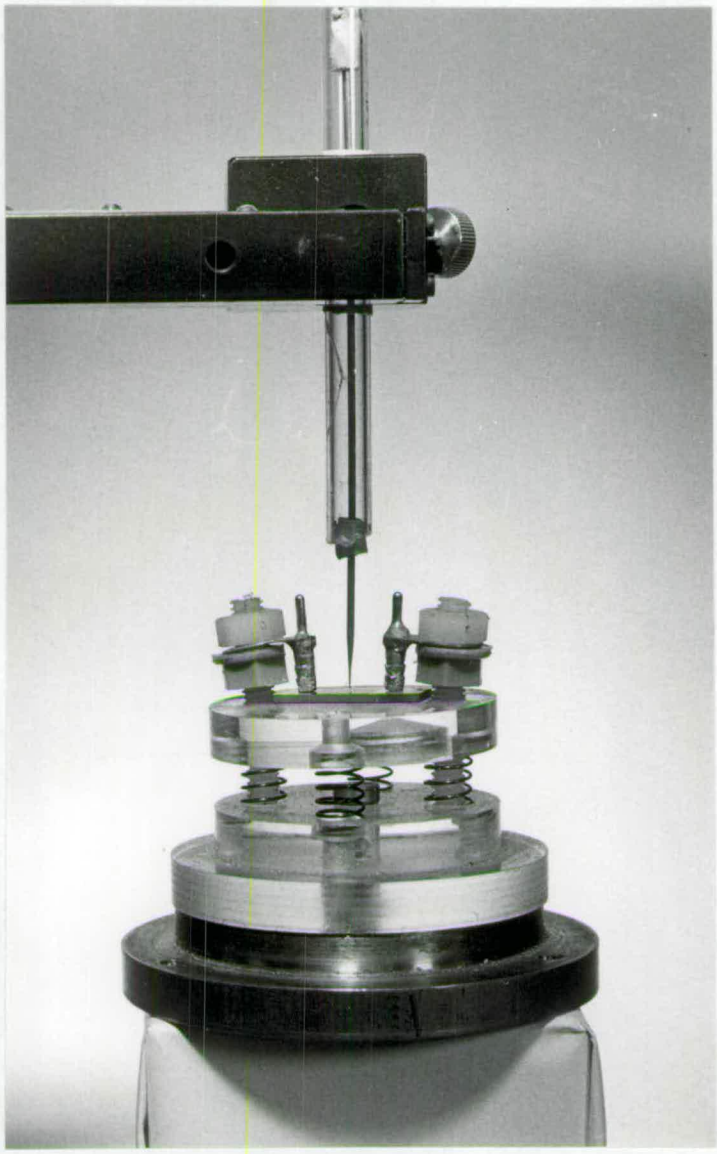

Figure 6.2 High field jig with probe in position.

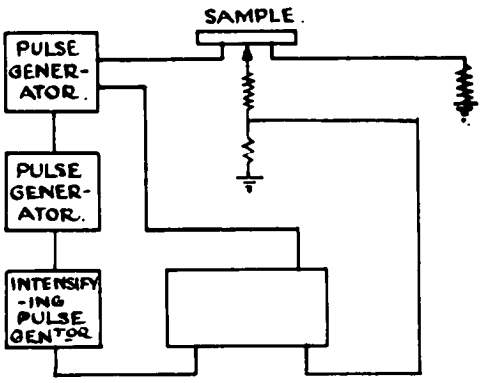

PROBE VOLTAGE VS. APPLIED VOLTAGE

A.

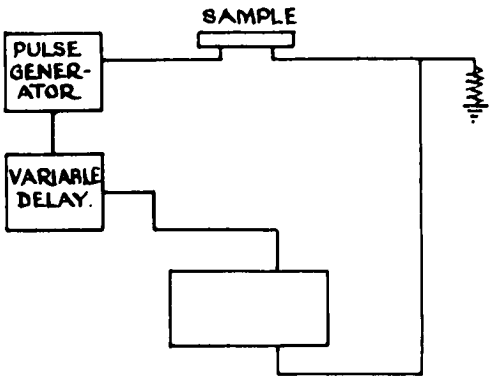

CURRENT VS. TIME

B.

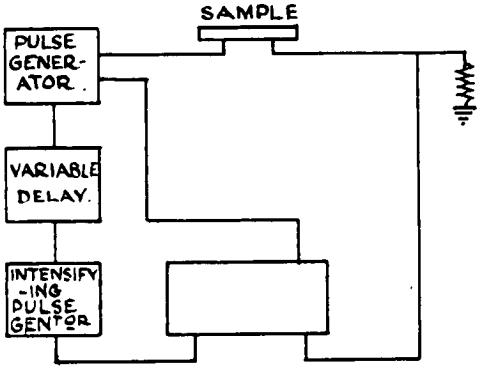

CURRENT VS. APPLIED VOLTAGE

C.

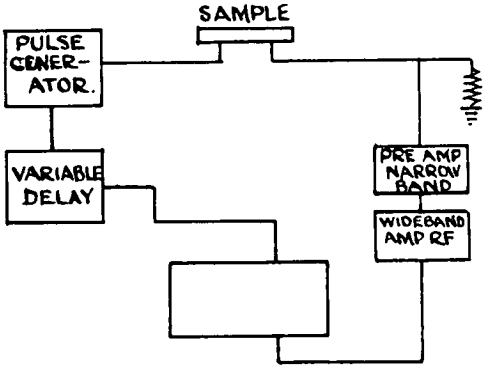

HIGH SENSITIVITY
CURRENT VS. TIME

D.

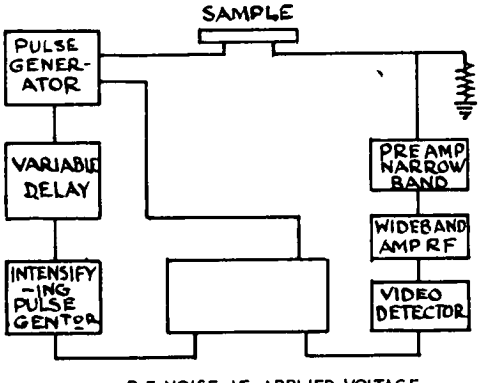

R.F. NOISE VS. APPLIED VOLTAGE

E.

AUXILIARY CIRCUITRY

FIGURE 6·3

breakdown event appeared to increase the probability of succeding events, and, as evidenced by the appearance of small black "scorch" marks, degraded film uniformity, thereby introducing unnecessary ambiguities into the interpretation of subsequent experimental results. Specimens exhibiting any tendency towards interelectrode breakdown at applied voltages of up to 7 kV were immediately rejected as being unsuitable for further investigation.

Using an indium tipped, high voltage insulated, tungsten needle mounted in a three dimensional manipulator, a search was made for anomalous field distributions in the vicinity of either contact (Figure 6.3). Field anomalies, suggestive of non-ohmic contact processes, were found in a disturbingly high proportion of the samples examined (50%), and underline the urgent necessity for further research into the behaviour of metal-to-polycrystalline-CdS junctions.

After treating non-ohmic contacts by carefully melting a thin slice of indium placed between the offending contact and the contacting stub of the testing jig, the field distribution search was repeated. In a number of cases the anomaly disappeared. Specimens exhibiting persistent non-ohmic contact effects were rejected as unsuitable for further study.

A further search was made for field dependent current instabilities under varying insensities of both uniform and non-uniform illumination (Figure 6.3). Photoresponse characteristics, while not directly under study, were noted, and the occurrence of coherent current oscillations of any amplitude at any frequency up to 20 MHz investigated in depth under a variety of pulsed high voltage, continuous E.H.T. and non-uniform carrier concentration conditions (see Chapter 4, section 7).

Current-voltage characteristics were recorded as a function of uniform illumination intensity. (Figure 6.3). Upon observation of high field photocurrent saturation, current vs. time, current vs applied voltage, and probe voltage vs. applied voltage characteristics of the specimen were investigated in depth, in an attempt to diagnose the mechanism underlying the observed sublinearity.

6.4 CURRENT IRREGULARITIES NOT ASSOCIATED WITH ACOUSTOELECTRIC INTERACTIONS.

During the course of investigation a bewildering variety of nonohmic, instability effects were observed. Many of these effects were poorly amenable to investigation, and, in terms of yielding evidence of acoustoelectric surface wave interactions, devoid of interest, being indicative only of the pathological quality of the majority of specimens investigated. A number of instability effects were however unusual, and a brief selective discussion may be of interest.

The capacitative contact effect, frequently observed upon rapid termination of the applied voltage pulse, is illustrated in Figure 6.4B. Potential probing frequently revealed the presence of associated high field concentrations in the vicinity of the positive contact, suggesting as one possible model chemisorbed surface layers giving rise to blocking barriers at the indium-CdS interfaces.

Characteristic features of the voltage dependent negative spike effect observed only once, (while testing a 6μ thick, vapour deposited, vacuum annealed, photosensitive film) included:-

(i) a time of occurence after application of the voltage pulse strongly dependent upon the applied voltage amplitude (Figure 6.4C)* but only

* Applied voltage reading, from top to bottom, 8.5 kV, 8.2 kV, 7.7 kV, 7.2 kV, 6.8 k

weakly dependent upon illumination intensity (and hence power input to the film)

(ii) a rise time and fall time independent both of applied voltage and illumination intensity

(iii) an amplitude strongly dependent upon illumination intensity but barely affected by localized shading of the contacts.

Figure 6.4D is a 28 shot photograph (taken at an applied voltage of 9.4 kV) illustrating the high field time stability of the negative spike. A single interelectrode breakdown event at 9.5 kV resulted in total disappearance of the phenomonon. No completely satisfactory explanation concerning its origin can be advanced.

The oscillating contact effect, originating probably in tunneling through a metal-insulator-metal cum heavily doped n-type semiconductor sandwich formed presumably by prolonged exposure of areas of indium to the atmosphere, is illustrated in Figure 6.4E (which shows, in addition, the slight effect on oscillation frequency of decreasing the level of control illumination). Since the phenomenon was easily detectable and could be removed by careful abrasion or localized heating, it proved interesting rather than troublesome.

Figure 6.4F shows four consecutive single shot current-time traces (taken at a set (7.5 kV) voltage level and separated, for clarity, by varying the oscilloscope trace position). The random current surges, typical of those observed in practically all non-post evaporation heat treated films, were often accompanied by the emission of visible (green-blue) radiation from minute spots in the film. Since the random current surges could readily be simulated by drawing fine scratches across the direction of current flow in an other-wise

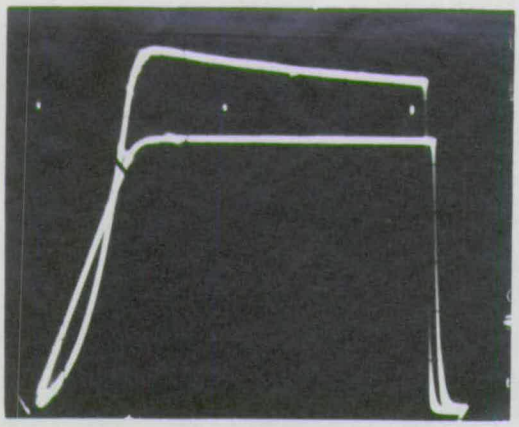

TYPICAL I,V, TRACES

A. H 0·2 msec/div.

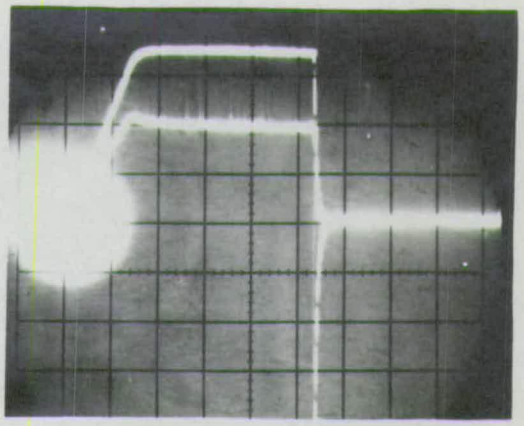

CAP. CONTACT

B. H 0·5 msec/div.

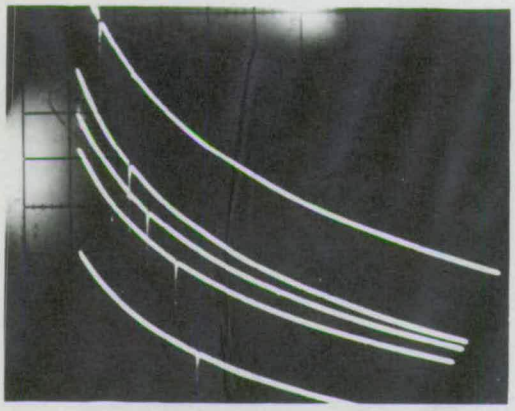

FIELD DEP., NEG. SPIKE

C. H 20 μsec/div.

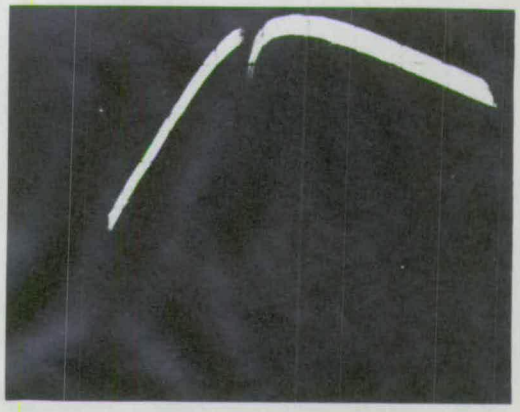

STABILITY, NEG. SPIKE

D. H 5·0 μsec/div.

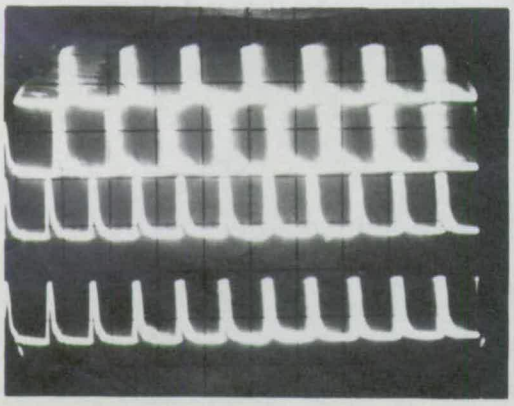

OSC. CONTACT

E. H 1·0 μsec/div.

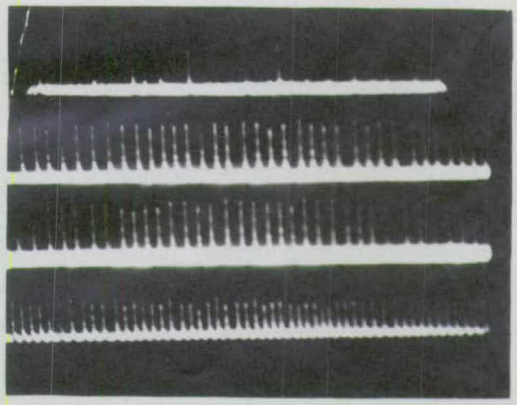

INTERCRYST. CHATTER

F. H 0·5 μsec/div.

FIGURE 6·4

stable film, they were attributed to intercrystallite N I N breakdown events (Chapter 5, section 7.2).

6.5 SWITCHING AND ASSOCIATED CURRENT OSCILLATIONS IN A VACUUM HEAT TREATED FILM.

Random switching effects, and associated current oscillations (reported in Electronics Letters, 3 (6) 1967) were observed while high voltage testing an even orange-yellow 4.7 μm thick specimen which had been post depostition vacuum annealed at 470°C, 1 x 10^{-5} Torr for 30 minutes before being cooled to room temperature and exposed to the atmosphere. Dark resistivity of the film was estimated at 6.5 x 10^{3} Ω cm, light resistivity at 3.2 x 10^{3} Ω cm. X-ray diffraction showed the crystals to be predominantly ⟨001⟩ oriented.

Pulsing the film with slow rise time, 2msec. length, variable amplitude voltage controlled pulses, the film resistance was observed, above a threshold pulse amplitude ($V_{t1} \doteq 3.4$ kV) to switch occasionally to a value between 90% and 96% of its preswitch value, and to remain in this switched condition until termination of the voltage pulse (Figure 6.5A. Upper trace: Voltage; middle trace: Current; lower trace:Switch detail).

Switching was characterized by a probability of occurrence which increased rapidly with increasing voltage above V_{t1}, by a switching time of less than 100nsec, by its repeatability with succeeding voltage pulses, and by the randomness of its amplitude within the stated limits, irrespective of voltage pulse amplitude (Figure 6.5E). V_{t1} did not appear to be markedly sensitive to the level of illumination.

Above a second threshold ($V_{t2} \doteq 3.9$ kV) in both uniform darkness and uniform light (the latter only occasionally) small amplitude (3μA peak to peak) undamped coherent oscillations were observed in the current trace after switching. No evidence of oscillation could be found after termination of the voltage pulse or prior to switching of the specimen resistance. The oscillatory waveform varied from quasi-triangular to quasi-sinusoidal with increase in voltage (Figure 6.5B).

Frequency (which increased slightly with increasing voltage) and increasing illumination intensity, was observed to cover a fairly wide band (6-7 MHz).

A strip of the specimen, adjacent and parallel to the positive contact, was shaded in an attempt to deliberately induce an acoustoelectrically unstable carrier distribution (see Chapter 4, section 7). As before, switching occurred. Oscillations of similar waveform and waveform voltage dependence were observed on the switched current trace. These oscillations were found to have far greater frequency stability than in the uniformly illuminated case, and were typically of approximately double the amplitude. Amplitude modulation of the oscillations at up to 3 MHz, reminiscent of the acoustoelectric beating effects described by Chun [164] was found to occur upon increasing aparallelism between the parallel diffused indium contact edges and the shading strip edge (Figure 6.5D).

In both light and dark, oscillation amplitude was found to be insensitive to changes in applied field. Rapid variation of frequency with variation in applied field was observed with the specimen differentially illuminated. The frequency/average field characteristics of the specimen are plotted in Figure 6.5E, (with variation in shaded strip width as a parameter).

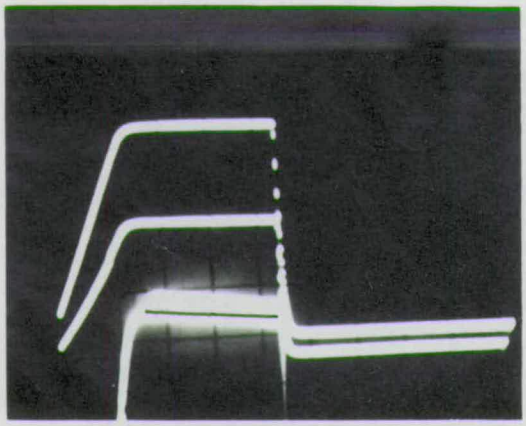

OSC. SWITCH EFFECT

A. H 0·5msec/div.

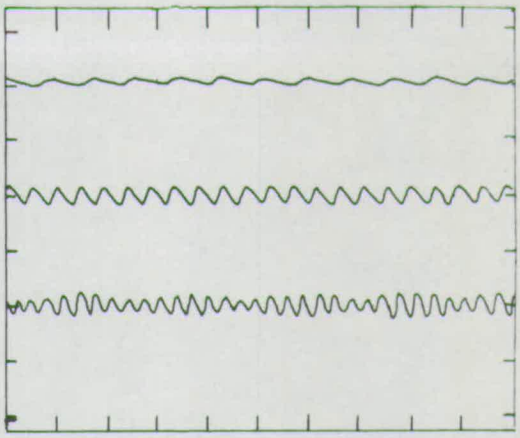

TYP. OSC. WAVEFORMS

B. H 0·2μsec/div.

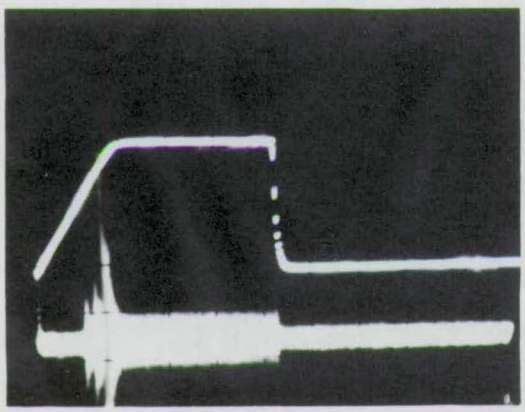

AMP. R.F. I COMPONENT

C. H 0·5msec/div.

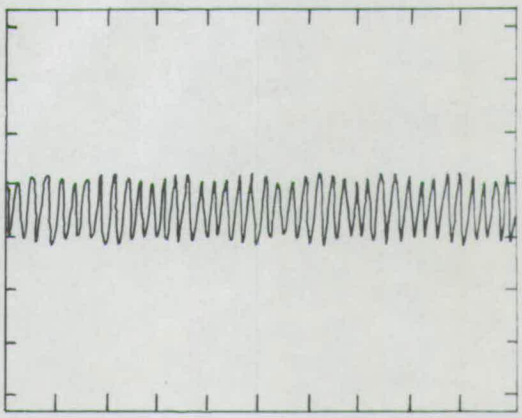

TRACE C (expanded time scale)

D. H 0·2μsec/div.

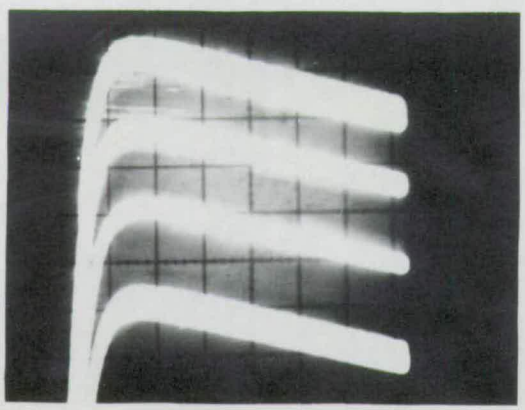

SUCCESSIVE I TRACES (V const > V_t)

E. H 0·2msec/div.

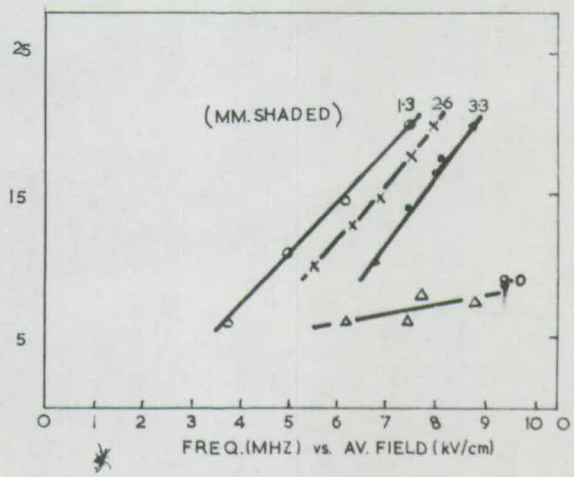

F.

FIGURE 6·5

It is believed that macroscopically distributed "bulk" interactions were responsible for the oscillatory phenomena observed. It is known that in a sufficiently imhomogeneous, low gain rate sample, acoustoelectric interactions may give rise to a wide variety of coherent current oscillations. While it might be possible to formulate an acoustoelectric model representing the situation, it is, bearing in mind the observations of Chapter 4, section 1 and Chapter 5, section 7, immediately apparent that any such model would be both complicated and difficult to defend in the face of competative models based, for example, upon high field tunneling, trapping, or impurity banding phenomena.

6.6 CURRENT SATURATION AND ASSOCIATED FIELD REDISTRIBUTION.

A detailed description of high field experiments on two particularly well behaved specimens is given in the following section. Both films were evaporated at 10^{-5} Torr (Chapter 5, section 4) heat treated at 620°C in the Boër-Esbitt-Kaufman apparatus (Chapter 5, section 5) and contacted with large area, parallel, diffused indium strip contacts (Chapter 6, section 3).

X-ray diffraction showed both films to be predominantly ⟨001⟩ oriented (Figure 6.6). The "crystallite size" of both specimens determined by scanning electron microscopy and confirmed, for one specimen by carbon replica micrography, was of the order of 2 microns (Figure 6.7). Optical examination showed both even, orange yellow films to be effectively free of pinholes and inclusions.

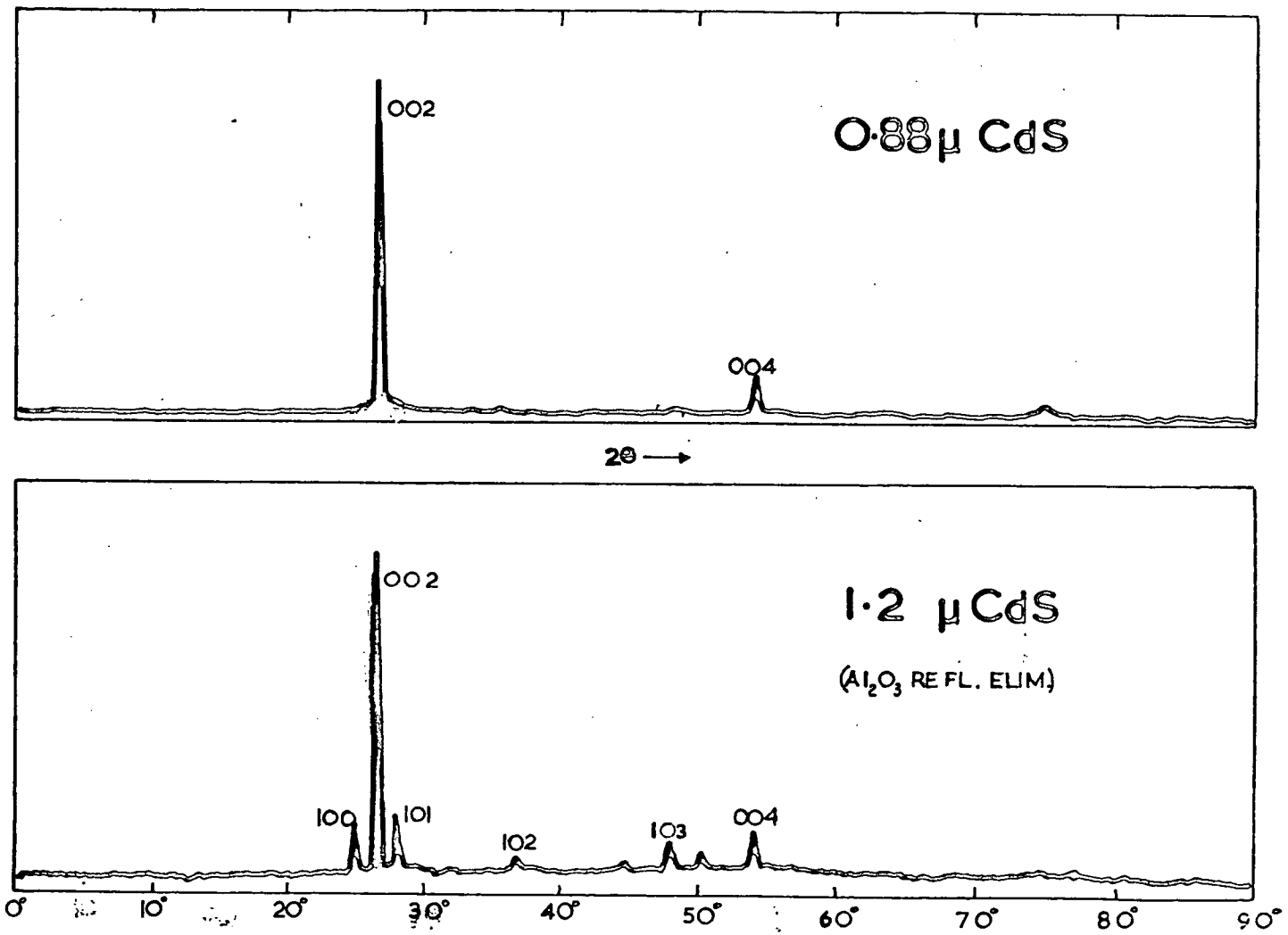
002
0·88μ CdS
004
2θ →
002
1·2 μ CdS
(Al2O3 REFL. ELIM.)
100
101
102
103
004
0°
10°
20°
30°
40°
50°
60°
70°
80°
90°

FIGURE 6·6

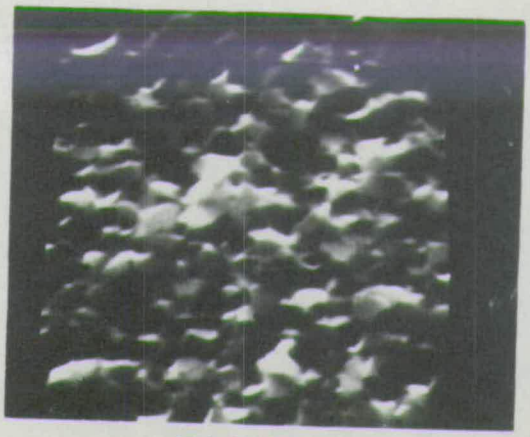

SCAN. ELECT. MICRO.

A. PRE HEAT-TREATMENT

24,000X

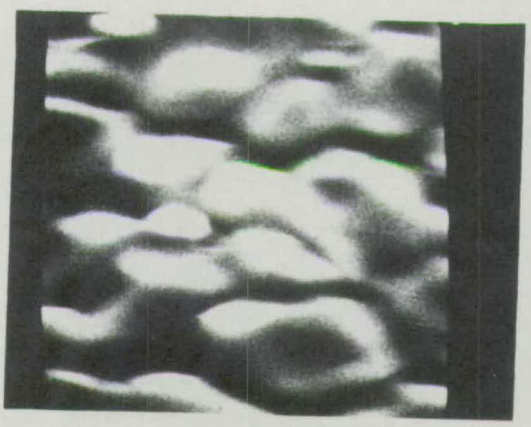

SCAN. ELECT. MICRO.

B. POST B.E.K HEAT-TREATMENT

10,000X

CARBON REPLICA

C. POST B.E.K. HEAT-TREATMENT

4,000X

FIGURE 6·7

Neither specimen displayed any detectable tendency towards current irregularity over the applied voltage range of interest (0 - 7kV) when voltage pulsed under uniform illumination. The potential drop was not localized at the electrodes, and at low fields appeared to vary approximately linearly (± 50%) with distance along both specimens. The light-to-dark resistivity ratio of both films was found to be greater than 10^4, and photoresponse speeds, while not accurately measured, were found to be unusually rapid (cf. [154]).

Power dissipation considerations permitted both pulsed (dotted line) and continuous (solid lines) I-V characteristics to be detected for the first specimen (0.88 microns thick) under a variety of uniform illumination intensities (Figure 6.8).

Concerning the current saturation observed above a certain voltage threshold (V_t), notice that for $V < V_t$ the sample acted ohmically, and that at high resistivities no saturation was observable. V_t appeared to be substantially independent of whether the voltage applied was pulsed or continuous. The sharpness of the "knee" increased with increasing illumination intensity, and its locus described a photo-Hall effect type curve.

Shading the anode (positive) half of the film in order to induce an acousto-electrically unstable carrier distribution (Chapter 4, section 7) a super threshold voltage was applied to the film. Large amplitude, 12.5 kHz, continuous current oscillations, of period apparently weakly dependent on the applied voltage, were observed. The large amount of jitter present frustrated attempts to internally trigger the oscilloscope in order to stabilize the displayed oscillatory trace. A detailed investigation of frequency and amplitude as a function of the three principal variables - applied voltage,

shade position, illumination intensity - was accordingly postponed in favour of an investigation by potential probing of the post-threshold field distribution as a function of applied voltage and uniform illumination intensity.

Two factors enter such an investigation. Firstly, meaningful probing of an extremely narrow thin film requires the use of a high precision, ultrahigh impedance potential probe. Secondly, a sample width comparable to the sample length introduces local probing complications in the form of a second dimension. These complications may effectively be removed by vapour depositing depositing, after McFee and Tien [109], a grating of thin parallel, indium strip contacts across the specimen (normal to the direction of current flow). While this arrangement might be ideal in the case of a freshly prepared crystal of thickness greater, by orders of magnitude, than the diffusion depth of indium, the difficulties inherent in being able to ensure adequate contact between the grating strips and a 0.88 micron thick, three day old thin film, without seriously disrupting the conduction or acoustoelectric interaction profile, will readily be appreciated.

Prior to narrowing the sample a preliminary investigation of the localized field distribution was made. During this investigation, the film was inevitably exposed to the atmosphere. As an unanticipated result (presumably) of gas adsorption during this exposure, an unmonitored tendency for V_t to drift to higher voltages was observed. The current saturation effect became less distinct and finally, two weeks after preparation of the film, disappeared completely. Heating the speciemn at 120°C under illumination in vacuum for 24 hours failed to reverse the deterioration, and an interpretable plot of the post-threshold field distribution was not obtained.

These observations were reported both to the Institute of Physics and the Physical Society Solid State Device Conference at Manchester in September 1967, and by invitation to the Sixteenth Meeting of the Thin Film Group at Electrical Research Association, Leatherhead in October 1967.

Bearing in mind the deterioration of the first sample, the second well-behaved specimen (1.2 microns thick) to exhibit photocurrent sublinearity above a threshold voltage was stored in vacuum while not directly under test. In order to avoid difficulties experienced previously in obtaining a one dimensional post-threshold field distribution plot, the width of the film was reduced, by scraping, to 1.35 ± 0.1 mm. (care being taken to avoid N-I-N structures along the film edges).

Current vs time characteristics for 0.15 μsec rise time, 4.0μsec length, and 0.1msec, 3msec length, variable amplitude square voltage pulses were compared. The time constant for post-threshold photocurrent decay to a steady state was found, in the latter case, to be of the order of 0.5msecs, suggesting field enhanced trapping as a possible mechanism underlying photocurrent sublinearity. Some evidence was however found, in the fast rise time case, for a more rapidly saturating interaction, with a time constant for photocurrent decay estimated at 0.25 μ secs. Detailed observation of this rapid decay was frustrated both by ring on the leading edge of the voltage pulse and by the voltage pulse's comparatively slow rise time (0.15 μ secs). The significance of these observations will be discussed in the following section.

Current-voltage characteristics of the 1.2μ thick specimen oscillographically plotted 1.5msecs after application of the variable amplitude 0.1msec rise time voltage pulse, are given in Figure 6.9. Resistivity variation was achieved by varying the intensity of uniform illumination.

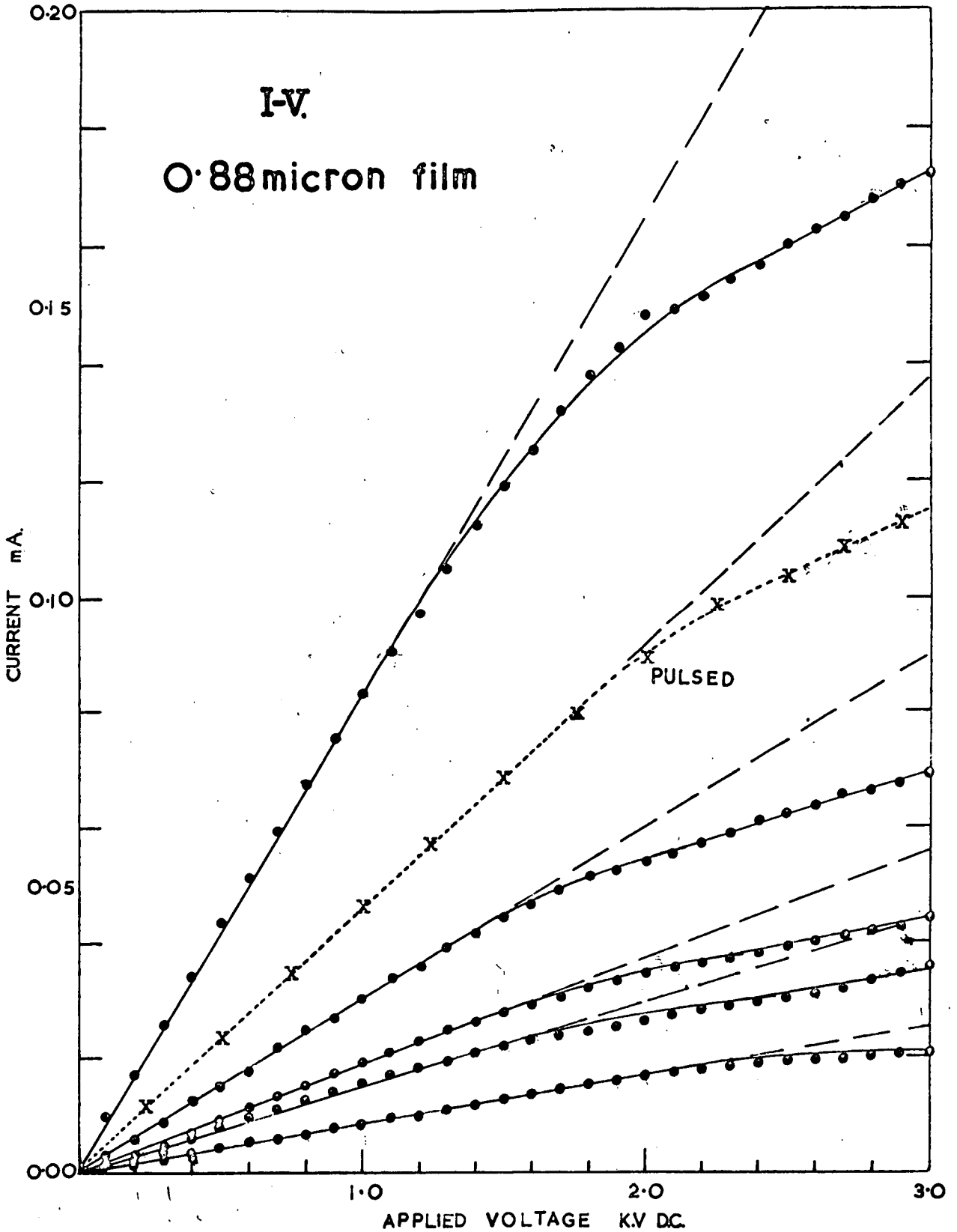
I-V.
0·88 micron film
0·20
0·15
0·10
0·05
0·00
CURRENT mA.
PULSED
1·0
2·0
3·0
APPLIED VOLTAGE K.V D.C.

FIGURE 6·8

Comparing these characteristics to Figure 6.8 (0.88 micron specimen) notice that the "knee" position was comparatively poorly defined. The degree of saturation again decreased with increase in resistivity. The "knee" voltage was, apparently, independent of pulse repetition rate (1 - 50 Hz) and its apparent locus again described a photo-Hall effect type curve. Below threshold the sample acted ohmically.

"Steady state" field distributions, obtained by sampling at 0.5 mm. intervals the voltage developed 1.5msecs after application of the variable amplitude, 0.1msec rise time, voltage pulse, are given in Figure 6.10. Note, firstly, the redistribution of local field with increase in the voltage applied to the sample, and secondly, the post-threshold ($V > V_t$) appearance of localized regions of low, and even negative field following regions of comparatively high field at points in the sample remote from the contacts. Discussion of the significance of these observations is again deferred to the following section.

In a study of the generation of r.f. noise power in bulk CdS crystals biased into the acoustic gain condition, A.R. Moore [100], employing a model similar to that of Chapter 4, sections 2 and 3, theoretically predicted that the acoustoelectrically generated noise power per unit bandwidth originating in transitions $S \longrightarrow 0$, $0 \longrightarrow S$ (Equation 4.2.25, Figure 4.2A) should be proportional to $(V - V_t)^2$ for $V > V_t$ and zero for $V < V_t$. This prediction was verified by plotting linearly the relative noise voltage [α (power)$^{\frac{1}{2}}$] developed across a resistor in series with a photoconducting CdS single crystal against the voltage applied to the crystal. Figure 6.11A shows the published result of Moore's experiment (Figure 9 of reference 100).

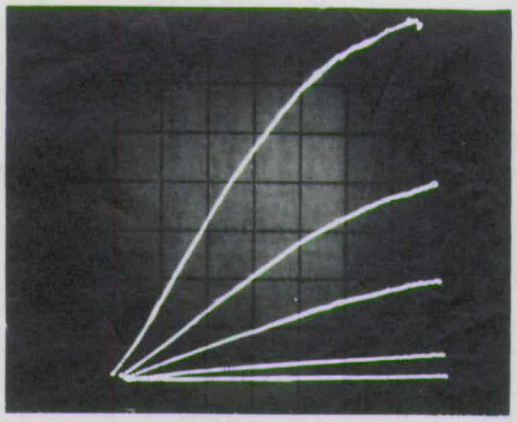

V 0·5mA/div. H 1kV/div.

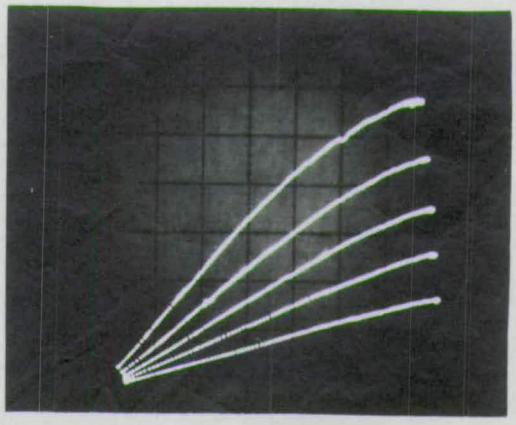

V 0·5mA/div. H 1kV/div.

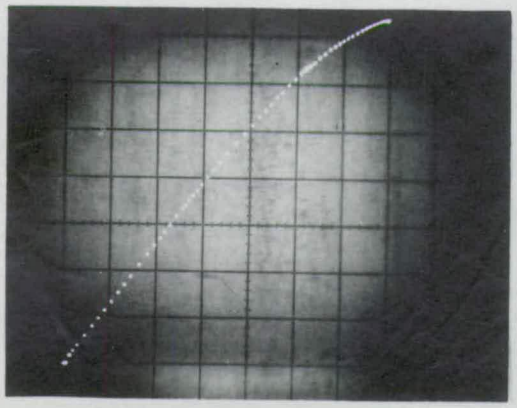

SAMPLE UNDER PROBE (SEE FIG. 6·10)

V 0·2mA/div. H 1kV/div.

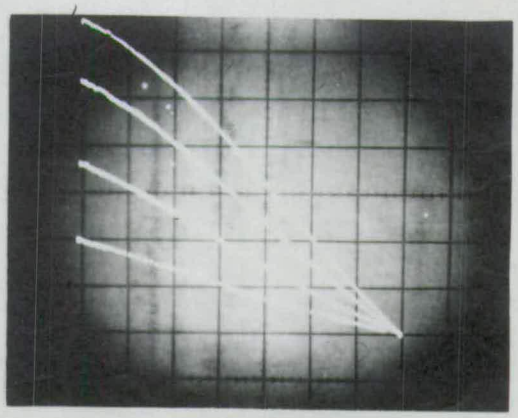

SAMPLE REVERSED

V 0·2mA/div. H 1kV/div.

PULSED IV CHARACTERISTICS

1·2 micron film

FIGURE 6·9

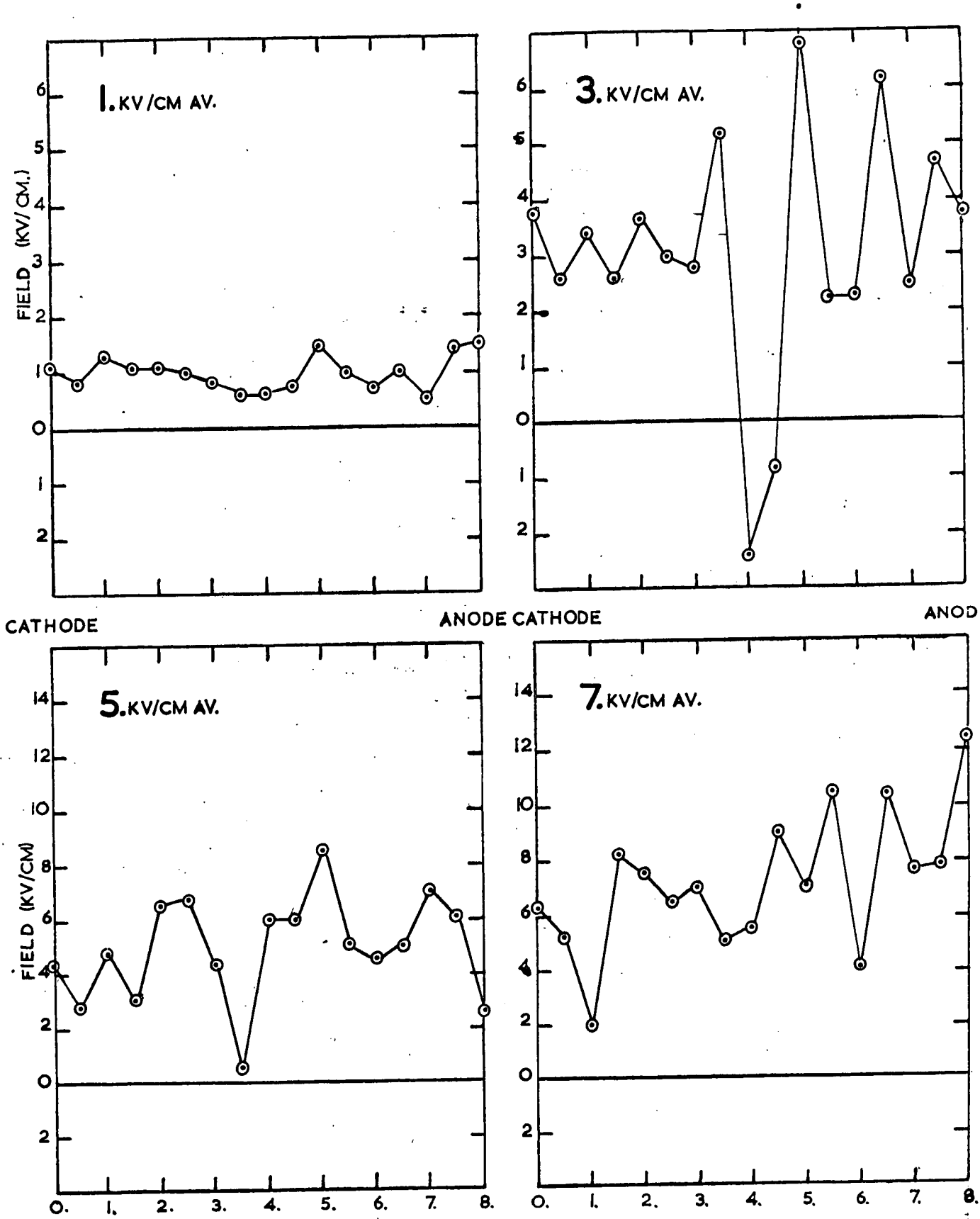
1. KV/CM AV.
3. KV/CM AV.
5. KV/CM AV.
7. KV/CM AV.
FIELD (KV/CM.)
FIELD (KV/CM)
CATHODE
ANODE CATHODE
ANOD
0. 1. 2. 3. 4. 5. 6. 7. 8.

FIGURE 6·10

Assembling auxiliary apparatus in configuration Figure 6.3, "steady state" pulsed noise voltage vs applied voltage characteristics of the narrowed thin film specimen were plotted, 1.5msecs after application of the 0.1msec voltage pulse for a variety of uniform illumination intensities. Two photographs of these plots, together with corresponding (inverted) current voltage characteristics for medium and low light levels, are given in Figures 6.11B and 6.11C.

Comparing these photographic plots with Figure 6.11A due to Moore, notice that in both cases the results appear to verify Moore's prediction that noise power is proportional to $(V - V_t)^2$ for $V > V_t$, zero for $V < V_t$. Deviations from this relationship may be seen to occur in the immediate vicinity of V_t, where Moore's analysis breaks down.

Failure of the E.H.T supply made further investigation of the saturated photo-current noise impossible for a period of two weeks, during which time the specimen was stored under vacuum in an attempt to avoid possible deterioration similar to that observed in the previously tested 0.88 micron thick specimen.

The attempt proved unsuccessful. While the contacts were found by probing to have remained substantially ohmic during the storage period, high field photo-current saturation localized field redistribution, and field dependent noise, were no longer detectable. Since it was, as a consequence, impossible to establish further correlation between A.R. Moore's high field bulk CdS experiments, and these high field thin film experiments, the experiments were terminated.

The results of these investigations were informally reported to the Acousto-electric Consortium, meeting at Standard Telecommunication Laboratories, Harlow, Essex, in February 1968 (unpublished).

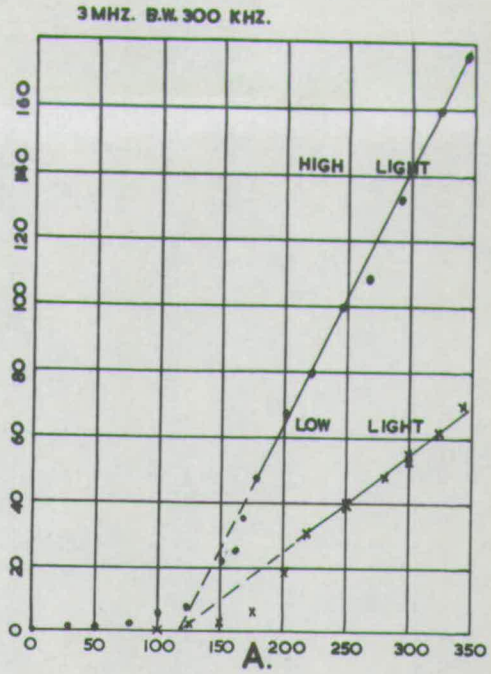

A.

NOISE VOLTAGE VS APPLIED VOLTAGE

(AFTER A.R.MOORE)

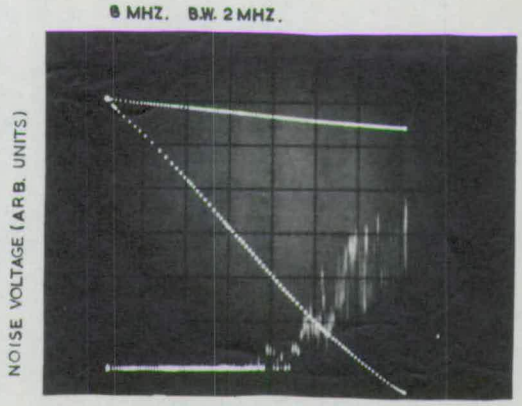

B.

H 1 KV/DIV.

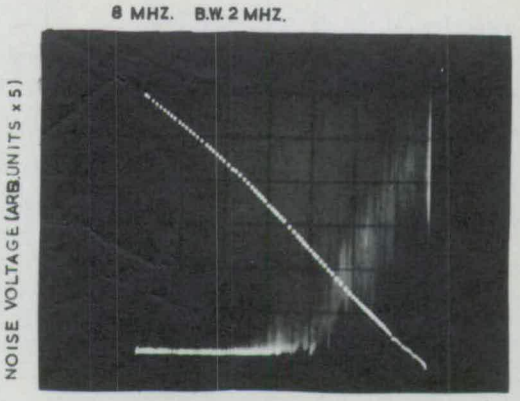

C.

H 1 KV/DIV.

FIGURE 6-11

6.7 DISCUSSION.

It is impossible to conclude, solely on the basis of observations of high field photocurrent saturation, that the overall experimental objective of demonstrating acoustoelectric surface wave interaction in a polycrystalline vapour deposited CdS thin film has been achieved. It will be shown however that the available evidence supports such a conclusion.

Any acceptable model must, in a simple framework, be able to reconcile simultaneously four features of the interaction in question, namely current saturation (Figures 6.8 and 6.9), localized field redistribution (Figure 6.10), the occurence of a region of negative field (Figure 6.10) and a superthreshold photosensitive, linear relationship between noise voltage and applied voltage (Figure 6.11).

Contact effects, impact ionization, field extraction, changes in the forbidden energy gap and changes in the wave functions of all but the most shallow trapping levels may be rejected as primary effects if it is accepted that the measured field distribution reflects the true microscopic field distribution. Arguments in support of electrochemically produced changes in the trap densities, dipole layer formation due to inhomogeneities with different conductivities or trap concentrations, Joule heating effects, and finally free carrier injection either as space charge or as double injection, as far as can be ascertained either fail to reconcile one or other of the observed features of the interaction or are forced to rely on a prior assumption which might be difficult to establish in a thin film situtation. It is therefore reasonable to seek explanations in terms either of acoustoelectric interactions or of field induced changes in the majority carrier capture probabilities.

Van Heek [165] and Karpovich et.al. [166] have observed high field photocurrent sublinearities in mobility enhanced, coplanar electrode CdSe thin films. Both investigators considered field enhanced electron capture to be more probable than acoustoelectric interaction. Karpovich and Zvonkov's adoption of the former explanation, based on correlations between high field photocurrent decay in the presence and absence of additional pulse illumination, appears to be realistic. A quantitative inconsistency does however exist between their time constants for photocurrent decay to saturation (10^{-3} secs) and Van Heek's statement that

"heating effects were not observed when the pulse width of a single sweep sawtooth voltage was changed from 10 microseconds to 1 second".

This apparent inconsistency justifies a critical comparison of the reasons advanced by the two investigators for the rejection of an acoustoelectric explanation.

Van Heek's rejection is based primarily upon the absence of correlation between the velocity of transverse waves in CdSe single crystal (1.5×10^5 cm/sec) and the drift velocity (sic) of the charge carrier at the "knee" voltage ($= \mu_H E_K = 70 \times 8.2 \times 10^3$ cm/sec). Moore and Smith [102] have pointed out that the effective carrier drift velocity is given by $\frac{n}{n + n_t}$ where n and n_t are, respectively, the densities of acoustoelectrically bunched, free and trapped carriers. Furthermore, for 0.36 micron thick films on pyrex, < 300 MHz fundamental mode surface waves travel at $\doteq 3 \times 10^5$ cm/sec (Figure 3.1). While it might be argued, on the basis of the White [17] theory, that the frequency for optimim gain of the system is in excess of 300 MHz, the question of into which surface wave mode energy would be pumped, has yet to be settled. Van Heek's secondary reason for rejection is based on the apparent stability of

the observed differential negative resistance and should be considered in the light of the acoustoelectric instability incubation length (Figure 4.1) and his small interelectrode drift length ($\sim 10\mu$ max).

Karpovich et.al.'s rejection of acoustoelectric interaction is based on the grounds of photocurrent decay observations and the absence of piezoelectric effects in unoriented polycrystalline structures. In an acoustoelectric framework both grounds are valid, and the question, of whether or not acoustoelectric interactions did in fact contribute to the observed current saturation cannot usefully be discussed here, since no studies of CdSe film orientation appear to have been published by these workers.

The two observed time constants for photocurrent decay to saturation (1.2μ thick specimen) are, respectively, compatible with diagnoses of acoustoelectric interaction ($\doteq 0.25 \times 10^{-6}$ secs) and field enhanced electron capture ($\doteq 0.5 \times 10^{-3}$ secs). It has already been noted that coulomb repulsive traps may exist in CdS and CdS-CdSe systems (Chapter 5, section 3). Since in imperfect experimental situations high field interactions may proceed in parallel, it is permissible to attempt to interpret the available evidence in terms of both mechanisms.

A 15% variation in ohmic (i.e. pre-saturation) field over the bulk of a commercial sample is regarded by McFee and Tien [109] as being typical of many "homogeneous" photoconducting CdS single crystals. The recorded (Figure 6.10), 1 kV applied, field variation need not, accordingly, be regarded as atypical of inhomogeneous photoconducting CdS specimens.

Redistributions of field with increasing applied voltage, in order to maintain current continuity in the face of spatially non-uniform current saturating

interactions, are to some extent, obscured by inherent specimen inhomogeneities (Figure 6.10). Normalization may profitably be accomplished by employing McFee and Tien's relation [109]

$$f(x) = -\frac{J_{ae}}{J_{sat}} = \frac{J_{ohmic.}}{J_{sat.}} \cdot \frac{E_{sat}(x)}{E_{ohmic}(x)} - 1$$

This equation describes (see Chapter 4, section 6) the relationship between the acoustoelectric current J_{ae}, and the post-threshold field profile $E_{sat}(x)$ in an inhomogeneous, low gain rate specimen. McFee and Tien's initial assumptions of spatially independent mobility and field independent carrier concentration may, to a greater or lesser degree, be inapplicable to the 1.2 μ thick sample.

Ignoring this difficulty, the observed high field regions (Figures 6.10 and 6.12) followed by regions of low, and even negative field may be explained simply on the basis of momentum exchange between drifting carriers and acoustic waves. Regions of positive f(x) in Figure 6.12 may be regarded as regions of acoustic gain, crossover points x_c where f(x) = 0 may be regarded as points of zero gain, and regions of negative f(x) may be regarded as regions of acoustic attenuation. In the absence of lattice attenuation, field measurements at points x_c may be used, through the relation

$$\mu_{eff}(x_c) = \frac{V_s}{E(x_c)}$$ to estimate the effective carrier drift mobility.

Ignoring further difficulties imposed by the dispersive nature of the thin film waveguide, effective drift mobility values obtained using this relation in conjunction with Figures 6.10 and 6.12, and the Rayleigh wave velocity for CdS ($\doteq 1.7 \times 10^5$ cm/sec) are tabulated as follows:

f(x) vs.x.

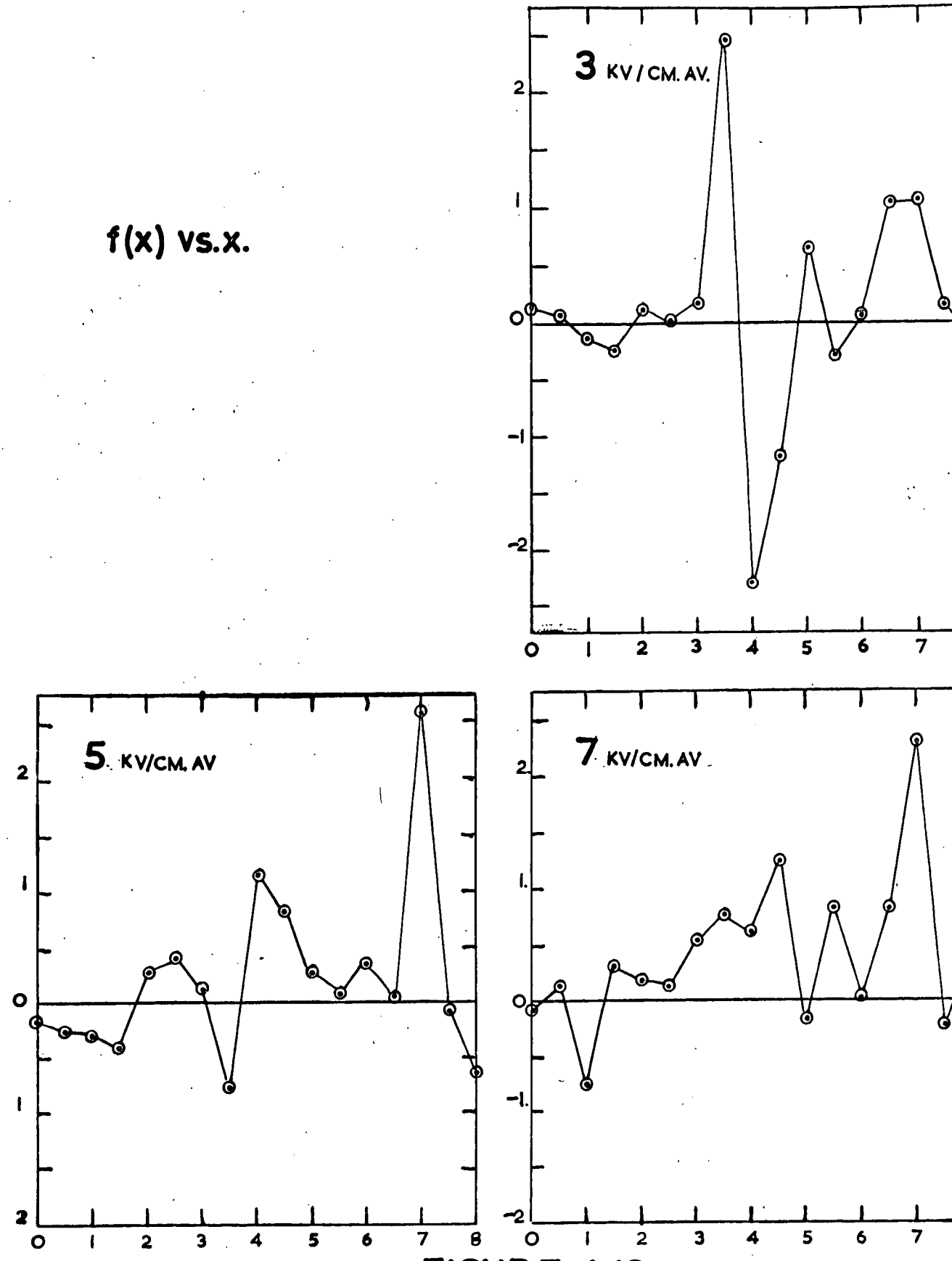

FIGURE 6·12

TABLE 6.1

Dist. from Cathode mm	Applied Field kV/cm	Local Field kV/cm	Effective Mobility cm^2/V sec
≐ 3.7	3	1.6	106
	5	5.4	31
≐ 7.5	3	4.4	39
	5	6.0	28
	7	7.9	22

These values for the effective drift mobility of a post evaporation heat treated thin film are made entirely plausible by Boër, Esbitt and Kaufmann's [154] Hall mobility measurements of 225 cm^2/V sec for similarly heat treated films. The decrease in effective drift mobility with increase in local field is at least qualitatively consistent with the previously mentioned Moore-Smith relation:-

$$\mu_{eff} = \frac{n}{n + n_t} . \mu_H . E_K$$

as applied to a sample in which n_t is an increasing function of field. Moore and Smith [102] observed acoustoelectric interactions at $\mu d/\mu_H$ ratios of 0.06, in single crystal CdS. Le Comber et.al.'s [160] criterion of $\mu d/\mu_L \geq 0.37$ for the occurence of transient acoustoelectric interactions would therefore appear to raise no significant difficulties, if the situation were to be represented by an acoustoelectric model.

The field reversal at 3 kV, between 3.8 mm and 4.6 mm (Figure 6.10), cannot easily be accounted for in terms of a simple trapping effect. Explanations

in terms of carrier extraction from accidental junctions may, in view of the width of the region and the absence of any visible discontinuity, be difficult to establish. The ease with which the negative region may be reconciled in terms of inhomogeneous acoustoelectric interactions lends strong support to the adpotion of a model similar to that advanced by McFee and Tien (Chapter 4, section 6).

Relationships between externally applied field and the internal generation of current noise have yet to be explored in detail. The possibility that conventional field dependent trapping interactions might have resulted in the observed photodependent linear relationship between noise power and $(V - V_t)^2$ cannot lightly be dismissed. Apparent verification of Moore's acoustoelectric noise power prediction (Figure 6.11) can, however, be viewed as an encouraging indication that acoustoelectric interactions made a significant contribution to the observed high field photocurrent sublinearity.

While uncontroversial proof may be lacking, the close similarity between the observed effects and those previously observed in acoustoelectrically active single crystal specimens of CdS, and the ease with which all the observed effects may be interpreted within an acoustoelectric framework, suggest that the experimental objective, of achieving acoustoelectric surface wave interaction in a CdS-on-Sapphire system, has been realised.

CHAPTER 7.

SUMMARY AND CONCLUSIONS.

7.1 SUMMARY.

Characteristic equations governing surface wave propagation in thin film waveguides were formulated as variants of the general, anisotropic, bimaterial, infinite plate problem. The primary influence exerted by the mechanical properties of the substrate on thin film propagation was deduced from a discussion, conducted in real space time, of the ranges of existence of solutions to these characteristic equations. The implications of system anisotropy were explored in some detail, and a number of dispersion "anomalies" were predicted.

A programme, potentially capable of extension to the numerical analysis of wave propagation in all variants of the bimaterial plate, was developed and applied to the experimentally imperative location of a crystallographic plane free from anisotropic surface wave propagation "anomalies". Slowness characteristics for shear vertical surface wave propagation over the principal planes of two trigonal media were presented in this context, and it was shown to be an adequate approximation to regard a suitably oriented CdS-on-Sapphire system as mechanically isotropic with respect to waveguide dispersion.

During the course of this investigation, a number of analyses leading to the prediction of high surface wave gain rates in a number of variants of the original electron beam piezoelectric surface wave amplifier were published. The variant of principal interest - the CdS-on-Sapphire waveguide - was shown

in this study to reduce, in low and high frequency limits respectively, to variants analysed by S. Kaliski and C-C Tseng. The numerical difficulties impeding extension of their arguments into the normalized frequency domain of strong dispersion were ennumerated, and the dispersive character of acousto-electric coupling was discussed within an alternative acoustic ray waveguide framework.

A general discussion of acoustic thermal noise amplification was applied both to the quasi-mathematical visualization of acoustoelectric domain formation in homogeneous single crystals and thin films, and to the low gain rate/inhomogeneity questions of current saturation, static domain formation and acoustoelectrically induced current oscillations.

The existing degree of control (during CdS film vapour deposition) over micro-precipitation, structural defect decoration and impurity trapping-complex formation, was shown to fall short of the heavy material demands made by high planar drift fields. Since available resources did not permit an elegant approach to defect density reduction, an unoptimized, relatively complex, post evaporation heat treatment procedure, aimed at compensation of native atom astoichiometries and at drift mobility enhancement through copper recrystallization catalysis, was developed.

A series of high field experiments performed on post evaporation heat treated CdS-on-Sapphire films led to the observation of both continuous and pulsed high field photocurrent saturation, the latter being accompanied by localized field redistribution and the generation of acoustoelectric-bunching-type noise. These observations were diagnosed as being indicative of low gain rate surface wave noise amplification in the presence of field dependent recombination.

7.2 CONCLUSIONS AND SUGGESTIONS FOR FURTHER WORK.

In spite of long standing seismological interest in the numerical structure of surface wave propagation, analysis of the classical monolayered halfspace problem is far from complete. Even in the highly degenerate isotropic case, many questions, involving propagation in complex space time, energy distribution among available modes for various noie inputs, and the detailed inter-relationship between material parameters, dispersion, stress and particle displacement, remain amenable to analysis but unanswered. Stoneley wave dispersion has yet to be examined in any detail, and higher mode cut-off has only been studied within the limited context of surface wave exponential decay with depth. In the more general anisotropic case, virtually nothing is known about the existence of Stoneley (interface) waves, many of the generalized Sezawa wave dispersion "anomalies" predicted in Chapter 3, section 3 are at present numerically unconfirmed, and only limited investigations into the influence of piezoelectric stiffening on bounded wave propagation have been made.

Permutation of the passive monolayered halfspace structure affords access to a wide variety of dispersive and non-dispersive surface acoustic waveguide devices, potentially capable (through manipulation of dispersion characteristics, higher mode cut-off points and forbidden directions of propagation) of performing many of of the circuit functions currently undertaken by bulky electromagnetic waveguides. Since thermal dissipation, round trip instability and cummulative round trip noise disadvantages of bulk acoustoelectric amplifiers have no direct surface wave analogue; since distributed gain may be used to advantage in a thin film waveguide network; and since surface wave acoustoelectric effects provide a versatile tool for the exploration of surface

transport and trapping mechanisms, it is anticipated that the thin film amplifier proposed in this study will not lack practical application.

It is reasonable to expect that the severe difficulties accompanying thermodynamic stabilization of high mobility, piezoelectric, semiconducting thin films (e.g. CdS, ZnO, GaAs) will be overcome in the near future.

REFERENCES.

1.	KROMER (H.)	Physical Review, 109, 1958, 1856-
2.	KROMER (H.)	Proc. I.R.E., 47, 1959, 231-
3.	VOIGT (W.)	Lehrbuch der Kristallphysik (Teubner, Leipzig, 1910).
4.	KYAME (J.J.)	Jnl. Acoustical Soc. Amer., 21, 1949, 159-
5.	KOGA (I.) et.al.	Physical Review, 109, 1958, 1467-
6.	MEIJER (H.J.G.) & POLDER (D.)	Physica, 19, 1953, 225-
7.	KYAME (J.J.)	Jnl. Acoustical Soc. Amer., 26, 1954, 990-
8.	WEINREICH (G.)	Physical Review, 104, 1956, 321-
9.	PARMENTER (R.H.)	Physical Review, 89, 1953, 996-
10.	NINE (H.D.)	Physical Review Letters, 4, 1960, 359-
11.	HUTSON (A.R.)	ibid. 4, 1960, 505-
12.	HUTSON (A.R.) et.al.	ibid. 7, 1961, 237-
13.	SMITH (R.W.)	ibid. 9, 1962. 87-
14.	HUTSON (A.R.)	ibid. 9, 1962, 296-
15.	WANG (W.C.)	ibid. 9, 1962, 443-
16.	McFEE (J.H.)	Jnl. Applied Physics, 34, 1963, 1548-
17.	WHITE (D.L.)	ibid. 33, 1962, 2547-
18.	KROGER (H.) et.al.	Physical Review Letters, 11, 1963, 246-
19.	KROGER (H.) et.al.	ibid. 12, 1964, 555-
20.	OKADA (J.) & MATINO (H.)	Jap. Jnl. Applied Physics, 2, 1963, 736-
21.	RIDLEY (B.K.) & WATKINS (T.B.)	Proc. Physical Society, 78, 1961, 293-
22.	RIDLEY (B.K.) & WATKINS (T.B.)	Jnl. Physics & Chemistry of Solids, 22, 1961, 155-

23.	RIDLEY (B.K.)	Proc. Physical Society, 82, 1963, 954-
24.	BOER (K.W.) et.al.	Zeit. Physik, 155, 1959, 170-
		Physica Status Solidi, 4, 1964-
		Solid State Communications, 5, 1967, 1967-
25.	RIDLEY (B.K.) & PRATT (R.G.)	Physics Letters, 4, 1963, 300-
26.	NORTHROP (D.C.) et.al.	Solid State Electronics, 7, 1964, 17-
27.	POLKE (M.) & HASLER (K.)	Physica Status Solidi, 9, 1965, 851-
28.	SILVA (P.O.) & BRAY (R.)	Physical Review Letters, 14, 1965, 372-
29.	HAYDL (W.H.) & QUATE (C.F.)	Applied Physics Letters, 7, 1965, 45-
30.	HERVOUET (C.) et.al.	Solid State Communications, 3, 1965, 413-
31.	ISHIGURO (T.) et.al.	Jap. Jnl. Applied Physics, 4, 1965, 703-
32.	GUNN (J.B.)	Solid State Communications, 1, 1963, 89-
		IBM Jnl. Research & Development, 8, 1964, 141-
33.	BARRAUD (A.)	Comptes Rendus Acad. Sci. Paris, 256, 1963, 367
34.	ALLEN (J.W.) et.al.	Applied Physics Letters, 7, 1965, 78-
		ibid. 9, 1966, 39-
35.	FOYT (A.G.) & McWHORTER (A.L.)	Trans. I.E.E.E. Electron Devices, ED-13, 1966, 79-
36.	LUDWIG (G.W.) et.al.	ibid. 13, 1966, 671-
37.	ZABOLOTSKAYA (E.A.) et.al.	Soviet Physics Acoustics, 12, 1967, 380-
38.	CLEMENSON (J.)	Proc. I.E.E.E., 55, 1967, 2168-
39.	BUTLER (M.B.N.) & SANDBANK (C.P.)	Trans. I.E.E.E. Electron Devices, ED-14, 1967, 663-
40.	RAYLEIGH (Lord S.J.W.)	Proc. London Mathematical Soc., 17, 1885, 4-
41.	LAMB (H.)	Proc. London Mathematical Soc., 13, 1882,
42.	OLDHAM (R.D.)	Phil. Trans. Royal Astronom. Soc., A 194, 1900 135-

43. LOVE (A.E.H.) — Some problems of geodynamics. Cambridge University Press, 1911.

44. STONELEY (R.) — Monthly Notes Royal Astronom. Soc., Geophys. Suppl. 1, 1925, 280-

45. STONELEY (R.) — Proc. Royal Society A, 106, 1924, 416-

46. EWING (W.M.) et.al. — Elastic waves in layered media. M'Graw-Hill, 1957.

47. ASH (E.A.) & MORGAN (D.P.) — Ministry of Aviation Interim Report, PD/47/029/AT. (Unpublished). 1967.

48. STONELEY (R.) — Monthly Notes Royal Astronom. Soc., Geophys. Suppl. 5, 1949, 343-

49. SYNGE (J.L.) — Jnl. Mathematical Physics, 35, 1957, 323-

50. BUCHWALD (V.T.) — Quart. Jnl. Mechanics & Applied Maths., 14, 1961 293-

51. BUCHWALD (V.T.) — ibid. 14, 1961, 461-

52. BUCHWALD (V.T.) & DAVIS (A.) — ibid. 16, 1963, 283

53. LIGHTHILL (M.J.) — Phil. Trans. A 252, 1960, 397-

54. DUFF (G.F.D.) — Phil. Trans. A 252, 1960, 249-

55. MUSGRAVE (M.J.P.) — Progress in Solid Mechanics, II, 1960, 63-85.

56. RAMAN (Sir C.V.) & VISWANATHAN (K.S.) — Proc. Indian Acad. Sci., A 42, 1955, 51-

57. MAKINSON (K.R.) — Proc. Int. Wool Textile Research Conf., Australi CSIRO Melbourne, Pt. D, 1955, pp. 54-

58. PILANT (W.L.) — Ph.D. Thesis, University of California, Los Angeles, 1960.

59. LIM (T.C.) & FARNELL (G.W.) — Ultrasonics Conference, Vancouver B.C., 1967.

60. TSENG (C-C). — Ph.D. Thesis, University of California, Berkeley, 1966.

& WHITE (R.M.) — Jnl. Applied Physics, 38, 1967, 4274-

61. GAZIS (D.C.) & WALLIS (R.F.) — Surface Science, 5, 1966, 482-

62. SYNGE (J.L.) Proc. Royal Irish Acad. A 58, 1956, 13-

63. SCHOLTE (J.G.) Monthly Notes Royal Astronom. Soc., Geophys. Suppl. 5, 1947, 120-

64. SEZAWA (K.) & KANAI (K.) Bull. Earthquake Research Inst. Tokyo, 17, 1939, 1-

65. MUSGRAVE (M.J.P.) Geophysical Journal Royal Astronom. Soc., 3, 1960, 406-

66. SCHOUTEN (J.A.) Tensor analysis for physicists, Ch. VII. 2nd. Edition, 1957. Clarendon Press.

67. PARSONS (M.K.) Trans. I.E.E.E. Sonics & ultrasonics, SU-14, 1967, 142-

68. KALISKI (S.) Proc. Conf. Acoustics of Solid Media, Warsaw, October, 1964.

69. MAYO (R.F.) Personal communication, 1966.

70. GULYAEV (Yu Y.) & PUSTOVOIT (V.I.) Soviet Physics JETP, 20, 1965, 1508-

71. WHITE (R.M.) Trans. I.E.E.E. Electron Devices, ED-14, 1967,

72. SAVVINYKH et.al. Soviet Physics Solid State, 7, 1966, 2585-

73. PUSTOVOIT (V.I.) & GERTSENSHTEIN (Soviet Physics Solid State, 6, 1964, 677-

74. KALISKI (S.) Proc. Vibration Problems, 4, 1965,

75. SOLYMAR (L.) & ASH (E.A.) Int. Jnl. Electronics, 20, 1966, 127-

76. JEFFREYS (H.) Monthly Notes Royal Astronom. Soc. Geophys. Suppl. 1. 1925, 282-

77. JEFFREYS (H.) ibid. 3, 1935,

78. MOONEY (H.M.) & BOLT (B.A.) Bull. Seismological Soc. Amer., 56, 1966, 43-

79. LIM (T.C.) & FARNELL (G.W.) Applied Physics Letters, To be published

80. ENGAN (H.) et.al. ibid. 10, 1967, 311-

81. ROLLINS (F.R.) et.al. ibid. To be published, 1968.

82. GAZIZ (D.C.) et.al. Physical Review, 119, 1960, 533-

83.	INGEBRITSEN (K.A.) & TONNING (A.)	Applied Physics Letters, 9, 1966, 16-
84.	ANDERSON (D.L.)	Jnl. Geophysical Research 66, 1961, 2953-
85.	SCHNITZLER (P.A.)	Applied Physics Letters, 11, 1967, 273-
86.	COQUIN (G.A.) & TIERSTEN (H.F.)	Jnl. Acoustical Soc. Amer., 41, 1967, 921-
87.	VEREVKINA (L.V.) et.al.	Soviet Physics Acoustics, 12, 1967, 254-
88.	SATO (Y.)	Bull. Earthquake Research Inst. Tokyo, 31, 1953, 81- and 255-
89.	TOLSTOY (I.) & USDIN (E.)	Geophysics, 18, 1953, 844-
90.	HADI (Z.M.A.)	M.Sc. Thesis, University College, London, 1967.
91.	CADY (W.G.)	Piezoelectricity. 1st Edition, M'Graw-Hill, 1946.
92.	McFEE (J.H.)	IN Physical acoustics, Vol. IVA, Academic Press, 1965. Mason (W.P.)
93.	PRESS (F.) & HEALY (J.)	Jnl. Applied Physics, 28, 1957, 1323-
94.	KALISKI (S.)	Proc. Vibration Problems, 4, 1966, 277-
95.	VASKOVA (V.I.) & VIKTOROV (I.A.)	Soviet Physics Acoustics, 13, 1967, 249-
96.	BREKHOVSKIKH (L.M.)	ibid. 5, 1959, 288-
97.	RISCHBIETER (F.)	Acoustica, 16, 1966, 75-
98.	MEITZLER (A.)	Jnl. Acoustical Soc. Amer., 34, 1962, 444-
99.	ROSE (A.)	RCA Review, 27, 1966, 98-
		ibid. 27, 1966, 600-
		ibid. 28, 1967,
100.	MOORE (A.R.)	Jnl. Applied Physics, 38, 1967, 2327-
101.	HAYDL (W.H.) et.al.	ibid. 38, 1967, 4295-
102.	MOORE (A.R.) & SMITH (R.W.)	Physical Review, 138, 1965, 1250-
103.	GREEBE (C.A.A.J.)	Trans. I.E.E.E. Sonics & Ultrasonics, SU-13, 1966, 54-

104.	AUTIN (P.)	Physica Status Solidi, 24, 1967, 501-
105.	PROHOFSKY (E.W.)	Jnl. Applied Physics, 37, 1966, 4729-
106.	BOER (K.W.)& DUSSEL (G.A.)	Physical Review, 154, 1967, 292-
		Physica Status Solidi, 21, 1967, K 145-
107.	POHLENDT (E.) & WETTLING (W.)	Physics Letters, A 25, 1967, 22-
108.	MACRAE (A.V.)	Surface Science, 2, 1964, 522-
109.	McFEE (J.H.) & TIEN (P.K.)	Jnl. Applied Physics, 37, 1966, 2754-
110.	PAIGE (E.G.S.)	Proc. Int. Conf. Physics Semiconductors, Kyoto, IN Jnl. Physical Soc. Japan, 21, 1966, Suppl. 397-
111.	FROOM (J.)	Trans. I.E.E.E. Electron Devices, ED-14, 1967, 656-
112.	FRERICHS (R.)	Naturwissenschaften, 33, 1946, 387-
113.	LORENZ (R.)	Chemische Berichte, 24, 1891, 1509-
114.	VEITH (W.)	Comptes Rendus Acad. Sci. Paris, 230, 1950, 947-
115.	WILSON (R.B.)	Jnl. Scientific Instruments, 44, 1967, 159-
116.	JACOBS (J.E.) & HART (C.W.)	Proc. National Electronics Conf., 111 1955, 1-
117.	CAPELLA (L.)	Comptes Rendus Acad. Sci. Paris, 261, 1965, 4053-
118.	ALBERS (W.)	IN Physics and chemistry of II-VI compounds, Ch. IV. *
119.	KROGER (F.A.)	The chemistry of imperfect crystals. North Holland, 1964.
120.	WOODBURY (H.H.)	IN Physics and chemistry of II-VI compounds, Ch.
121.	BOYN (R.) et.al.	Physica Status Solidi, 12, 1965, 57-
122.	DREEBEN (A.)	Jnl. Electrochemical Society, 115, 1968, 279-
123.	VAN GOOL (W.)	Philips Research Reports, Suppl. 3, 1961.
124.	BUBE (R.H.)	IN Physics and chemistry of II-VI compounds, Ch. XIII, *.

125.	WOODBURY (H.H.)	Jnl. Applied Physics, 36, 1965, 2287-
126.	VITRIKHOVSKII (N.I.) & KURIK (M.V.)	Soviet Physics Solid State, 6, 1966, 2714-
127.	CHERNOW (F.) et.al.	Applied Physics Letters, 9, 1966, 145-
128.	DRESNER (J.) & SHALLCROSS (F.V.)	Jnl. Applied Physics, 34, 1963, 2390-
129.	KARPOVICH (I.A.) & ZVANKOV (B.N.)	Soviet Physics Solid State, 6, 1965, 2714-
130.	WOODBURY (H.H.)	Jnl. Physics & Chemistry of Solids, 27, 1966, 1257-
131.	MARK (P.)	RCA Review, 26, 1965, 461-
132.	MARK (P.)	Jnl. Physics & Chemistry of Solids, 26, 1965, 959-
133.	FAETH (P.A.)	Jnl. Electrochemical Society, 114, 1967, 511-
134.	AITCHISON (R.E.)	Nature, 167, 1951, 812-
135.	BROMLEY (A.)	Physical Review, 98, 1955, 246-
136.	NELSON (R.C.)	Jnl. Optical Society Amer., 45, 1955, 774-
137.	BUBE (R.H.)	Photoconductivity of solids. Academic Press, New York, 1960.
138.	DE KLERK (J.)	IN Physical acoustics, Vol. IVA, Academic Press, 1966. Mason((W.P.).
139.	SHALLCROSS (F.V.)	RCA Review, 28, 1967,
140.	LORENZ (M.R.)	IN Physics and chemistry of II-VI compounds, Ch. II. *
141.	GOLDFINGER (P.) & JEUNEHOMME (M.)	Trans. Faraday Society, 59, 1963, 2851-
142.	SOMORJAI (G.A.)	Surface Science, 2, 1964, 298-
143.	ADDISS (R.R.)	Trans. 10th Nat. Vacuum Symp., 1963, pp. 354-63. Macmillan, New York.
144.	ZULEEG (R.) & SENKOVITZ (E.J.)	Enlarged Abstracts Elect. Div. Electrpchem. Soc., 12, 1963, 110-
145.	MILLER (R.J.) & BACHMAN (C.H.)	Jnl. Applied Physics, 29, 1958, 1277-

146. PIZZARELLO (F.A.) — Jnl. Applied Physics, 35, 1964, 2730-

147. DE KLERK (J.) & KELLY (E.F.) — Review of Scientific Instruments, 36, 1965, 506-

148. HUDOCK (P.) — Trans. Metall. Soc. AIME, 239, 1967, 338-

149. BRUNSCHWEILER (A.) — Nature, 209, 1966, 492-

150. REID (M.A.) — Ph.D. Thesis, University of Edinburgh, 1968.

151. FOSTER (N.F.) — Jnl. Applied Physics, 38, 1967, 149-

152. GILLES (J.M.) & VAN CAKENBERGHE (J.) — Nature, 182, 1958, 862-

153. DRESNER (J.) & SHALLCROSS (F.V.) — Solid State Electronics, 5, 1962, 205-

154. BOER (K.W.) et.al. — Jnl. Applied Physics, 37, 1966, 2664-

155. BOER (K.W.) et.al. — Physica Status Solidi, 16, 1966, 697-

156. FOSTER (N.F.) et.al. — Unpublished Report AL-2634, Bell Telephone Labs. In.

157. MOREHEAD (F.F.) — IN Physics and chemistry of II-VI compounds. Ch. XII. *

158. SCHAFFT (H.A.) & FRENCH (J.C.) — Trans. I.E.E.E. Electron Devices, ED-13, 1966, 613-

159. VIKTOROV (I.A.) — Soviet Physics Acoustics, 8, 1962, 118-

160. LE COMBER (P.G.) et.al. — British Jnl. Applied Physics, 17, 1966, 467-

161. ELLIS (D.J.) & CORNWALL (M.G.) — Physics Letters, A 25, 1967, 756-

162. ARTZ (R.M.) & DRANSFELD (K.) — Applied Physics Letters, 7, 1965, 156-

163. WHITE (R.M.) & VOLTMER (F.M.) — Applied Physics Letters, 7, 1965, 314-

164. CHUN (M.K.) — Proc. I.E.E.E, 53, 1965, 1678-

165. VAN HEEK (H.F.) — Physics Letters, A 26, 1968, 175-

166. KARPOVICH (I.A.) & ZVONKOV (B.N.) — Soviet Physics Solid State, 8, 1967, 2994-

167. WACHTMAN (J.B.) et.al. — Jnl. Research Nat. Bureau Standards, A 64, 1960, 213-

* AVEN (M.) & PRENER (J.S.) eds. — Physics and chemistry of II-VI compounds, North-Holland, 1967.